

Aus der Neurologischen Klinik und Poliklinik

Klinikum der Ludwig-Maximilians-Universität München

Vorstand: Prof. Dr. Marianne Dieterich

# **Alpha-Synuclein defects autophagy flux by impairing SNAP29-mediated autophagosome-lysosome fusion**

Dissertation

zum Erwerb des Doktorgrades der Medizin

an der Medizinischen Fakultät der

Ludwig-Maximilians-Universität zu München



vorgelegt von

Qilin Tang

aus

Shandong, V.R. China

2021

---

Mit Genehmigung der Medizinischen Fakultät  
der Universität München

Berichterstatter:	Prof. Dr. Kai Bötzel
Mitberichterstatter:	Prof. Dr. Christian Behrends Prof. Dr. Harald Steiner
Mitbetreuung durch den promovierten Mitarbeiter:	Dr. Thomas Köglsperger
Dekan:	Prof. Dr. med. Thomas Gudermann
Tag der mündlichen Prüfung:	18.11.2021

## Table of Contents

<b>TABLE OF CONTENTS.....</b>	<b>3</b>
<b>ZUSAMMENFASSUNG (DEUTSCH).....</b>	<b>7</b>
<b>ABSTRACT (ENGLISH) .....</b>	<b>9</b>
<b>LIST OF FIGURES.....</b>	<b>11</b>
<b>LIST OF TABLES .....</b>	<b>12</b>
<b>LIST OF ABBREVIATIONS.....</b>	<b>13</b>
<b>1. INTRODUCTION.....</b>	<b>15</b>
<b>1.1 Parkinson's disease .....</b>	<b>15</b>
1.1.1 Clinical characterization .....	15
1.1.2 Neuropathological characteristics and the role of $\alpha$ -Syn in PD.....	18
1.1.3 The development of PD and $\alpha$ -Syn propagating hypothesis .....	21
<b>1.2 Autophagy .....</b>	<b>23</b>
1.2.1 The initiation and regulation of autophagy.....	23
1.2.2 Autophagy as a hub for protein degradation and secretion.....	25
1.2.3 The connection between autophagy defects and PD pathology .....	26
<b>1.3 Extracellular vesicles.....</b>	<b>27</b>
1.3.1 The biogenesis and biochemical composition of EVs.....	27
1.3.2 Aggregated $\alpha$ -Syn transmission may be mediated by EVs .....	29
<b>1.4 Aim of the study .....</b>	<b>30</b>
<b>2. METHODS .....</b>	<b>32</b>
<b>2.1 Cell biology.....</b>	<b>32</b>
2.1.1 Cell culture .....	32

Table of Contents	4
2.1.2 Small interfering RNA transfection .....	34
2.1.3 LDH assay and MTT assay .....	34
2.1.4 LC3B-GFP-RFP autophagy reporter assay.....	35
<b>2.2 Molecular biology.....</b>	<b>36</b>
2.2.1 RNA extraction and reverse transcription.....	36
2.2.2 Real time PCR .....	37
<b>2.3 Protein biochemistry .....</b>	<b>37</b>
2.3.1 Protein extraction.....	38
2.3.2 BCA assay.....	38
2.3.3 Western blot.....	38
2.3.4 Co-Immunoprecipitation .....	39
2.3.5 Florescent immunohistochemistry.....	40
<b>2.4 Extracellular vesicle isolation .....</b>	<b>41</b>
<b>2.5 Nanoparticle tracking analysis .....</b>	<b>42</b>
<b>2.6 Bioinformatics analysis .....</b>	<b>42</b>
2.6.1 Three-dimensional structure prediction and validation .....	42
2.6.2 Protein docking simulation.....	43
<b>2.7 Statistical analysis .....</b>	<b>43</b>
<b>3. RESULTS.....</b>	<b>44</b>
<b>3.1 <math>\alpha</math>-Syn overexpression inhibits autophagy initiation and defects autophagy turnover.....</b>	<b>44</b>
3.1.1 $\alpha$ -Syn overexpression inhibits autophagy initiation in an mTOR-dependent manner.....	44
3.1.2 The abundance of the autophagy marker LC3B-II is increased in $\alpha$ -Syn transduced LUHMES cells .....	46



<b>3.2</b>	<b>EVs release is changed in response to attenuating autophagy flux .....</b>	<b>50</b>
3.2.1	Rapamycin treatment increases autophagy by inhibiting AKT-mTOR signaling pathway. ....	50
3.2.2	$\alpha$ -Syn overexpression and rapamycin treatment increase EV release form cultured neurons. ....	50
3.2.3	Bafilomycin blocks autophagosome-lysosome fusion and inhibits autophagy ....	52
3.2.4	Bafilomycin treatment increases EVs release .....	53
3.2.5	Both bafilomycin treatment and $\alpha$ -Syn overexpression increase the abundance of autophagy-associated markers in EV-enriched pellets from cell culture medium.....	53
<b>3.3</b>	<b>The effect of <math>\alpha</math>-Syn overexpression on autophagolysosome fusion depends on SNAP29 .....</b>	<b>56</b>
3.3.1	$\alpha$ -Syn overexpression leads to a decreased expression of SNAP29 in transduced LUHMES cells .....	56
3.3.2	The abundance of LC3B-II is increased in SNAP29-deficient cells.....	58
3.3.3	SNAP29 knockdown impairs autophagosome-lysosome fusion .....	59
3.3.4	Loss of SNAP29 increases the abundance of EVs in cell medium .....	59
<b>3.4</b>	<b>Co-expressing SNAP29 attenuates autophagy defects and cell death in <math>\alpha</math>-Syn-transduced LUHMES cells.....</b>	<b>62</b>
3.4.1	Co-expressing SNAP29 attenuates the increased LC3B-II abundance in $\alpha$ -Syn transduced LUHMES cells .....	62
3.4.2	Co-expressing SNAP29 rescues the defected autophagy turnover in $\alpha$ -Syn transduced LUHMES cells .....	63
3.4.3	Co-expressing SNAP29 attenuates the cytotoxicity of $\alpha$ -Syn overexpression .....	64
3.4.4	Co-expressing SNAP29 attenuates the abundance of EVs in $\alpha$ -Syn-transduced LUHMES cell medium.....	66
<b>3.5</b>	<b><math>\alpha</math>-Syn directly interacts with SNAP29 .....</b>	<b>68</b>

Table of Contents	6
3.5.1 SNAP29 three-dimensional structure was predicted with good quality.....	68
3.5.2 Protein-protein docking simulations indicates sufficiently strong binding between a-Syn and SNAP29.....	70
3.5.3 Co-IP indicated a direct binding between $\alpha$ -Syn and SNAP29 .....	70
<b>3.6 SNAP29 is lost from neuromelanin-positive neurons of the human SNc in LBP cases.....</b>	<b>73</b>
<b>4. DISCUSSION .....</b>	<b>76</b>
4.1 $\alpha$ -Syn overexpression induces a complex modulation of autophagy.....	76
4.2 Impaired autophagy and $\alpha$ -Syn accumulation form a bidirectional pathogenic loop in synucleinopathies .....	78
4.3 The potential role of SNAP29 in $\alpha$ -Syn overexpression related autophagy defects.	80
4.4 The “crosstalk” between $\alpha$ -Syn-related autophagy defects and increased release of EVs.....	81
<b>5. SUMMARY .....</b>	<b>84</b>
<b>REFERENCES .....</b>	<b>85</b>
<b>APPENDIX A: CELL CULTURE MATERIALS AND REAGENTS .....</b>	<b>94</b>
<b>APPENDIX B: BUFFERS AND SOLUTIONS .....</b>	<b>95</b>
<b>APPENDIX C: ANTIBODIES .....</b>	<b>96</b>
<b>APPENDIX D: PCR PRIMERS .....</b>	<b>97</b>
<b>APPENDIX E: INFORMATION OF HUMAN BRAIN SAMPLES.....</b>	<b>98</b>
<b>ACKNOWLEDGEMENTS .....</b>	<b>99</b>
<b>AFFIDAVIT .....</b>	<b>101</b>

## Zusammenfassung (Deutsch)

Die Parkinson-Krankheit (PD) ist die häufigste neurodegenerative Bewegungsstörung, die durch den fortschreitenden Verlust dopaminergener Neuronen in der Substantia nigra pars compacta (SNc) gekennzeichnet ist. Der neuronale Zelltod bei PD ist mit dem allmählichen Auftreten von neuronalen Proteinaggregaten verbunden, die als Lewy-Körper (LBs) bezeichnet werden und aus vesikulären Membranstrukturen und dysomorphen Organellen in Verbindung mit dem Protein Alpha-Synuclein ( $\alpha$ -Syn) bestehen. Obwohl der genaue Mechanismus der neuronalen Aggregatbildung und des Unterganges von Neuronen bislang nicht bekannt ist, deuten neuere Forschungen auf  $\alpha$ -Syn-vermittelte Veränderungen des lysosomalen Abbaus von aggregierten Proteinen und Organellen hin -- ein Prozess, der als Autophagie bezeichnet wird. In der vorliegenden Arbeit verwendeten wir eine Kombination aus Molekularbiologie und Immunocytochemie, um die Wirkung von  $\alpha$ -Syn auf den Autophagieumsatz in kultivierten menschlichen dopaminergen Neuronen und in menschlichem postmortalem Hirngewebe zu untersuchen.

Wir fanden heraus, dass eine Überexpression von  $\alpha$ -Syn den Autophagie-Umsatz verringert, indem die Fusion von Autophagosomen mit Lysosomen beeinträchtigt wird, was zu einer Verringerung der Bildung von Autophagolysosomen führt. In Übereinstimmung mit einem kompensatorischen Anstieg der Plasmamembranfusion von Autophagosomen erhöhte  $\alpha$ -Syn die Anzahl der extrazellulären Vesikel (EV) und die Häufigkeit von Autophagie-assoziierten Proteinen in diesen EVs. Mechanistisch interagierte  $\alpha$ -Syn mit dem v-SNARE-Protein SNAP29, einem Mitglied des SNARE-Komplexes, der die Autophagolysosomen-Fusion vermittelt, und verringerte dessen Proteinexpression. In Übereinstimmung damit ahmte der Knockdown von SNAP29 mittels RNAi die Wirkung von  $\alpha$ -Syn auf die Autophagie nach, während die SNAP29-Coexpression die  $\alpha$ -Syn-induzierten Veränderungen beim Autophagie-Umsatz und der

EV-Freisetzung umkehrte und den Zelltod reduzierte. In Übereinstimmung mit unseren Ergebnissen aus kultivierten Neuronen fanden wir eine Stadien-abhängige Reduktion von SNAP29 in Neuromelanin-positiven SNc Neuronen aus menschlichem postmortalem Hirngewebe von Fällen mit Lewy-Körperpathologie (LBP). Zusammenfassend zeigen unsere Ergebnisse somit eine bisher unbekannte Wirkung von  $\alpha$ -Syn auf intrazelluläre Autophagie-assoziierte SNARE-Proteine und infolgedessen eine verringerte Autophagolysosomenfusion. Daher werden unsere Ergebnisse die Untersuchung Autophagie-assoziiierter pathologischer Veränderungen der Parkinson-Krankheit unterstützen.

## Abstract (English)

Parkinson's disease (PD) is the most common neurodegenerative movement disorder characterized by the progressive loss of dopaminergic (DAergic) neurons in the substantia nigra pars compacta (SNc). DAergic neuronal death in PD is associated with the gradual appearance of neuronal protein aggregates termed Lewy bodies (LBs) that are comprised of vesicular membrane structures and dysmorphic organelles in conjunction with the protein alpha-Synuclein ( $\alpha$ -Syn). Although the exact mechanism of neuronal aggregate formation and death remains elusive, recent research suggests  $\alpha$ -Syn-mediated alterations in the lysosomal degradation of aggregated proteins and organelles -- a process termed autophagy. Here, we used a combination of molecular biology and immunchemistry to investigate the effect of  $\alpha$ -Syn on autophagy turnover in cultured human DAergic neurons and in human postmortem brain tissue.

We found  $\alpha$ -Syn overexpression to reduce autophagy turnover by compromising the fusion of autophagosomes with lysosomes, thus leading to a decrease in the formation of autophagolysosomes. In accord with a compensatory increase in the plasma membrane fusion of autophagosomes,  $\alpha$ -Syn enhanced the number of extracellular vesicles (EV) and the abundance of autophagy-associated proteins in these EVs. Mechanistically,  $\alpha$ -Syn interacted with and decreased the abundance of the v-SNARE protein SNAP29, a member of the SNARE complex mediating autophagolysosome fusion. In line, SNAP29 knockdown mimicked the effect of  $\alpha$ -Syn on autophagy whereas SNAP29 co-expression reversed the  $\alpha$ -Syn-induced changes on autophagy turnover and EV release and ameliorated DAergic neuronal cell death. In accord with our results from cultured neurons, we found a stage-dependent reduction of SNAP29 in SNc DAergic neurons from human postmortem brain tissue of Lewy body pathology (LBP) cases. In summary, our results thus demonstrate a previously unknown effect of  $\alpha$ -Syn on intracellular autophagy-associated SNARE proteins and, as a consequence, a reduced autophagolysosome fusion.

---

As such, our findings will therefore support the investigation of autophagy-associated pathological changes in PD.

## List of figures

Figure 1 Schematic representation of nigrostriatal pathway and neuropathology of PD.....	19
Figure 2 Immunohistochemical labeling of Lewy bodies in a SNpc dopaminergic neuron. ....	20
Figure 3 Progression of PD-related intraneuronal pathology.....	22
Figure 4 Main types of autophagy. ....	24
Figure 5 Different types of EVs can be distinguished by their mechanism of generation and size.....	28
Figure 6 $\alpha$ -Syn overexpression activates mTOR associated signaling molecules.....	45
Figure 7 $\alpha$ -Syn overexpression impairs autophagy initiation and turnover.. ....	47
Figure 8 $\alpha$ -Syn overexpression attenuates autophagy turnover. ....	49
Figure 9 Both $\alpha$ -Syn overexpression and rapamycin treatment increase EVs release .....	51
Figure 10 Blocking autophagosome-lysosome fusion impairs autophagy turnover.....	52
Figure 11 Blocking autophagosome-lysosome fusion increases EVs release.....	54
Figure 12 EVs from $\alpha$ -Syn-transduced or bafilomycin A1 treated neurons carried an increased amount of the autophagy-associated proteins. ....	55
Figure 13 $\alpha$ -Syn overexpression reduces the abundance of SNAP29 in cultured human DA neurons. ....	57
Figure 14 Knocking down SNAP29 mimics the effect of $\alpha$ -Syn overexpression on autophagy turnover. ....	58
Figure 15 Knocking down SNAP29 mimics the effect of $\alpha$ -Syn overexpression on autophagosome-lysosome fusion.....	60
Figure 16 Knocking down SNAP29 mimics the effect of $\alpha$ -Syn overexpression on EVs release.....	61
Figure 17 SNAP29 co-expression rescues the $\alpha$ -Syn-induced impairment of autophagy turnover. ....	62

<b>Figure 18 SNAP29 co-expression rescues the <math>\alpha</math>-Syn-induced impairment of autophagosome-lysosome fusion.</b>	<b>63</b>
<b>Figure 19 <math>\alpha</math>-Syn overexpression induces cell death.</b>	<b>64</b>
<b>Figure 20 co-expressing SNAP29 in <math>\alpha</math>-Syn transduced neurons attenuated cellular death.</b>	<b>65</b>
<b>Figure 21 SNAP29 co-expression attenuated <math>\alpha</math>-Syn-induced increase on EVs release.</b>	<b>67</b>
<b>Figure 22 The computationally modelled tertiary structure of SNAP29 and <math>\alpha</math>-Syn.</b>	<b>69</b>
<b>Figure 23 Potential binding sites and complexes between SNAP29 and <math>\alpha</math>-Syn.</b>	<b>71</b>
<b>Figure 24 <math>\alpha</math>-Syn physically interacts with SNAP29 in cultured neurons.</b>	<b>72</b>
<b>Figure 25 The abundance of SNAP29 is stage-dependently decreased in neuromelanin-positive neurons from LBP cases.</b>	<b>74</b>

## List of tables

<b>Table 1 Genes and mutations implicated in heritable forms of PD.</b>	<b>18</b>
<b>Table 2 Rosetta scores and protein structure geometry evaluation scores of the SNAP29 models.</b>	<b>69</b>
<b>Table 3 The bioenergetic and biophysical characteristics of the indicated complexes between SNAP29 and <math>\alpha</math>-Syn.</b>	<b>71</b>



## List of abbreviations

$\alpha$ -Syn	alpha-Synuclein
AAVDJ/8	adenovirus-associated viruses serotype DJ/8
AMPK	AMP-activated protein kinase
AV5	adenoviruses serotype 5
BECN1	Beclin 1
CNRQ	Comparative normalized relative quantities
CNS	central nervous system
Co-IP	co-immunoprecipitation
CSF	cerebrospinal fluid
CT	cycle threshold
CTSD	cathepsin D
DAergic	dopaminergic
DBS	deep brain stimulation
Dibutyl cyclic-AMP	N6,2'-O-Dibutyladenosine 3',5'-cyclic monophosphate sodium salt
DLB	dementia with Lewy bodies
DMEM/F-12	Dulbecco's modified Eagle's medium/nutrient mixture F-12 Ham
DMV	dorsal motor nucleus of the vagus nerve
DPBS	Dulbecco's phosphate-buffered saline
ENS	enteric nervous system
ESCRT	endosomal sorting complex required for transport
EV	extracellular vesicle
GWAS	genome-wide association studies
HMGB1	high mobility group box 1
LB	Lewy body
LBP	Lewy body pathology
LDH	lactate dehydrogenase
LUHMES	Lund human mesencephalic
miRNA	microRNA
MOI	multiplicity of infection
MPTP	1-methyl-4-phenyl-1,2,3,6-tetrahydropyridine

---

mTORC1	mammalian target of rapamycin complex 1
MTT	5-diphenyltetrazolium bromide
MVB	multivesicular body
NTA	nanoparticle tracking analysis
PAS	phagophore assembly site
PD	Parkinson's disease
PDB	Protein Data Bank
PET	positron emission tomography
PKB, Akt	mTOR-activating protein kinase B
PLO	poly-L-ornithine solution
PPI	protein-protein interaction
PVDF	polyvinylidene difluoride
qRT-PCR	quantitative real-time PCR
Rab	Ras-related protein in brain
ROI	Regions of interest
RUBCN	Rubicon
S6K1	ribosomal protein S6 kinase
SAVES	Structure Analysis and Verification Server
SCAMP5	secretory membrane carrier protein 5
siRNA	small interfering RNA
SNARE	soluble N-ethylmaleimide sensitive factor attachment protein receptor
SNc	Substantia Nigra pars compacta
SQSTM1, p62	sequestosome 1
STX17	syntaxin17
TBST	Tris-buffered saline with 0.05 % (v/v) Tween20
TPPP, p25 $\alpha$	tubulin polymerization-promoting protein
ULK1	Unc-51 like autophagy activating kinase 1
UVRAG	UV radiation resistance associated gene
WB	Western blot

# 1. Introduction

## 1.1 Parkinson's disease

### 1.1.1 Clinical characterization

Parkinson's disease (PD), first described in 1817 by the English physician and pharmacist James Parkinson (1755-1824) in his "Essay on the Shaking Palsy", is the most common movement disorder and second most prevalent neurodegenerative diseases [1]. The prevalence of PD in the elderly aged over 65 years was 1.8%, which increased to up to 2.4% in those aged 65 – 69 and to 4.4% in those over 85 [2]. When it comes to young-onset PD, which affects 5–10% of patients, initial symptoms sometimes may arise between the age 21 and 40 (sometimes 50) years [3, 4].

The clinical features of PD can be divided into motor symptoms and non-motor symptoms [5]. The typical motor symptoms include resting tremor, muscular rigidity, bradykinesia, and postural instability [1], which are the result of dopaminergic (DAergic) neuron degeneration in the substantia nigra pars compacta (SNc). Among them, resting tremor is the most common symptom. Besides, some patients may suffer from other motor symptoms, such as gait and posture disturbance, reduced arm swing, hypomimia (facial masking), micrographia (cramped handwriting), and dystonia (sustained muscle contractions). On the other hand, PD patients also show a wide range of non-motor symptoms that contributes significantly to PD morbidity, especially in advanced stages of the disease. Mood disturbance is the most common non-motor symptom. A systematic review and meta-analysis including 21 studies found more than 20% of PD patients suffering from depression [6]. As the disease progresses, some patients develop cognitive dysfunction and eventually become demented. Whereas the diagnosis of PD is predominantly made clinically, functional neuroimaging of the nigrostriatal dopaminergic pathway

by positron emission tomography (PET, DaT Scan) may be helpful in uncertain cases or early during the disease course [7-9].

Since dopamine deficiency is the pathophysiological hallmark of PD's motor symptoms, the major treatment for PD are dopamine replacement therapies aiming at either temporarily replenishing dopamine or mimicking the action of dopamine. Dopamine replacement medication includes precursor levodopa, dopamine agonists, as well as medications interfering with different enzymatic steps of dopamine metabolism, nerve terminal release and re-uptake [10]. These current medications generally help alleviate muscle rigidity, ameliorate speed and coordination of movement, and reduce tremor, although their efficiency decreased over time, and none of them halts or retards the degeneration of DAergic neurons. In addition, when medical treatment options have been exhausted for tremor or the patient suffered profound motor fluctuations with standard medical treatment, deep brain stimulation (DBS) surgery may help to control the debilitating symptoms. However, similar to the abovementioned medication, DBS does not slow PD progression either. Therefore, a further understanding of the molecular and biochemical pathogenesis of PD is critical for the development of novel neuroprotective (to prevent cell death) or neuro-restorative (to repair neurons) therapies [11].

Like other neurodegenerative diseases, most PD cases occur sporadically. Most people (up to 90%) with PD do not have a family history of PD [12]. Except for the few patients who were exposed to 1-methyl-4-phenyl-1,2,3,6-tetrahydropyridine (MPTP) or have a known gene mutation, the cause of this disorder is unknown. Multiple factors likely contribute to PD, which include genetic susceptibility, environmental agents, and aging. For familial PD, the first gene found to link to familial disease is *PARK1* (HUGO-approved name *SNCA*) which codes the  $\alpha$ -Syn protein. Thereafter, several autosomal dominant or recessive Parkinsonism related genetic loci have been successfully discovered (**Table**

1). The identification of these loci associated with the heritable forms of PD was a breakthrough for the comprehensive understanding of the molecular mechanisms of this disease and the discovery of ways to treat and prevent PD.

Locus	Gene	Inheritance	Onset	Location	Variants	Function
PARK1/4	SNCA	Dominant Risk factor	EO	4q21.3-q22	5 point-mutations, multiplications Rep1 risk variant in the promoter	Synaptic vesicles trafficking
PARK2	PARKIN	Recessive	EO	6q25.2-q27	>250 point-mutations, ins/de and exon rearrangements	Mitophagy
PARK3	Unknown	Dominant	LO	2p13	?	?
PARK5	UCHL1	Dominant	LO	4p13	1 missense variant in one sibling pair	Proteasome
PARK6	PINK1	Recessive	EO	1p36.12	>100 point-mutations, ins/del and exon rearrangements	Mitophagy
PARK7	DJ-1	Recessive	EO	1p36.23	>20 point-mutations and deletions	Mitophagy
PARK8	LRRK2	Dominant Risk factor	LO	12q12	7 point-mutations, risk variants p.R1628P and p.G2385R	Autophagy?
PARK9	ATP13A2	Recessive	EO	1p36	>20 point-mutations	Lysosomes
PARK10	Unknown	Risk factor	?	1p32	?	?
PARK11	GIGYF2	Recessive	EO	2q36-7	7 missense variants	Insulin-like growth factors (IGFs) signaling
PARK12	Unknown	Risk factor	?	Xq21-q22	?	?
PARK13	HTRA2	Dominant	?	2p13.1	1 missense variant	Mitophagy,
PARK14	PLA2G6	Recessive	EO	22q13.1	>18 missense variants	Lipids metabolism
PARK15	FBXO7	Recessive	EO	22q12.3	4 point-mutations	Mitophagy
PARK16	Unknown	Risk factor	?	1q32	?	?
PARK17	VPS35	Dominant	LO	16q12	2 point-mutations	Endosomes
PARK18	EIF4G1	Dominant	LO	3q27.1	1 missense variant	Protein translation
PARK19	DNAJC6	Recessive	EO	1p31.3	9 missense variants	Endosomes

Locus	Gene	Inher- itance	On set	Location	Variants	Function
PARK20	SYNJ1	Recessive	EC	21q22.11	3 missense variants	Endosomes
PARK21	DNAJC13	Dominant	LO	3q22.1	1 missense variant	Endosomes
PARK22	CHCHD2	Dominant	LO/ EO	7p11.2	1 missense variant, 1 truncation	Mitochondria- mediated apoptosis and metabo- lism?
PARK23	VPS13C	Recessive	EO	15q22.2	2 missense variants, 1 truncation	Mitophagy
–	GBA	AD, AR in GD Risk factor	LO	1q22	>10 missense variants	Lysosomes
–	MAPT	Sporadic Risk factor		17q21.31	H1 haplotype increase PD risk and disease severity	Microtubules

**Table 1 Genes and mutations implicated in heritable forms of PD.** (From Del Rey et al., Front Neuroanat 2018 [13])

### 1.1.2 Neuropathological characteristics and the role of $\alpha$ -Syn in PD

Pathologically, PD is characterized by the demise of dopaminergic neurons in the SNc and the loss of nigrostriatal dopamine projections to the putamen, resulting in a striatal DA deficit (**Figure 1**). Apart from dopaminergic neurons, neuronal degeneration likewise occurs in the cholinergic, noradrenergic, and serotonergic systems of the brain. In addition, neuronal degeneration affects the olfactory bulb, cerebral cortex, and autonomic nervous system as well [14].

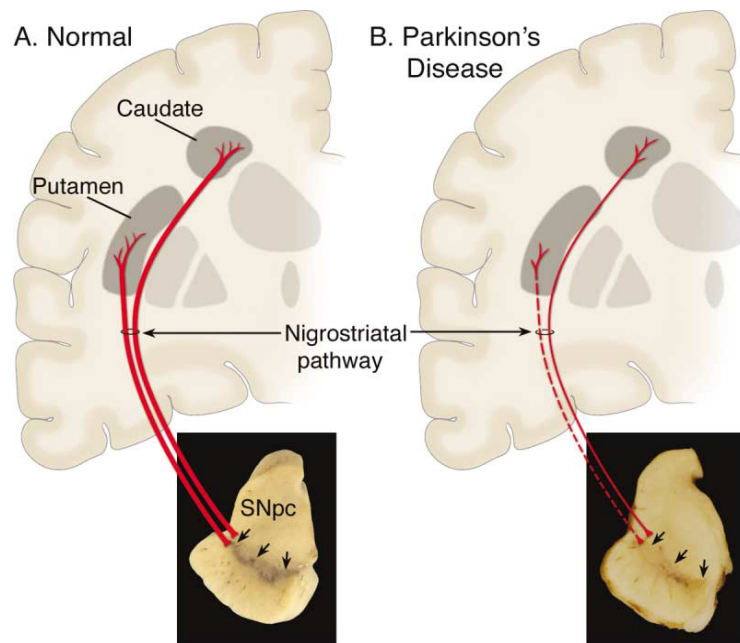


**Figure 1 Schematic representation of nigrostriatal pathway and neuropathology of PD.** **A** Normal nigrostriatal pathway is demonstrated in the red line. The photograph shows the normal pigmentation produced by neuromelanin within the dopaminergic neurons in SNpc. **B** The diseased pathway is demonstrated in the dashed red line. The photograph shows significantly reduced pigment neuromelanin due to degeneration of dopaminergic neurons. (From Dauer and Przedborski, *Neuron* 2003 [14])

Apart from the neuronal degeneration in PD, another specific neuropathological feature of PD is the concomitant existence of intracytoplasmic inclusion bodies. In 1912, Friedrich Heinrich Lewy first discovered these microscopic particles in PD brains, which were therefore later named “Lewy bodies” [15]. Lewy bodies (LBs) and Lewy neurites are the defining neuropathological characteristics of PD and dementia with Lewy bodies (DLB) [16, 17]. In PD, LBs are found in a wide variety of brain regions, including the substantia nigra, hypothalamus, nucleus basalis, locus ceruleus, cranial nerve motor nuclei, and cerebral cortex, as well as the central and peripheral autonomic nervous system[1, 18].

After the characterization of LBs in DA neurons, it took almost a whole century until  $\alpha$ -Synuclein ( $\alpha$ -Syn) was identified as one of the main protein components of LBs [16] (**Figure 2**). Human  $\alpha$ -Syn is encoded by the *SNCA* gene located on Chr 4: 89.7 - 89.84 Mb.  $\alpha$ -Syn is a 140-amino acids protein that is highly evolutionarily conserved and abundantly expressed in the nervous system of vertebrates, and predominantly localized at pre-synaptic terminals of neurons [19]. It is predominantly a neuronal protein expressed in the neocortex, substantia nigra, hippocampus, thalamus, and cerebellum, but can also be found in the neuroglial cells [20, 21]. Although this highly abundant presynaptic protein is involved in many biological processes [22], its exact function and mechanism of mediating toxicity remains unclear [23].

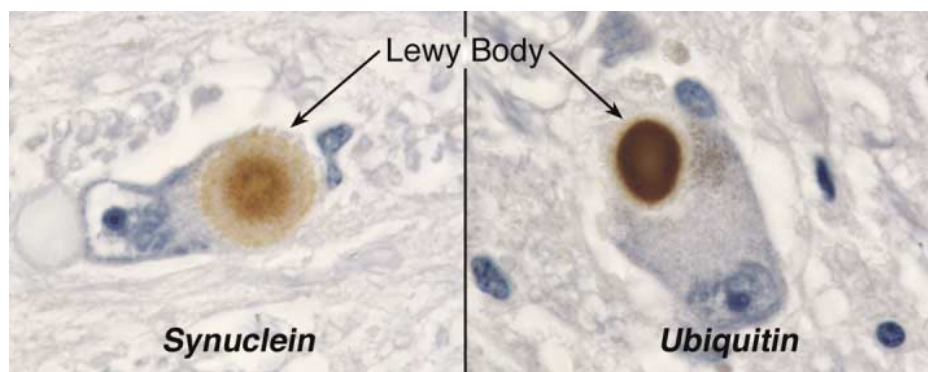


**Figure 2 Immunohistochemical labeling of Lewy bodies in a SNpc dopaminergic neuron.** Left: immunostaining with an  $\alpha$ -Syn antibody; right: immunostaining using an antibody against ubiquitin. (From Dauer and Przedborski, Neuron 2003 [14])

$\alpha$ -Syn is composed of an amphipathic N-terminus, an acidic C-terminus, and a hydrophobic central domain which was reported to be responsible for its oligomerization and fibrillization. Natively,  $\alpha$ -Syn is an unfolded protein that is soluble[24]. *In vitro*,  $\alpha$ -Syn has an intrinsic propensity to self-assemble into aggregates. Small aggregates (oligomers) of  $\alpha$ -Syn are demonstrated to cause cell toxicity in several ways, fundamentally including binding to lipid vesicles and affecting the electrophysiological properties of lipid bilayers, as well as interacting with membrane bound proteins [25, 26]. Several factors render  $\alpha$ -



Syn more prone to misfolding and aggregation according to literature. The factors include duplication and triplication of the locus, as well as missense mutations (e.g., A53T, A30P, E46K, and H50Q) [27-30]. Notably, all these factors have been reported as contributors to PD development [18, 31-33]. This connection between genetics and pathology suggests that the altered  $\alpha$ -Syn proteins in PD patients with genetic abnormalities may promote PD pathological processes, including  $\alpha$ -Syn aggregation, LBs formation, and neurotoxicity [16, 18, 34]. Besides, the post-translational modification of  $\alpha$ -Syn phosphorylation, which occurs predominantly at serine residues S129 [35], was reported to play a role in  $\alpha$ -Syn aggregation. For instance, in dementia with DLB brains, approximately 90% of insoluble  $\alpha$ -Syn is phosphorylated at S129, while the percentage for soluble cytosolic  $\alpha$ -Syn is only 4% [36]. Because of the limitation of appropriate model systems [37], the exact mechanism of LBs formation has not yet been comprehensively investigated. Baba et al. reported that the metabolisms that render  $\alpha$ -Syn insoluble and prone to aggregate may lead to the selective incorporation of  $\alpha$ -Syn into LBs [38]. These aggregates cause neuronal function disruption and result in the death of affected neurons as a long-term consequence [38].

### 1.1.3 The development of PD and $\alpha$ -Syn propagating hypothesis

As mentioned above, PD is a progressive disease with continuously deteriorating motor symptoms. Braak et al. found the pathology process in an ascending course with little interindividual variation by analyzing post mortem brain tissue from pre-symptomatic persons (possible exception: loss of smell) with LBs and PD patients at different stages.[39]. In stages 1 and 2, LBs are mainly restricted to the dorsal IX/X motor nucleus and/or intermediate reticular zone (stage 1), and additionally to the gigantocellular reticular nucleus, caudal raphe nuclei, and coeruleus–subcoeruleus complex (stage 2). In accord, Braak stage 1 and 2 is characterized by non-motor symptoms, such as loss of olfaction. In stage 3 and 4, pathology progresses to the lower and upper brain stem including the

SNc (stage 3) or with initial affection of the anteromedial temporal mesocortex (stage 4). Usually, the motor dysfunction is barely noticeable in stage 3 and begins to appear from stage 4. In stage 5 and 6, these changes become more pronounced as the previously mentioned damage in subcortical and mesocortical structures becomes more severe (**Figure 3**). In addition, several key neocortical areas are involved in the final two stages, therefore patients frequently display impaired cognition [40].

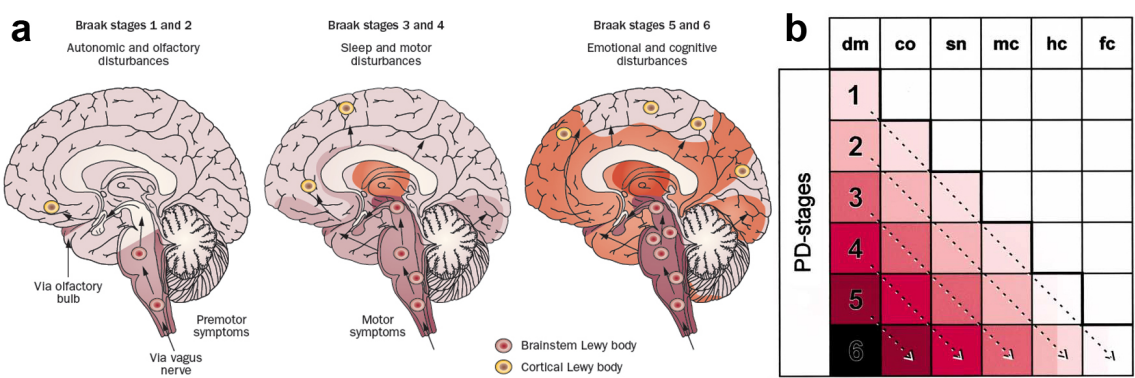


**Figure 3 Progression of PD-related intraneuronal pathology.** co, coeruleus–subcoeruleus complex; dm, dorsal motor nucleus of the glossopharyngeal and vagal nerves; fc, first order sensory association areas, premotor areas, as well as primary sensory and motor fields; hc, high order sensory association areas and prefrontal fields; mc, anteromedial temporal mesocortex; sn, substantia nigra. (**a** from Doty et al. Nat Rev Neurol 2012 [41], **b** from Braak et al., Neurobiol Aging 2003 [39].)

The ascending distribution of  $\alpha$ -Syn in patient brains has been interpreted as a result of  $\alpha$ -Syn propagating (‘spreading’) across connected brain regions. The spreading pattern of pathology following the disease progression was supported by the identification of LBs in transplanted midbrain neurons [42-44].

Besides, studies also found the earliest sporadic PD-related lesions within the nervous system in the enteric nervous system (ENS) [45]. Thus,  $\alpha$ -Syn aggregates are thought to be retrogradely transported to the preganglionic visceromotor neurons of the dorsal

motor nucleus from the intramural plexus of the ENS along the vagal nerve. The hypothesis is supported by results showing PD pathology spread from the gastrointestinal tract to the brain in animals, while vagotomy, on the other hand, halted the progression [46, 47]. Furthermore, an epidemiologic study showed individuals who had full truncal vagotomy have a significantly lower risk of developing sporadic PD than the general population, while the risk in persons with selective vagotomy, however, was not reduced [48].

All these results from previous studies suggest the transneuronal transmission of  $\alpha$ -Syn between vulnerable nerve cells to be a crucial factor in the development of PD, thus emphasizing the need to further understand the molecular mechanism of  $\alpha$ -Syn transmission for the development of effective therapy that halts disease progression.

## 1.2 Autophagy

### 1.2.1 The initiation and regulation of autophagy

Cells need to adapt to continuously changing environmental conditions, and respond to endogenous as well as a variety of exogenous stress, requiring a continuous remodeling and recycling of intracellular proteins and organelles. Eukaryotic cells, therefore, apply two major degradation systems, the lysosome, and the proteasome. Autophagy is a transport pathway, which delivers cellular components to the lysosome for degradation. Autophagy, coming from the ancient Greek “auto”-on self and “phagy”-to eat, was first discovered by Christian De Duve who also invented the term in the 1960s [49]. Autophagy is crucial for cell survival since it maintains cellular homeostasis and helps to get rid of toxic protein aggregates and pathogens. Thus, autophagy defects are associated with a wide variety of diseases, including cancer, metabolic diseases, neurodegenerative diseases, etc. [50]. Three kinds of autophagy have been described to date: macroautophagy, microautophagy, and chaperone-mediated autophagy (**Figure 4**). Macroautophagy,

the best-characterized form of autophagy, is an evolutionarily conserved process for cytosolic proteins degradation, in which the double membrane sequestered vesicles are delivered to lysosomes. In this research, the focus was placed on macroautophagy and hereafter referred to as autophagy.

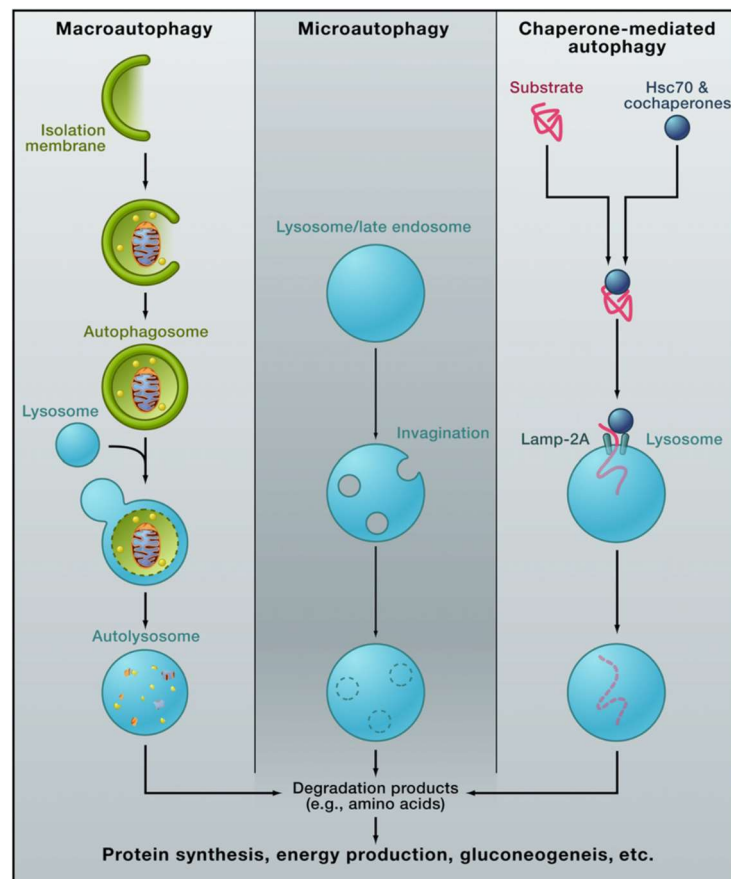


**Figure 4 Main types of autophagy.** (From Mizushima and Komatsu, Cell 2011 [51])

Autophagy occurs at a low basal level in almost all cell types under inhibition of autophagy regulators to maintain cellular homeostasis [52]. Upon induction of autophagy, small autophagy-specific vesicles (Atg9 positive membrane vesicles) fuse at the site of autophagosome biogenesis. Once the first small vesicles are fused at the phagophore assembly site (PAS) to form a phagophore, this cup-shaped membrane elongates and engulfs

cytoplasmic constituents including organelles and aggregated proteins to form an autophagosome. At last, the autophagosome will close up and fuse with the lysosome to deliver the inner membrane sac and the cargo for degradation.

The fusion process is controlled by small GTPases of the Ras-related protein in brain (Rab) family and other co-factors including membrane-tethering factors (HOPS, ATG14) and regulatory molecules (RILP, TECPR1, BRUCE, PLEKHM1, Pacer) [53-56]. Like any membrane fusion event, the fusion of the outer membrane of the matured autophagosome with the lysosome needs the mediation of soluble N-ethylmaleimide sensitive factor attachment protein receptors (SNAREs). SNARE proteins drive the two opposing membranes to fuse by a zipper-like mechanism, which involves the formation of a four-helix bundle of a Qa-, Qb, Qc, and R-SNARE. Previous studies reported the SNARE syntaxin17 (STX17) to be recruited to the autophagosome by direct interaction with Atg14 homo-oligomers [57]. The SNARE STX17 and SNAP-29 on the autophagosome, then interact with the R-SNARE VAMP8 on the lysosomal membrane to mediate the fusion [58]. Upon the fusion of autophagosome and lysosome, the contents and the inner membrane are degraded rapidly by lysosomal proteases.

### **1.2.2 Autophagy as a hub for protein degradation and secretion**

From the outside, cells take up soluble molecules, receptor-associated ligands, and membrane components, which is called endocytosis. Initially, vesicles containing extracellular material or plasma membrane proteins form at the plasma membrane. The budding endocytic vesicles first merge together to form an early endosome, and the cargo is immediately sorted out either for recycling or to be degraded. Thereafter, the early endosomes are transported towards the cell center, accompanied by a replacement of Rab5 by Rab7 as the key regulatory protein, and matured to become late endosomes. Late endosomal membranes invaginate and produce intraluminal vesicles, therefore also

called multivesicular bodies (MVBs). The MVBs are either delivered to lysosomes for cargo degradation or fuse with the plasma membrane for content release.

Notably, complete autophagosomes were found to fuse either directly with lysosomes or first with early/late endosomes to form amphisomes. Conventionally, amphisomes are degraded upon fusion with lysosomes. Interestingly, in contrast to degradative autophagy, the autophagic machinery may lead to a secretion of the intraluminal vesicles as extracellular vesicles (EVs) instead of their degradation. The mechanism and biological functions are different, but cells may dispose of cytoplasmic materials either way. The autophagosome-lysosome system thus connects endosomal, secretory, and lysosomal pathways [59, 60]. In this way, it acts as a major hub for cargo recycling, secretion, or degradation [61-64], although the mechanism of how autophagosomes interact with the endosomal system is still to be investigated.

Since impaired autophagy is associated with PD pathology, and evidence shows EVs might mediate the transmission of  $\alpha$ -Syn and thus promote PD progression (see 1.3.2), further investigation aiming at elucidating the effect of impaired autophagy on EVs release and the underlying molecular mechanism will contribute to antagonize the progression of the PD.

### **1.2.3 The connection between autophagy defects and PD pathology**

Autophagy is known to be involved in the change of cellular homeostasis of the aging organism. One characteristic of aging is the accumulation of ubiquitinated protein aggregates. As mentioned above, the histological hallmark of PD are LBs, mainly composed of aggregated  $\alpha$ -Syn. In addition, comprehensive analyses of protein elements in LBs showed that, LBs consist of molecules implicated in the autophagy, indicating autophagy

defects to play a role in disease progression[65, 66]. Consistently, a wide variety of familial forms of PD are related with a broad range of gene mutations, most of which are associated with autophagy-lysosome pathway (**Table 1**).

Furthermore, evidence suggests  $\alpha$ -Syn to impair autophagic protein degradation in PD. For instance,  $\alpha$ -Syn was found to interact with autophagy related factors, while autophagy defects could be corrected by normalization of affected factors or signaling pathway [64, 67, 68]. Furthermore, several studies showed restoration of impaired autophagy rescues neurons from experimental synucleinopathies [69-71]. Conversely, the effect of deficiency in autophagy in turn exacerbates  $\alpha$ -Syn pathology thus forming a bidirectional pathogenic loop [62, 72-75]. Taken together, these results functionally connect impaired autophagy and PD pathology, and investigating the effect of  $\alpha$ -Syn on the autophagy will therefore support the understanding of cell death and disease progression in PD.

## 1.3 Extracellular vesicles

### 1.3.1 The biogenesis and biochemical composition of EVs

EVs are small globular particles encircled by a lipid bilayer with different diameters (from 40 nm to a few  $\mu$ m), released by almost all cells ranging from prokaryotes to eukaryotes. They are widely distributed and can be detected in a wide variety of body fluids. Among the different types of EVs, there are the exosomes (40-120 nm) that are generated via the endo-lysosomal pathway and are released upon the fusion of MVBs with the plasma membrane, microvesicles (0.1-1  $\mu$ m) formed by outward blebbing of the plasma membrane, and apoptotic bodies (1-3  $\mu$ m) released by cells undergoing apoptosis. In addition, evidence showed some cancer cells can generate 1–10  $\mu$ m EVs which are termed oncosomes (**Figure 5**). The collective term “extracellular vesicles” is recommended for this

cell released vesicle population, as the current EV isolation methods are not able to separate these subpopulations distinctly.

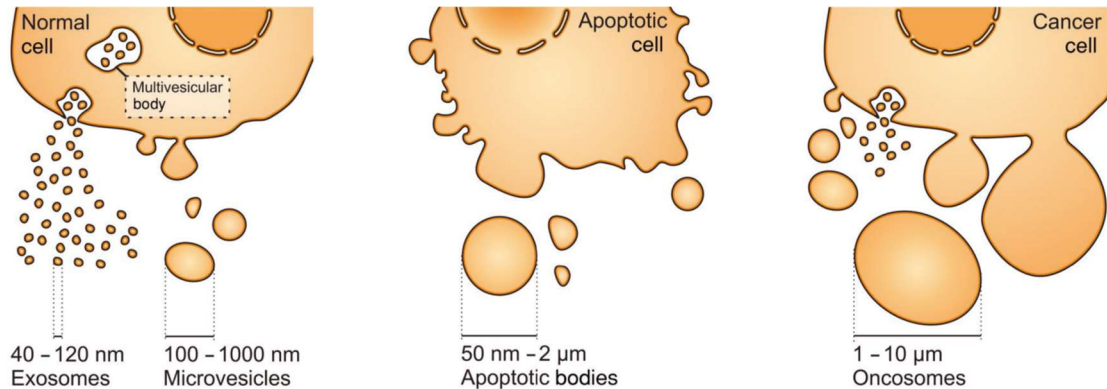


**Figure 5 Different types of EVs can be distinguished by their mechanism of generation and size.** (From Zaborowski et al., Bioscience 2015 [76])

The content of EVs includes lipids, DNA, RNA, and proteins. While the EVs composition is associated with the mode of biogenesis and donor cell type, studies on EV-carried proteins revealed a set of conserved proteins in most cell types, which including proteins involved in the formation of MVBs (e.g., TSG101 and Alix), endosome-related proteins (e.g., Rab GTPases, flotillin, and SNAREs), and tetraspanins (e.g., CD9, CD63, and CD81) [77, 78]. The conserved expression of these proteins permits their use as markers for the quantification of EVs. A breakthrough in EV research was, apart from proteins, EVs carry nucleic acids. Most RNA transported by EVs is less than 200 nucleotides [nt], which is shorter than the average cellular fraction [79, 80]. Sequencing of total RNA from serum-derived EVs detected both coding and non-coding RNA, among which microRNAs (miRNAs) were the most abundant. Evidence showed EVs carried miRNAs may regulate the translation of target mRNAs in recipient cells [81], which later was confirmed also *in vivo* [82].



For a long time, EVs were considered to be cellular “garbage bags” helping cells to discard unnecessary protein until evidence showed they play an important role in mediating cell-to-cell communication [83, 84].

Today the features of EVs still need further investigation, but there is no doubt that they act as important messengers in intercellular communication, mediating a wide variety of biological effects in neurodegenerative disease, immune response, and tumor growth and metastasis, etc. The presence of EVs in cerebrospinal fluid (CSF) further underscores their implication in the central nervous system (CNS) [85]. For example, evidence suggested EVs support neuronal survival under ischemic stress [86-88], and play a role in neuroinflammation and under conditions of brain injury [89, 90].

### **1.3.2 Aggregated $\alpha$ -Syn transmission may be mediated by EVs**

Aggregated  $\alpha$ -Syn likely contributes to the demise of DAergic neurons [18, 31, 32, 91, 92], and the cell-to-cell transmission of aggregated  $\alpha$ -Syn (“spreading”) is assumed to promote the progression of pathology throughout the nervous system in PD [93-96]. Evidence showed stress conditions or degenerating processes enable neurons to release  $\alpha$ -Syn toxic species, which contribute to the spreading of the pathology [97, 98]. In line with the prion-like spreading hypothesis [99], their implication in the cell-to-cell transmission of aggregated  $\alpha$ -Syn in PD is increasingly being recognized.

The ability of EVs to carry misfolded or aggregated proteins might promote the progression of neurodegenerative diseases. Similar to other neurodegenerative conditions [100-103], aggregated  $\alpha$ -Syn transmission may be mediated by small EVs including exosomes [104]. According to a previous study,  $\alpha$ -Syn is related to the MVB compartment at an ultrastructural level [105]. And MVB resident protein ATPase13A2 was found to regulate  $\alpha$ -Syn EV release [106]. Besides,  $\alpha$ -Syn was identified in exosomes in vitro  $\alpha$ -

Syn overexpression models [107-109], and particularly noteworthy, in human cerebrospinal fluid (CSF) [107, 110]. A study on DLB revealed a correlated  $\alpha$ -Syn level in CSF with the severity of cognitive impairment [110]. Furthermore, evidence showed exosomes in PD- and DLB-derived CSF induce oligomerized forms of  $\alpha$ -Syn in a reporter cell line [110]. Further understanding of EVs mediated aggregated  $\alpha$ -Syn transmission will not only help to establish an efficient biomarker for early diagnosis or prognosis of  $\alpha$ -Syn-related neurodegenerative disorders but also will provide further insight into the prevention of disease development.

## 1.4 Aim of the study

Autophagy is a critical process as it maintains cellular homeostasis and recycles damaged organelles. The perturbation of the the autophagolysosomal system has been implemented in the onset and progression of neurodegenerative diseases. Autophagy-related molecules are associated with PD pathology, and deficiency in autophagic degradation exacerbates  $\alpha$ -Syn pathology. Conversely, accumulated  $\alpha$ -Syn aggregates were shown to defect autophagy and thus forms a bidirectional pathogenic loop. Taken together, these findings functionally link autophagy and PD pathology. Therefore, the motivation of my study was to investigate how  $\alpha$ -Syn affects autophagy mechanistically and in which way it influences disease progression in PD, which will help to understand cell death and disease progression in PD .

The **first aim** of this study was to identify which specific steps of autophagy are affected by  $\alpha$ -Syn in dopaminergic neurons.

The **second aim** addressed how EV release changes upon  $\alpha$ -Syn impaired autophagy in DA neurons mechanistically.

---

The ***third aim*** of the study was to investigate whether the above results have a disease-relevant implication and are replicated in SNc DAergic neurons from human postmortem brain tissue of LBP cases.

Taken together, a more nuanced understanding of  $\alpha$ -Syn impaired autophagy and the knowledge of the connection between autophagy and EVs release will contribute to the development of future therapy against the progression of PD.

## **2. Methods**

### **2.1 Cell biology**

To study the effect of  $\alpha$ -Syn overexpression in autophagy and EV release, we used the Lund human mesencephalic (LUHMES) cell line which is derived and immortalized from embryonic human mesencephalon. Adenoviruses were used to achieve  $\alpha$ -Syn overexpression, while adenovirus-associated viruses and small interfering RNAs (siRNA) were applied to modulate SNAP29. We performed lactate dehydrogenase (LDH) assay and 5-diphenyltetrazolium bromide (MTT) assay to evaluate cell viability, and carried out LC3B-GFP-RFP autophagy reporter assay to address the autophagosome-lysosome fusing process.

#### **2.1.1 Cell culture**

Proliferating LUHMES cells were maintained in Thermo Scientific™ Nunc™ EasYFlask™ Cell Culture Flasks, while differentiated LUHMES cells were plated in Thermo Scientific™ Nunc™ Cell-Culture Dishes/Multidishes (Thermo Fisher Scientific). Proliferating and differentiated LUHMES cells were cultured at 37 °C with 5 % CO<sub>2</sub> and water-saturated air.

Before plating the cells for proliferating and differentiation, tissue culture vessels were coated with 0.1 mg/mL poly-L-ornithine solution (PLO, Sigma-Aldrich) at 37 °C for 24 hours, followed by three times washing with Dulbecco's phosphate-buffered saline (DPBS, Sigma-Aldrich). As for cell differentiation, cell culture vessels were further coated with 5 µg/ml bovine fibronectin (Sigma-Aldrich) at 37°C for 24h in addition.

The proliferation medium consisted of Dulbecco's modified Eagle's medium/nutrient mixture F-12 Ham (DMEM/F-12, Sigma-Aldrich) with 1% N-2 supplement (Life Technologies) and 0.04 µg/ml recombinant human FGF-basic (Peprotech). The differentiation medium consisted of DMEM/F-12 supplemented with 1% N-2 supplement, 1 µg/ml tetracycline (Sigma-Aldrich), 0.5 µg/ml N6,2'-O-Dibutyryl adenosine 3',5'-cyclic monophosphate sodium salt (Dibutyryl cyclic-AMP, Sigma-Aldrich), and 2 ng/mL recombinant human GDNF (Bio-Techne).

For differentiation, unless stated otherwise, the cells were seeded at a density of 100,000 cells/cm<sup>2</sup> to achieve a final confluence of ~ 50%, and differentiated for 6 days in differentiation medium into post-mitotic neurons with a dopaminergic phenotype [111, 112].

In order to achieve viral overexpression of α-Syn or GFP as a control, adenoviruses serotype 5 (AV5)-α-Syn or AV5-GFP at a multiplicity of infection (MOI) of 2.15 were added to the cell culture medium 24 h after plating as described previously [12]. As for SNAP29 overexpressing experiments, adenovirus-associated viruses serotype DJ/8 (AAVDJ/8)-SNAP29 or AAVDJ/8-GFP at an MOI of 4000 were added 6 h after AV5-α-Syn application. After the virus application, the cells were incubated for 24 h. Thereafter, virus medium was removed and cells were washed three times with DPBS before fresh differentiation medium was added.

Cell culture medium was changed 24 h before harvesting on day 6 of differentiation. For rapamycin or bafilomycin A1 (both Sigma-Aldrich) treatment, the compound was dissolved in DMSO and added to cells at a final concentration of 100nM after the medium change. The same volume of DMSO was added to cells as a control. The final concentration of DMSO < 0.1% (v/v).

### 2.1.2 Small interfering RNA transfection

LUHMES cells were knocked-down for SNAP29 by using siRNA. For that, a magnetic nanoparticle transfection kit (NeuroMag Starting Kit, OZ Biosciences) and Silencer Select siRNAs™ targeting SNAP29 (siRNA ID: s17859, Thermo Fisher Scientific) was used according to the manufacturer's instructions. In brief, SNAP29 siRNA or Silencer™ Select Negative Control No. 1 siRNA (# 4390843) was incubated with NeuroMag reagent in Optimum medium (Thermo Fisher Scientific) for 15 min at room temperature before the mixture was added to the cells. Thereafter, cell culture vessels were put back in the incubator, and placed on a magnetic plate for 30 min to allow transfection.

### 2.1.3 LDH assay and MTT assay

Cell death in cultured dopaminergic neurons was quantified using LDH assay and MTT assay on day 6 of differentiation. LUHMES cells were seeded in 300 µL differentiation medium per well in 48-well plates, followed by virus transduction and/or rapamycin treatment as described above.

For LDH assay, 30 µL of medium of each well was transferred to a 96 well plate and 70 µL of 80 mM Tris/HCl / 200 mM NaCl (pH 7.2) buffer containing 10 mM NADH and 100 mM pyruvate (Sigma-Aldrich) was added. The absorption of NADH at 340 nm was monitored with a reference measurement at 420 nm using a microplate reader (ClarioStar, BMG labtech, Ortenburg, Germany). For the positive control, cells were lysed using Triton™ X-100 (Sigma-Aldrich) for maximal LDH release. The percentage of LDH release was calculated by taking the ratio of LDH released into the supernatant to the total LDH in the supernatant and the cell lysate.

For MTT assay, 30 µL MTT (5 mg/ml in sterile DPBS) was added to each well and incubated back in the incubator for 1 h. After careful removal of the medium, the plate was

frozen at -80 °C for 1 h. Thereafter, 300µL of DMSO was added to each well and the plate was put on a plate shaker to homogenize. After the violet crystals are dissolved, the absorption at 590 nm was monitored with a reference measurement at 630 nm using a microplate reader (ClarioStar, BMG labtech, Ortenburg, Germany).

#### **2.1.4 LC3B-GFP-RFP autophagy reporter assay**

The RFP-GFP-LC3B fusion protein was expressed in LUHMES cells using BacMam 2.0 RFP-GFP-LC3B reagent from Premo™ Autophagy Tandem Sensor RFP-GFP-LC3B Kit (Thermo Fisher Scientific). This tandem RFP-GFP sensor capitalizes on the pH difference between the acidic autolysosome and the neutral autophagosome, and the exhibited green/red (yellow) or red fluorescence enables the visualization of the autophagosome to autolysosome progression.

LUHMES cells were plated and grown on PLO and fibronectin-coated µ-Slide 8-Well Ibidi chambers (Ibidi) and were transduced and treated as described above. Baculoviral infection was performed on day 4 of differentiation according to the manufacturer's instructions. The cells were fixed using 4% formaldehyde for 20 min at room temperature on day 6 of differentiation. Pictures were captured under a Leica SP5 confocal microscope (Leica, Wetzlar, Germany). Images were processed and GFP or RFP dots counts were carried out using the open-source image analysis platform FIJI (<http://fiji.sc/Fiji>). More than 25 cells were analyzed for each condition. The average number of GFP or RFP dots per cell was determined.

## **2.2 Molecular biology**

To investigate the transcriptional level of SNAP29 upon  $\alpha$ -Syn overexpression, total RNA was extracted from cells and reverse transcription was performed. cDNAs were thereafter subjected to real-time PCR to determine mRNA expression.

### **2.2.1 RNA extraction and reverse transcription**

For total RNA extraction, an RNeasy Plus Kit was used according to the manufacturer's protocol (Qiagen). In brief, the cell culture medium was removed and cells were washed with DPBS before 350  $\mu$ L of Buffer RLT Plus were added to the cells. The cell lysate was transferred into a microcentrifuge tube and homogenized by vortexing for 30 s, followed by centrifugation for 30 s at 8000 x g in a gDNA Eliminator spin column. The flow-through was mixed with 350  $\mu$ L of 70% ethanol, transferred to an RNeasy spin column, and centrifuged for 15 s at 8000 x g. Thereafter, the column was washed by adding 700  $\mu$ L of Buffer RW1 to the column, followed by another centrifugation for 15 s at 8000 x g. Subsequently, the column was washed twice with 500  $\mu$ L of Buffer RPE by centrifugation at 8000 x g, for 15 s and 2 min, respectively. The RNeasy spin column was placed in a new 2 ml collection tube and the membrane was dried by centrifugation at full speed for 1 min. After supplying a new 1.5 mL collection tube, RNA was eluted by adding 30  $\mu$ L of RNase-free water directly to the spin column membrane and centrifugation for 1 min at 8000 x g. Total RNA concentration was quantified using a Nanodrop 2000 spectrophotometer (NanoDrop).

Reverse transcription was performed using an iScript™ cDNA Synthesis Kit (Bio-Rad Laboratories). For each reverse transcription extraction, 1  $\mu$ g extracted RNA, 10  $\mu$ L iScript Reaction Mix, and 2ul iScript Reverse Transcriptase were used. The reaction was



performed using the following protocol: 5 min at 25 °C, 20 min at 46 °C, and 1 min at 95 °C.

### 2.2.2 Real time PCR

Gene expression of SNAP29 was validated using semi-quantitative real-time PCR (qRT-PCR) in a Step One Plus instrument (Thermo Fisher Scientific). For qRT-PCR analysis, SYBR™ Select Master Mix (Thermo Fisher Scientific), 2.5 ng complementary DNA from total RNA, and 0.2 µM forward and reverse primers were used. The PCR primer sequences are listed in **Appendix B**. The reaction was performed according to the following protocol: 2 min at 50 °C, 2 min at 95 °C, and 40 cycles of 15 seconds at 95 °C and 60 seconds at 60 °C. The melting curves were recorded, and the cycle threshold (CT) values were set within the exponential phase of the PCR. Four housekeeping genes (ACTB, GAPDH, GPBP1, and RPL22) were tested in total, and two of them (GPBP1 and RPL22) was used for data normalization according to geNorm analysis. Comparative normalized relative quantities (CNRQ) were used to calculate the relative expression levels using qBase Plus software (Biogazelle). Gene expression was statistically evaluated by two-tailed Student's t-test on the assumption of equal variances.

## 2.3 Protein biochemistry

The expression of target proteins was studied using Western blot (WB) and florescent immunohistochemistry. Co-immunoprecipitation (Co-IP) experiment was conducted to study the physical protein-protein interaction between  $\alpha$ -Syn and SNAP29. Before WB and Co-IP, total protein extraction and BCA Assay was performed.

### **2.3.1 Protein extraction**

For total protein extraction from LUHMES cells or EVs enriched medium pellets, bio-material was lysed in pre-chilled RIPA buffer freshly supplemented with protease and phosphatase inhibitors (Complete™ Protease Inhibitor Cocktail, PhosStop™ Phosphatase Inhibitor Cocktail, both Roche). The lysates were incubated for 30 min on ice and centrifuged at 13000 x g for 15 min at 4 °C. The supernatants were obtained and subjected to the following experiments.

### **2.3.2 BCA assay**

BCA Assay was performed to evaluate total protein concentration by using a Pierce™ BCA Protein Assay Kit (Thermo Fisher Scientific) according to the manufacturer's instructions. Briefly, a BCA working solution was prepared by mixing 50 volume of Reagent A and 1 volume of Reagent B together. Thereafter, the BCA working solution was thoroughly mixed with a sample and incubated for 30 min at 60°C. The optical density was measured at 562 nm using a Nanodrop 2000 spectrophotometer (NanoDrop).

### **2.3.3 Western blot**

Total protein concentration was normalized according to BCA assay prior to WB unless stated otherwise. Thereafter, samples were denatured by heating to 95 °C for 5 min in Laemmli sample buffer containing 10 %  $\beta$ -mercaptoethanol, and run on AnyKD™ Criterion™ TGX™ precast gels (Bio-Rad Laboratories) with tris-glycine-based running buffer. Proteins were transferred from polyacrylamide gels onto polyvinylidene difluoride (PVDF) membranes using a semi-dry transfer system (Trans-Blot® Turbo™ System, Bio-Rad). Non-specific binding sites were blocked with 5 % (w/v) skimmed milk in Tris-buffered saline with 0.05 % (v/v) Tween20 (TBST) for 1 h and the membrane was incubated at 4 °C overnight under gentle shaking with the primary antibody in TBST with 5 % (w/v)

BSA (Cell Signaling Technology). The membrane was washed and incubated with the respective HRP-conjugated secondary antibody (Vector Labs) in TBST for 2 h at room temperature.

The protein bands were detected by using Clarity™ Western ECL Substrate Kit (Bio-Rad Laboratories) or ECL Prime™ (GE Healthcare), and LI-COR Odyssey® Fc Imaging system (LI-COR Biosciences). Band intensities were quantified using Image Studio™ software (LI-COR Biosciences). For proteins of interest, band intensities were normalized to the housekeeping protein GAPDH. All antibodies used for Western blot are listed in **Appendix C**.

### 2.3.4 Co-Immunoprecipitation

Co-IP assays were performed using a Pierce™ Co-Immunoprecipitation Kit (Thermo Scientific) following the manufacturer's instructions with subtle modifications.

Formaldehyde in-cell crosslinking was performed prior to co-immunoprecipitation. Formaldehyde is a mild and reversible crosslinker with a very short spacer length (2.3–2.7 Å) and cross-links only closely associated proteins[113]. Cells were washed once with DPBS before incubated with 1% (w/v) formaldehyde in DPBS for 20 min at room temperature. Thereafter, 1/10 volume of 1.25M glycine was added to quench cross-linking for 5 min. The cells were washed twice with Modified Dulbecco's PBS (0.008M sodium phosphate, 0.002M potassium phosphate, 0.14M sodium chloride, and 0.01M KCl; pH 7) and subsequently lysed with pre-chilled IP Lysis/Wash Buffer (0.025M Tris, 0.15M NaCl, 0.001M EDTA, 1% NP-40, 5% glycerol; pH 7.4) freshly supplemented with protease and phosphatase inhibitors (Complete™ Protease Inhibitor Cocktail, PhosStop™ Phosphatase Inhibitor Cocktail, both Roche). The lysates were incubated for 30 min on ice and centrifuged at 13000 x g for 15 min at 4 °C, and supernatants were obtained and the total protein concentrations were normalized according to BCA assay.

For each sample, 50  $\mu$ L AminoLink Plus Coupling Resin slurry was transferred to Pierce Spin Columns and incubated with 10  $\mu$ L of anti-SNAP29 antibody (Abcam) for 2.5 h on a rotator at room temperature for antibody immobilization. For the negative control, Pierce Control Agarose Resin was used in the same conditions. After antibody immobilization, 500  $\mu$ g of the lysate's proteins were diluted with IP Lysis/Wash Buffer to a final volume of 500  $\mu$ L per column and incubated with the resins on a rotator for 6 h at 4 °C. The resin was washed with Modified Dulbecco's PBS according to the manufacturer's instructions. Thereafter, 40  $\mu$ L of the elution buffer was passed through each resin to elute SNAP29 together with its associated-proteins. For protein denaturalization, the 5X sample buffer containing 10 %  $\beta$ -mercaptoethanol was added to eluted fractions which were subsequently heated at 95 °C for 5 min. Finally, Co-IP fractions as well as the input fractions were subjected to Western blot analysis for SNAP29 and  $\alpha$ -Syn detection.

### **2.3.5 Florescent immunohistochemistry**

Human brain slices were provided with approval from Ludwig Maximilian University ethics commission by the Munich Brain Bank, Department of Neuropathology, Ludwig Maximilian University Munich. The selected cases were staged by a trained neuropathologist according to the presence of LBs in the dorsal motor nucleus of the vagus nerve (DMV), locus coeruleus, the SN and the cortex.

Human SNc sections were deparaffinized in xylene and rehydrated in graded ethanol series. Antigen retrieval was performed by incubating the slices with 10  $\mu$ g/ml proteinase K (Qiagen) in TE buffer (pH = 8) for 15 min at 37 °C. The sections were subsequently blocked in 5 % normal serum (Vector Laboratories) for 1 h at room temperature, followed by incubating with anti-SNAP29 primary antibody (R&D Systems) overnight at 4 °C in a humidified chamber. Thereafter, tissue sections were washed with PBS and incubated with anti-mouse biotinylated secondary antibodies (Vector Laboratories) for 2 h at room

temperature. After washing with PBS, the sections were incubated with ABC solution (ABC kit, Vector) for 1 h, and subsequently with 10  $\mu$ M biotinylated tyramide containing 0.005 % Hydrogen peroxide for 20 min for signal amplification[114]. The sections were subsequently incubated with Alexa Fluor™ 488-conjugated streptavidin (Invitrogen) for 2 h. Finally, nuclei were stained with DAPI for 10 min followed by washing and mounting with Fluoroshield™ mounting medium (Sigma-Aldrich).

All images were captured using a Leica SP5 confocal microscope with the same setting and analyzed using the open-source image analysis platform FIJI (<http://fiji.sc/Fiji>). Regions of interest (ROI) of neuromelanin-positive cells were selected manually based on both the brightfield channel and green channel, and the mean SNAP29 fluorescent intensity was quantified. The background fluorescent intensity of SNAP29 in each field was acquired and subtracted from corresponding cell fluorescent intensity for normalization. At least three fields or 30 cells were used for analysis for each case. The average SNAP29 intensity per case was determined. All antibodies used are listed in **Appendix C**.

## 2.4 Extracellular vesicle isolation

To prepare EV-enriched pellets from cell culture medium, the medium was changed at day 5 of differentiation and was harvested after 24 h. EVs were isolated by differential ultracentrifugation. The cell culture medium was first centrifuged at 300 x g for 10 min at 4 °C to pellet cells. The supernatant was then centrifuged at 2000 x g for 10mins and at 10000 x g for 30mins. The supernatant was subsequently transferred to ultracentrifuge tubes and centrifuged twice in a TLA-55 rotor (Beckman) at 100000 x g for 90 min at 4 °C. The supernatant was removed and the pellet was resuspended with DPBS between the two ultra-centrifugations. After centrifugation, the supernatant was discarded, and the pellet was lysed in an equal volume of pre-chilled RIPA buffer supplemented with

protease inhibitors for further Western blot analysis. For autophagy markers blots, the total protein concentration of the lysates was normalized according to BCA assay, while for EV quantification, the lysates were directly subjected to EV markers blots.

## 2.5 Nanoparticle tracking analysis

For EV size distribution profiles and EV quantification, nanoparticle tracking analysis (NTA) was carried out using a NanoSight LM10 system (Malvern), which analyses particle size based on Brownian motion. Cell culture medium was changed at day 5 of differentiation and was harvested after 24 h. For each sample, three 60-second videos were recorded. Replicate histograms were generated from the videos, using the NanoSight software 3.0 (Malvern), representing mean and confidence intervals of the three recordings for each sample.

## 2.6 Bioinformatics analysis

### 2.6.1 Three-dimensional structure prediction and validation

To simulate the protein interaction between SNAP29 with  $\alpha$ -Syn, the three-dimensional structure model of  $\alpha$ -Syn was obtained from the Protein Data Bank (PDB) database (DOI: 10.2210/pdb1XQ8/pdb [115], accessed on 03/08/2020).

The complete protein structure of the SNAP29 protein was not available in the PDB, thus the structure model of SNAP29 was computationally modeled using Robetta webserver [116] (<http://rosetta.bakerlab.org>), which predicted protein structure using the Rosetta ab initio and homology comparative modeling structure prediction methods [117, 118]. The sequence of SNAP29 used for the computation was retrieved from UniProt online database (<https://www.uniprot.org/uniprot/O95721>, accessed on 03/08/2020).

The predicted SNAP29 models were further optimized using PyRosetta FastRelax [119-123], and the returned full-atom relaxed structures were evaluated for protein geometry using PROCHECK (Ramachandran plot) [124], VERIFY 3D [125], and ERRAT [126] on the Structure Analysis and Verification Server (SAVES, <https://servicesn.mbi.ucla.edu/SAVES>), and ProSA-web [127, 128] (<https://prosa.services.came.sbg.ac.at/prosa.php>). The best SNAP29 model was selected based on the results of the abovementioned evaluations.

### 2.6.2 Protein docking simulation

Protein docking simulations were performed using the protein docking prediction server SwarmDock [129-131] (<https://bmm.crick.ac.uk/~svc-bmm-swarmdock/index.html>), which performed flexible modeling of SNAP29-a-Syn complexes using the SwarmDock algorithm which incorporates a normal modes approach. Properties and inference on probable SNAP29-a-Syn complexes assemblies were evaluated using jsPISA [132, 133] (<http://www.ccp4.ac.uk/pisa>). The structural figures were produced with an open-source version of Pymol (<https://github.com/schrodinger/pymol-open-source>).

## 2.7 Statistical analysis

Prism 7 (GraphPad Software) was used for statistical analysis and for creating line and bar graphs. Two datasets were compared by *t*-tests. When there were more than two datasets, assays with one variable with were compared by one-way ANOVAs with Tukey's or LSD post hoc test. Data are shown as mean  $\pm$  SEM.  $P < 0.05$  was considered to be significant.

### 3. Results

#### 3.1 $\alpha$ -Syn overexpression inhibits autophagy initiation and defects autophagy turnover

##### 3.1.1 $\alpha$ -Syn overexpression inhibits autophagy initiation in an mTOR-dependent manner

To investigate the role of  $\alpha$ -Syn overexpression in autophagy, the effect of  $\alpha$ -Syn overexpression on autophagy initiation was first examined. mTORC1 and AMPK are the two main signaling molecules conversely regulating autophagy initiation. mTORC1 phosphorylates ULK1 at Ser757 and suppress autophagy initiation, while AMPK phosphorylates ULK1 at Ser317, Ser555, and Ser777 to activate this process [134-136]. Differentiated LUHMES cells, a human DAergic cell line that acquires a neuronal phenotype upon differentiation, was used for investigating the effect of  $\alpha$ -Syn overexpression on autophagy [112]. Upon  $\alpha$ -Syn overexpression, the phosphorylation level of the mTOR-activating protein kinase B (PKB, Akt) and ribosomal protein S6 kinase (S6K1) was increased in LUHMES cells (**Figure 6**). The latter results are in accord with previous results from our lab, which demonstrated a stimulatory effect of  $\alpha$ -Syn overexpression on the mTOR signaling pathway [12].



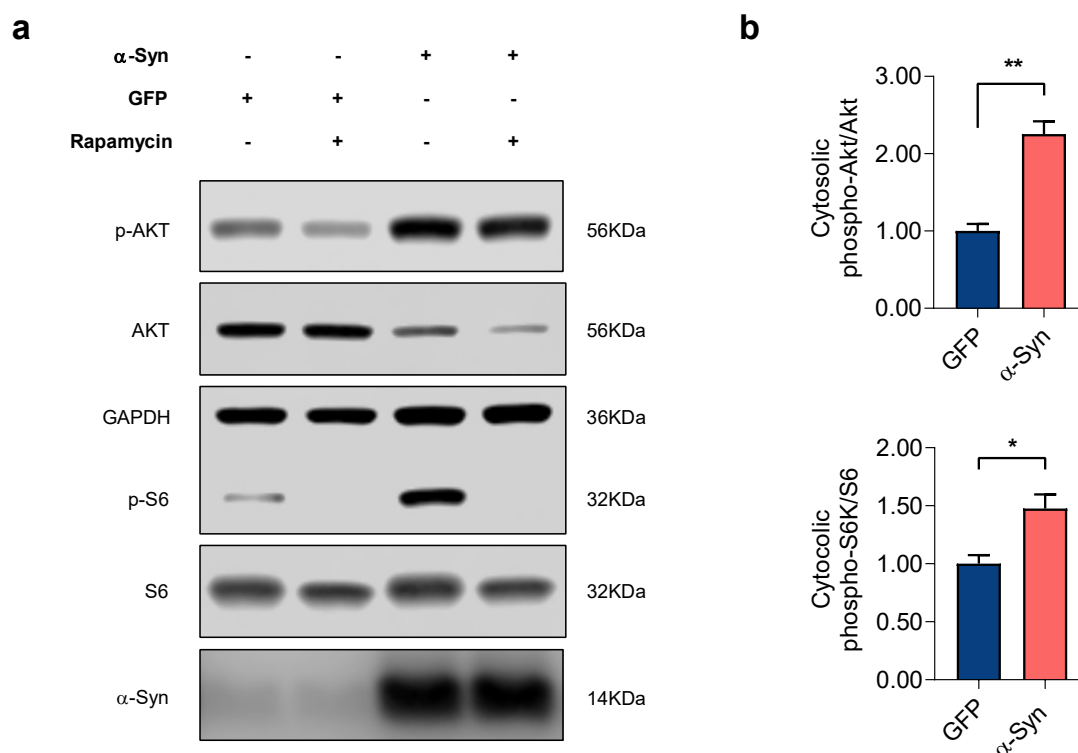


**Figure 6  $\alpha$ -Syn overexpression activates mTOR associated signaling molecules.**

Western blot (a) and bar graphs (b) illustrating the abundance and phosphorylation of mTOR associated signaling molecules (Akt and S6) in response to  $\alpha$ -Syn overexpression and in response to treatment with rapamycin (100 nM; 24 hrs) (n = 3/condition). For comparison of the means, a two-tailed unpaired t-test was used in panel b. \*\*P < 0.01, \*P < 0.05. Data are shown as means  $\pm$  SEM.

p62, also called sequestosome 1 (SQSTM1), is a receptor for cargo that is destined to be degraded by autophagy. It targets the ubiquitinated proteins to autophagosomes by binding to both ubiquitin and LC3, thus facilitates the clearance. p62 decreases when autophagy is activated, whereas an increased p62 level can be observed upon autophagy suppression. Therefore, p62 is often used as a marker to study autophagic flux [137].

Western blot results showed the abundance of p62 to be increased upon  $\alpha$ -Syn overexpression, indicating that autophagy initiation was inhibited under these conditions. Taken

the above results together, this suggests that  $\alpha$ -Syn overexpression inhibits autophagy initiation in an mTOR-dependent manner.

### **3.1.2 The abundance of the autophagy marker LC3B-II is increased in $\alpha$ -Syn transduced LUHMES cells**

The next step was to investigate the effect of  $\alpha$ -Syn overexpression on autophagy turnover and therefore assess the abundance of LC3B-I and II in cultured DAergic neurons in response to  $\alpha$ -Syn overexpression. In the autophagy pathway, LC3B is a key protein participating in autophagosome biogenesis and substrate selection, and it is the most widely used marker of autophagosomes, used to quantify their abundance [138]. As is shown in **Figure 7** the abundance of LC3B-II increased when  $\alpha$ -Syn was overexpressed in LUHMES cells. Since LC3B-I is cytosolic and LC3B-II is membrane-bound, the increased LC3B-II abundance indicates an increased accumulation of autophagosomes in response to  $\alpha$ -Syn.

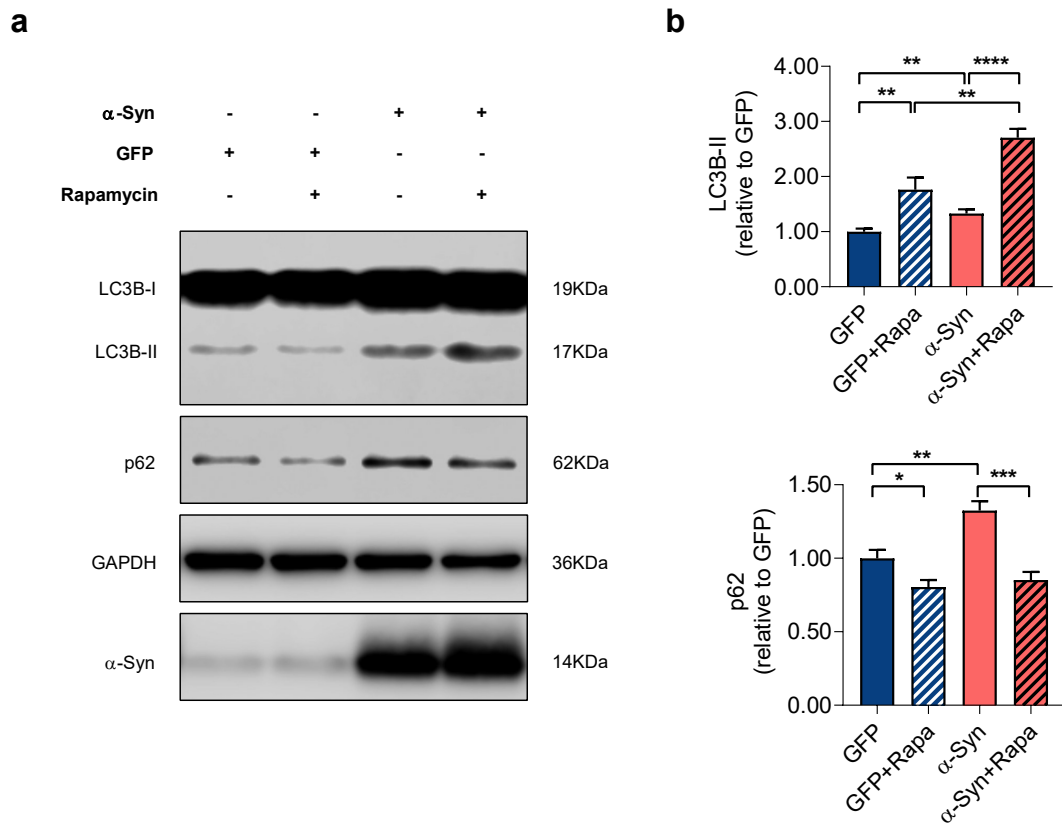


**Figure 7  $\alpha$ -Syn overexpression impairs autophagy initiation and turnover.** Western blot (**a**) and bar graphs (**b**) illustrating the abundance of LC3B-I and -II in response to  $\alpha$ -Syn overexpression and in response to treatment with rapamycin (100 nM; 24 hrs) (n = 10/condition). For comparison of the means, one-way ANOVA with Tukey's post hoc test was used in panel b. \*\*\*\*P < 0.0001, \*\*\*P < 0.001, \*\*P < 0.01, \*P < 0.05. Data are shown as means  $\pm$  SEM.

$\alpha$ -Syn overexpression blocks autophagosome-lysosome fusion The above results showed that  $\alpha$ -Syn overexpression leads to an increased abundance of LC3B-II, but at the same time attenuated mTOR-mediated autophagy initiation, as illustrated by an increased p62 abundance. We thus hypothesized that  $\alpha$ -Syn overexpression caused LC3B-II accumulation by impairing autophagy turnover downstream of the autophagosome. In order to test this hypothesis, a fusion protein GFP-RFP-LC3B [138] was expressed in LUHMES cells together with  $\alpha$ -Syn or Luciferase. This fluorescence-based assay allows to examine the different stages of autophagy flux by quantifying the abundance of autophagosomes and autophagolysosomes separately. In accordance with our Western blot data, we found an increased amount of both GFP and RFP positive autophagosomes in response to  $\alpha$ -Syn overexpression, whereas the abundance of RFP-positive autophagolysosomes was decreased. Bafilomycin A1 (100 nM, 24 hrs), which inhibits autophagolysosome fusion by blocking the vacuolar  $H^+$ -ATPase-mediated lysosome acidification, was used as a reference. In bafilomycin A1 treated cells, the fusion between autophagosomes and lysosomes was inhibited and likewise led to an accumulation of autophagosomes (**Figure 8**). Taken together, these results thus suggest that  $\alpha$ -Syn overexpression impairs autophagosome-to-lysosome fusion, and as a consequence, leads to the accumulation of autophagosomes and a decreased abundance of autophagolysosomes.

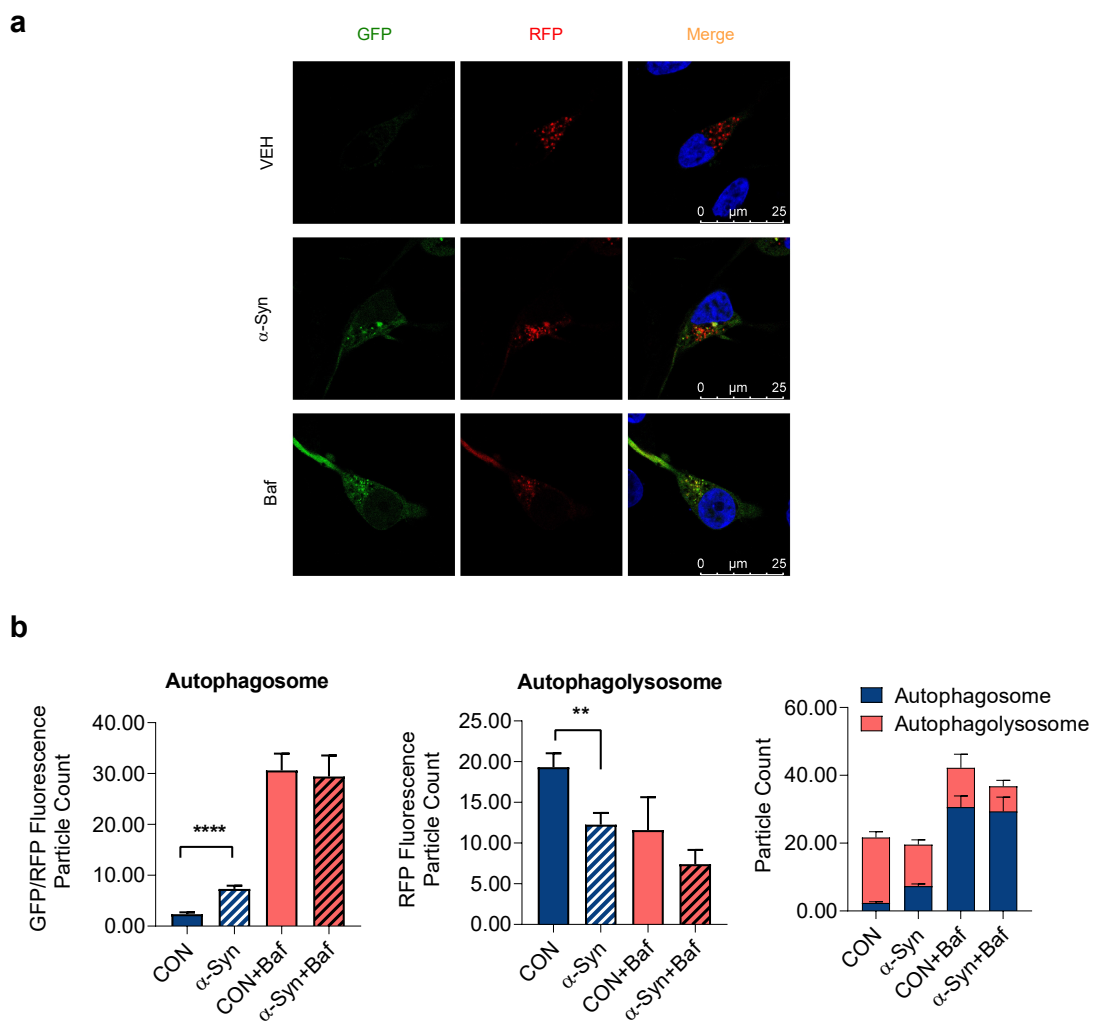


**Figure 8  $\alpha$ -Syn overexpression attenuates autophagy turnover.** **a** Photomicrographs from confocal microscopy of neurons transduced with GFP-RFP-LC3B and either co-transfected with vehicle (VEH),  $\alpha$ -Syn or treated with bafilomycin A1 (Baf; 100 nM; 24 hrs) (for VEH n = 25 cells, for  $\alpha$ -Syn n = 26 cells, for Baf n = 5 cells) **b** Bar graphs illustrating the count of fluorescence positive particles.  $\alpha$ -Syn overexpression and Baf both lead to a significant increase in GFP/RFP fluorescence positive particles (left graph), whereas RFP-fluorescence positive particles was decreased (middle graph). The ratio of GFP/RFP double-positive autophagosomes to RFP-positive autophagolysosomes is decreased in response to  $\alpha$ -Syn overexpression and Baf (right graph). For comparison of the means, a one-way ANOVA with Tukey's post hoc test was used in panel b. \*\*\*\*P < 0.0001, \*\*P < 0.01. Data are shown as means  $\pm$  SEM.

## **3.2 EVs release is changed in response to attenuating autophagy flux**

### **3.2.1 Rapamycin treatment increases autophagy by inhibiting AKT-mTOR signaling pathway**

As described above, mTORC1 regulates autophagy by inhibiting the ULK complex. We next studied the effect of the mTOR inhibitor rapamycin on autophagy in our cell model. As expected, treatment with rapamycin (100 nM, 24 hrs) led to a decreased phosphorylation of the mTOR-associated signaling molecules (**Figure 6**). In addition, rapamycin treatment decreased the abundance of p62, suggesting an enhanced autophagy initiation. Co-application of rapamycin together with  $\alpha$ -Syn overexpression further increased the abundance of LC3B-II. Because  $\alpha$ -Syn, at the same time, inhibited autophagy turnover (**Figure 7**), these results suggest that  $\alpha$ -Syn overexpression and rapamycin act on different distinct stages of autophagy, with  $\alpha$ -Syn overexpression inhibiting both autophagy initiation and turnover.

### **3.2.2 $\alpha$ -Syn overexpression and rapamycin treatment increase EV release from cultured neurons.**

The abundance of EVs released to the cell culture medium were investigated by Western blot and nanoparticle tracking analysis. EVs were isolated from cell culture medium by ultracentrifuge, and subjected to Western blot for EV marker. As shown in **Figure 9**, the abundance of the EV-associated proteins Alix/AIP1, Flotillin-1, and CD81 increased upon  $\alpha$ -Syn overexpression. In addition, co-application of rapamycin further potentiated this effect, mirroring the effect of  $\alpha$ -Syn overexpression and rapamycin on LC3B-II. In according with our Western blot results, the extracellular particle concentration increased in  $\alpha$ -Syn transduced cell medium as measured by NTA, and rapamycin co-application

further potentiated the increase, thus further confirming a stimulatory effect of  $\alpha$ -Syn overexpression and rapamycin on EV release.

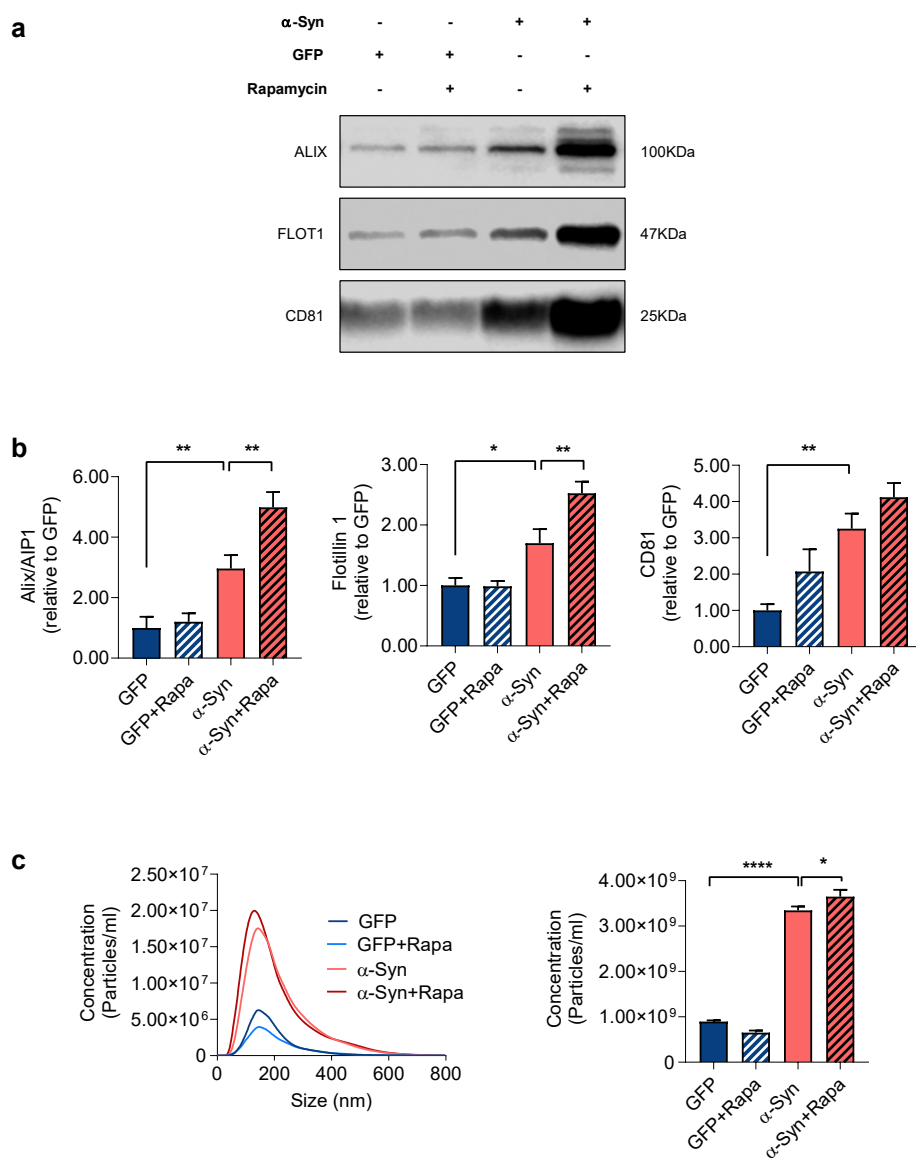


**Figure 9 Both  $\alpha$ -Syn overexpression and rapamycin treatment increase EVs release.** **a,b** Western blot (**a**) and bar graphs (**b**) illustrating the abundance of the EV-associated proteins Alix/AIP1, Flotillin-1 and CD81 in EV-enriched medium pellets from cultured cells in response to  $\alpha$ -Syn overexpression and in response to treatment with rapamycin (100 nM; 24 hrs) ( $n = 9$ /condition). **c** Results from Nanoparticle Tracking Analysis (NTA) illustrating an increased amount of EVs in response to  $\alpha$ -Syn overexpression

or to treatment with rapamycin (100 nM; 24 hrs) (n = 9/condition). For comparison of the means, one-way ANOVA with Tukey's post hoc test was used in panels b and c. \*\*\*\*P < 0.0001, \*\*P < 0.01, \*P < 0.05. Data are shown as means  $\pm$  SEM.

### 3.2.3 Bafilomycin blocks autophagosome-lysosome fusion and inhibits autophagy

As shown by the RFP-GFP-LC3B autophagy reporter assay, bafilomycin A1 treatment led to an increased amount of both GFP and RFP positive autophagosomes, whereas decreased the abundance of RFP-positive autophagolysosomes (**Figure 8**). For bafilomycin A1 treatment, cell lysates were further analyzed by Western blot. The results showed an increase in LC3B-II abundance in bafilomycin treated cell lysates (**Figure 10**), indicating accumulated autophagosomes upon bafilomycin A1 treatment. Taken together, these results suggested that bafilomycin A1 blocks autophagosome-lysosome fusion and inhibits autophagy turnover.

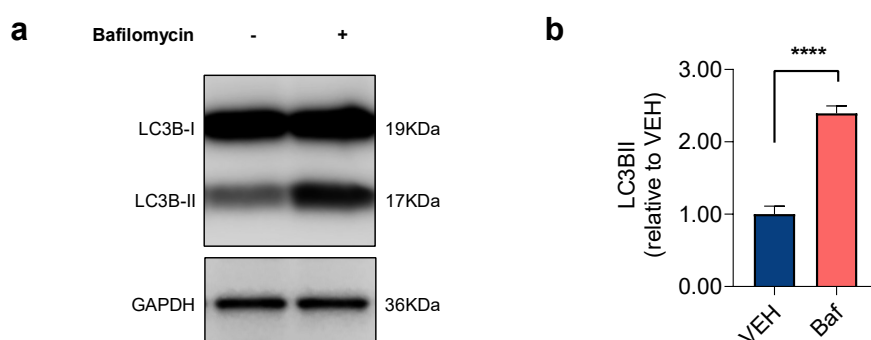


**Figure 10 Blocking autophagosome-lysosome fusion impairs autophagy turnover.**

Western blot (a) and bar graphs (b) illustrating the increased abundance of LC3B-II in response to bafilomycin (100 nM; 24 hrs) (n = 7/condition). For comparison of the means, a two-tailed unpaired t-test was used in panel b. \*\*\*\*P < 0.0001. Data are shown as means  $\pm$  SEM.



### **3.2.4 Bafilomycin treatment increases EVs release**

Similar to  $\alpha$ -Syn, bafilomycin A1 treatment resulted in an increased abundance of the EV-associated proteins Alix/AIP1, Flotillin-1 and CD81 in EV-enriched medium pellets. Consistent with our Western blot results, NTA analysis showed an increased extracellular particle concentration in bafilomycin A1 treated cell medium (**Figure 11**). Notably, in both Western blot and NTA results, the effect of bafilomycin A1 treatment in increasing EVs release was mirroring the effect of  $\alpha$ -Syn overexpression comparing to GFP-transduced cells.

### **3.2.5 Both bafilomycin treatment and $\alpha$ -Syn overexpression increase the abundance of autophagy-associated markers in EV-enriched pellets from cell culture medium**

In addition to investigating EV abundance, we further investigated the protein composition of EVs. The results showed that EVs from  $\alpha$ -Syn-transduced or bafilomycin A1 treated neurons carried an increased amount of the autophagy-associated proteins LC3B-II and p62, thus suggesting their origin from the autophagy pathway (**Figure 12**). Based on these results, we concluded that  $\alpha$ -Syn overexpression impairs autophagy turnover by blocking autophagolysosome fusion, leading to a compensatory increase in the release of neuronal EVs that carry the molecular signature of autophagy-derived organelles.

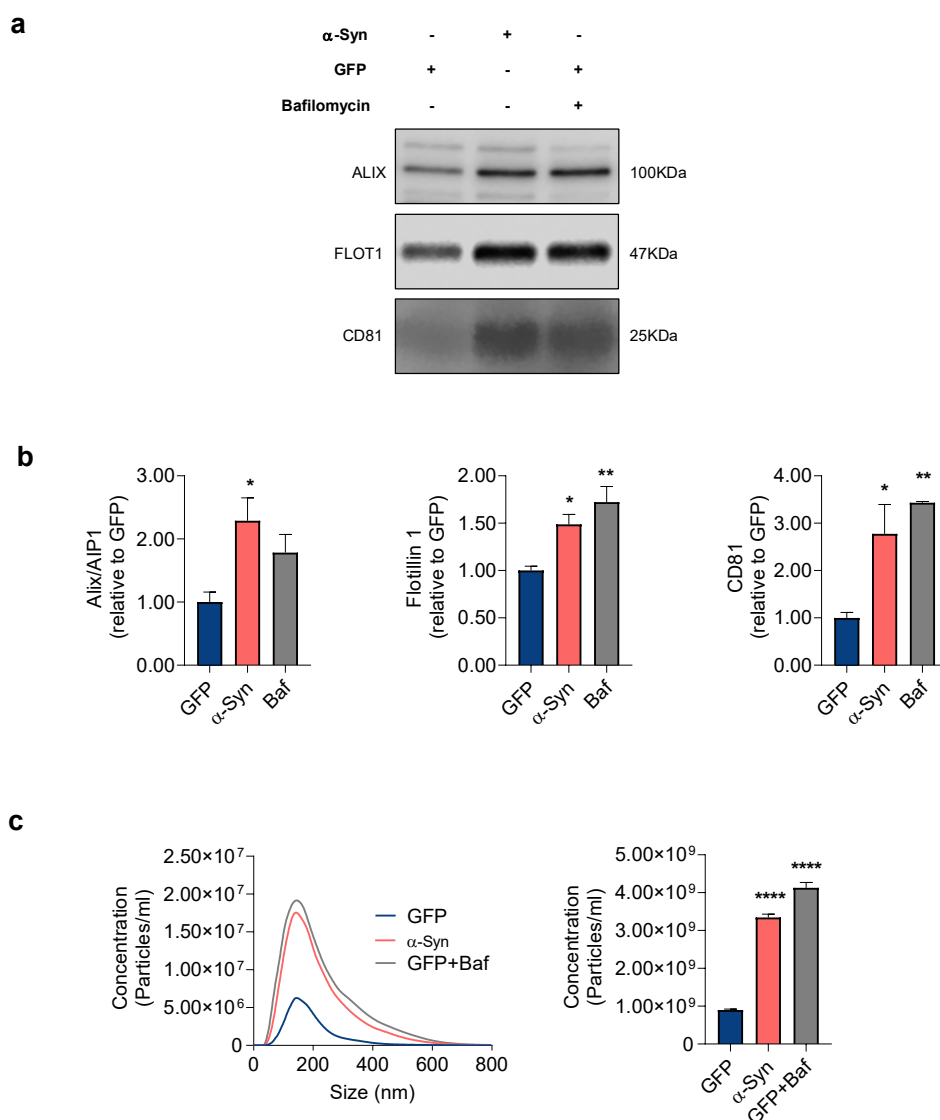


**Figure 11 Blocking autophagosome-lysosome fusion increases EVs release. a,b** Western blot (a) and bar graphs (b) illustrating the increased abundance of the EV-associated proteins Alix/AIP1, Flotillin-1 and CD81 in EV-enriched medium pellets from cells in response to  $\alpha$ -Syn overexpression and in response to treatment with bafilomycin (Baf; 100 nM; 24 hrs) ( $n = 3$ /condition). **c** Results from NTA illustrating an increased amount of EVs in response to  $\alpha$ -Syn overexpression or to treatment with Baf (100 nM; 24 hrs) ( $n = 9$ /condition). For comparison of the means, one-way ANOVA with Tukey's post hoc test was used in panels b and c. \*\*\*\* $P < 0.0001$ , \*\* $P < 0.01$ , \* $P < 0.05$ . Data are shown as means  $\pm$  SEM.

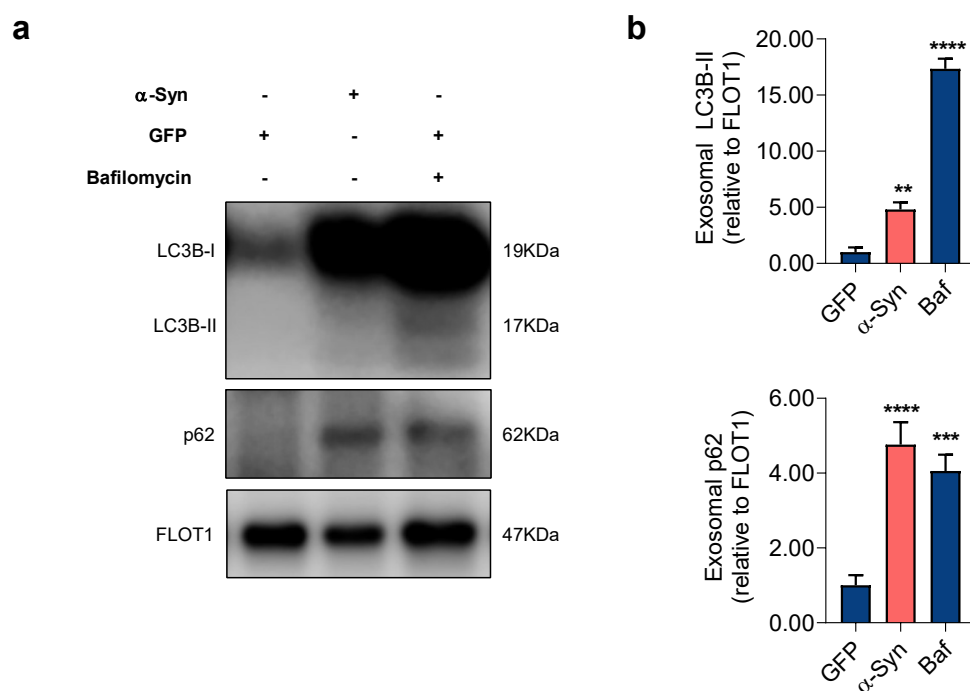


**Figure 12 EVs from  $\alpha$ -Syn-transduced or bafilomycin A1 treated neurons carried an increased amount of the autophagy-associated proteins.** Western blot (**a**) and bar graphs (**b**) illustrating the increased abundance of LC3B-II and p62 in EV-enriched medium pellets from  $\alpha$ -Syn-transduced and bafilomycin (Baf) treated cells. Note that a similar amount of total protein (i.e., a comparable total number of EVs) has been loaded on each lane. The result thus represents the relative content of LC3B-II and p62 per vesicle. For comparison of the means, one-way ANOVA with Tukey's post hoc test was used in panel b. \*\*\*\*P < 0.0001, \*\*\*P < 0.001, \*\*P < 0.01. Data are shown as means  $\pm$  SEM.

### **3.3 The effect of $\alpha$ -Syn overexpression on autophagolysosome fusion depends on SNAP29**

#### **3.3.1 $\alpha$ -Syn overexpression leads to a decreased expression of SNAP29 in transduced LUHMES cells**

In principal, the fusion of autophagosomes and lysosomes depends on a set of specific SNARE molecules, where the autophagic Qa-SNARE STX17 forms a SNARE core complex with the cytosolic Qbc-SNARE SNAP29 and the lysosomal R-SNARE VAMP8 or YKT6 [57, 58, 139-142]. Because  $\alpha$ -Syn is well known to interact with synaptic SNARE proteins [143, 144], we therefore hypothesized that  $\alpha$ -Syn overexpression may impair autophagosome-to-lysosome fusion by affecting one or more of these SNARE molecules. When we examined the abundance of the autophagy-associated SNARE molecules in cultured neurons in response to  $\alpha$ -Syn overexpression, we found indeed a significant decrease of the SNAP25 SNARE family members SNAP23 and SNAP29 in  $\alpha$ -Syn-transduced cells. On the other hand, the abundance of VAMP8, STX17 and YKT6 remained unchanged, suggesting a family-specific effect of  $\alpha$ -Syn. Interestingly,  $\alpha$ -Syn overexpression had no effect on SNAP29 gene expression as measured by qRT-PCR, suggesting a posttranscriptional effect of  $\alpha$ -Syn overexpression on SNAP29 abundance (**Figure 13**).

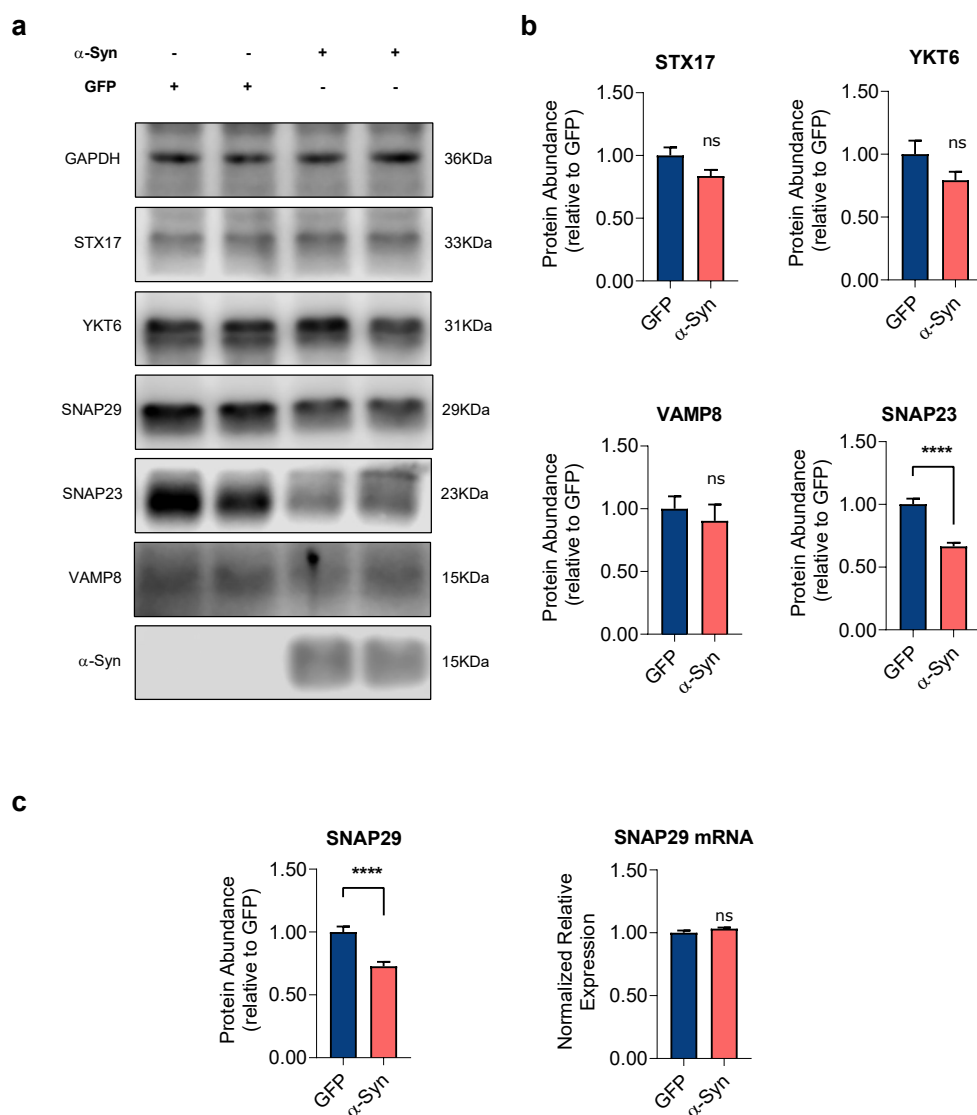


**Figure 13  $\alpha$ -Syn overexpression reduces the abundance of SNAP29 in cultured human DA neurons.** **a,b** Western blot (**a**) and bar graphs (**b** and left of **c**) illustrating the SNARE proteins STX17, YKT6, VAMP8, SNAP29 and SNAP23 in  $\alpha$ -Syn- and GFP-transduced neurons.  $\alpha$ -Syn overexpression specifically leads to a decreased protein abundance of the SNAP25 family members SNAP23 and SNAP29, whereas the other SNARE proteins remain unchanged ( $n = 6/\text{condition}$ ,  $n = 11$  for SNAP29). **c** Bar graph showing a decreased protein level but similar mRNA expression levels for SNAP29 in  $\alpha$ -Syn-transduced neurons as compared to GFP-transduced cells ( $n = 3/\text{condition}$ ). For comparison of the means, an unpaired t-test was used in panels **b** and **c**; \*\*\*\* $P < 0.0001$ ; Data are shown as means  $\pm$  SEM.

### 3.3.2 The abundance of LC3B-II is increased in SNAP29-deficient cells.

Based on the above results, it would be conceivable that  $\alpha$ -Syn overexpression impairs autophagosome-to-lysosome fusion by affecting SNAP29, and as a consequence the functional integrity of the autophagolysosomal SNARE complex. In order to test this hypothesis, the effect of knocking-down SNAP29 on autophagy turnover was investigated. Consistent with what has been reported about the role of SNAP29 in autophagolysosome fusion [58], our Western blot results showed an increased abundance of LC3B-II upon SNAP29 knockdown in cultured DAergic neurons (**Figure 14**).

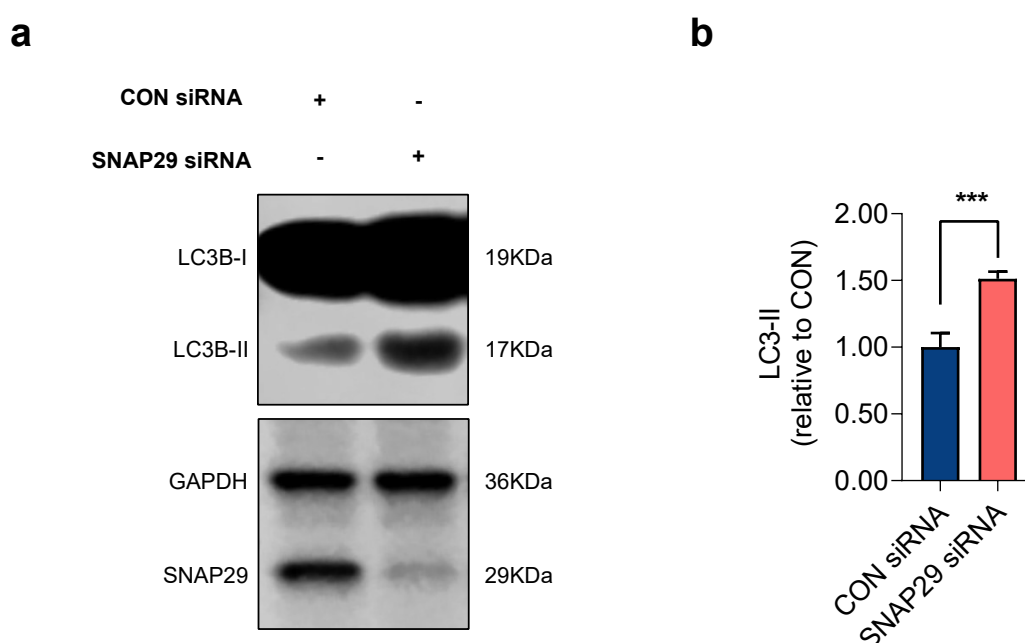


**Figure 14 Knocking down SNAP29 mimics the effect of  $\alpha$ -Syn overexpression on autophagy turnover.** Western blot (**a**) and bar graphs (**b**) illustrating an increased abundance of LC3B-II in response to transfection with SNAP29 siRNAs (30 nM) ( $n = 4/\text{condition}$ ). For comparison of the means, an unpaired t-test was used; \*\*\* $P < 0.001$ . Data are shown as means  $\pm$  SEM.

### 3.3.3 SNAP29 knockdown impairs autophagosome-lysosome fusion

To further confirm the effect of SNAP29 knockdown on autophagy turnover, we carried out an RFP-GFP-LC3B autophagy reporter assay. Similar to  $\alpha$ -Syn overexpression, SNAP29 knockdown likewise decreased the abundance of autophagolysosomes which are only RFP positive, thus increasing the ratio of autophagolysosomes to autophagosomes (**Figure 15**). Taken together, these results confirmed SNAP29 to play a key role in the fusion between autophagosomes and lysosomes in our model system.

### 3.3.4 Loss of SNAP29 increases the abundance of EVs in cell medium

To investigate the effect of SNAP29 knockdown on EV release in LUHMES cells, EV abundance was measured by Western blot and NTA. Western blot showed an increased abundance of EV markers in EV-enriched medium pellets from SNAP29 siRNA treated neurons, and nano-particle tracking analysis confirmed the increased particle concentration. Both results suggest an increased abundance of EVs in the culture medium due to the loss of SNAP29 (**Figure 16**). In summary, these results thus demonstrate SNAP29 knockdown to mimic the effect of  $\alpha$ -Syn overexpression on autophagy turnover, further implicating SNAP29 in  $\alpha$ -Syn-associated autophagy changes.

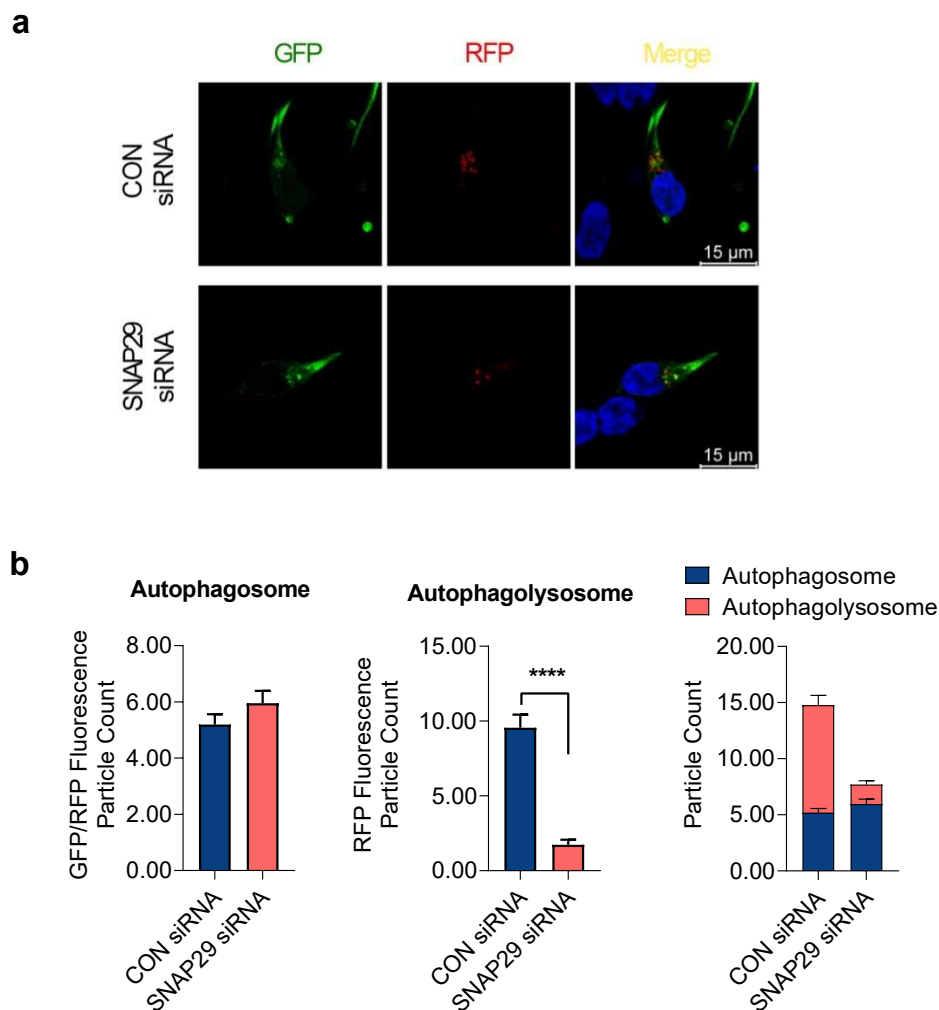


**Figure 15 Knocking down SNAP29 mimics the effect of  $\alpha$ -Syn overexpression on autophagosome-lysosome fusion.** **a** Photomicrographs from confocal microscopy of neurons transduced with GFP-RFP-LC3B and either co-transfected with SNAP29 or negative control (CON) siRNAs (for CON siRNA  $n = 41$  cells, for SNAP29 siRNA  $n = 42$  cells). **b** Bar graphs illustrating the count of fluorescence positive particles. SNAP29 siRNA led to a significant decrease in RFP fluorescence positive particles (middle graph), whereas GFP/RFP-fluorescence positive particles remained unchanged (left graph). The ratio of GFP/RFP double-positive autophagosomes to RFP-positive autophagolysosomes is decreased in response to SNAP29 siRNA transfection. For comparison of the means, an unpaired t-test was used; \*\*\*\* $P < 0.0001$ . Data are shown as means  $\pm$  SEM.



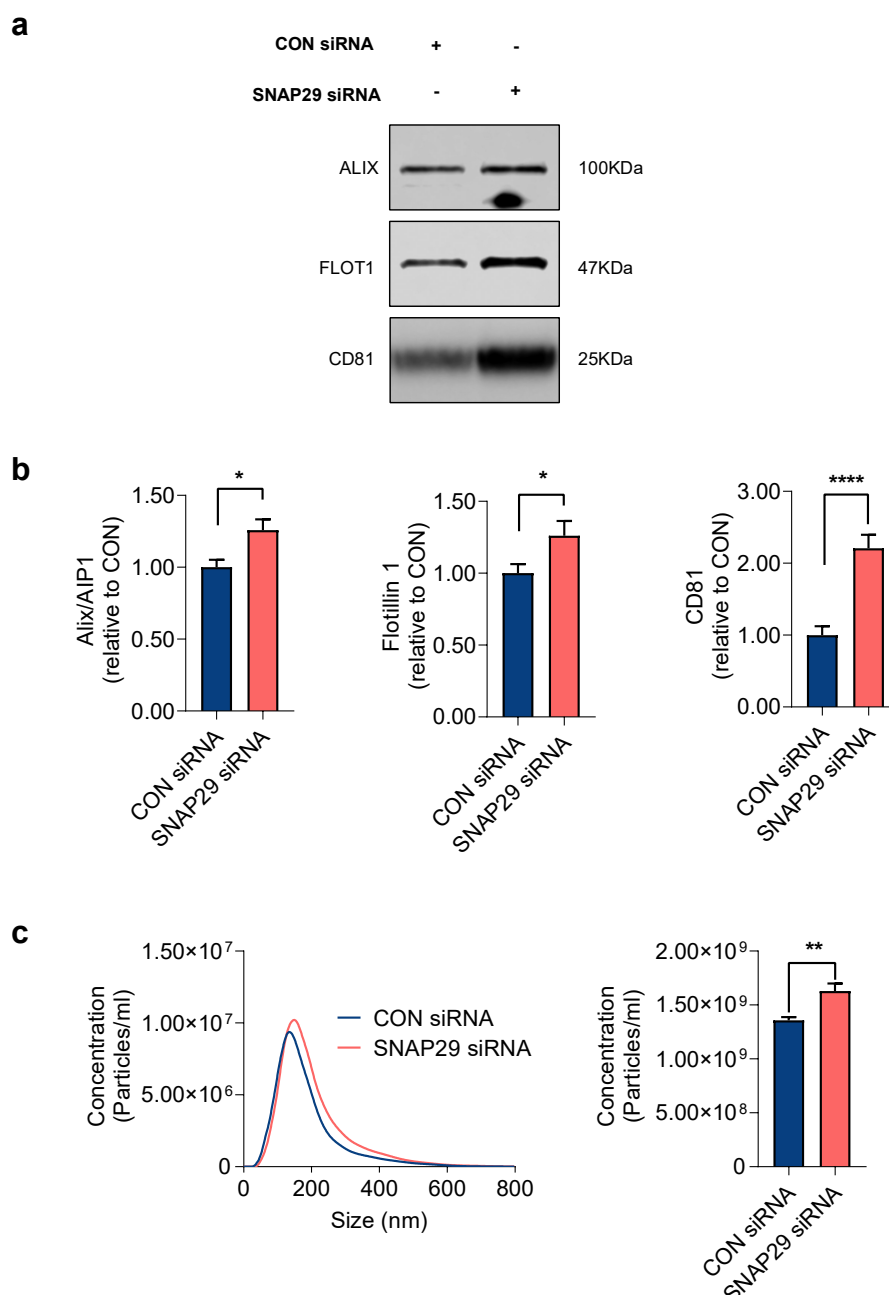


**Figure 16 Knocking down SNAP29 mimics the effect of  $\alpha$ -Syn overexpression on EVs release.** **a,b** Western blot (**a**) and bar graphs (**b**) illustrating the increased abundance of the EV-associated proteins Alix/AIP1, Flotillin-1 and CD81 in EV-enriched medium pellets from cells in response to SNAP29 knock-down ( $n = 9/\text{condition}$ ). **g** Results from NTA illustrating an increased amount of EVs in response to transfecting cells with SNAP29 siRNAs ( $n = 9/\text{condition}$ ). For comparison of the means, an unpaired t-test was used; \*\*\*\* $P < 0.0001$ , \*\* $P < 0.01$ , \* $P < 0.05$ . Data are shown as means  $\pm$  SEM.

### 3.4 Co-expressing SNAP29 attenuates autophagy defects and cell death in $\alpha$ -Syn-transduced LUHMES cells

#### 3.4.1 Co-expressing SNAP29 attenuates the increased LC3B-II abundance in $\alpha$ -Syn transduced LUHMES cells

In order to further establish the functional interplay between SNAP29 and  $\alpha$ -Syn, the effect of SNAP29 co-expression in  $\alpha$ -Syn transduced neurons was investigated. Consistent with our previous results, co-expression of SNAP29 attenuated the  $\alpha$ -Syn-mediated increase in LC3B-II, thus indicating a restored autophagy flux upon SNAP29 co-expression (**Figure 17**).

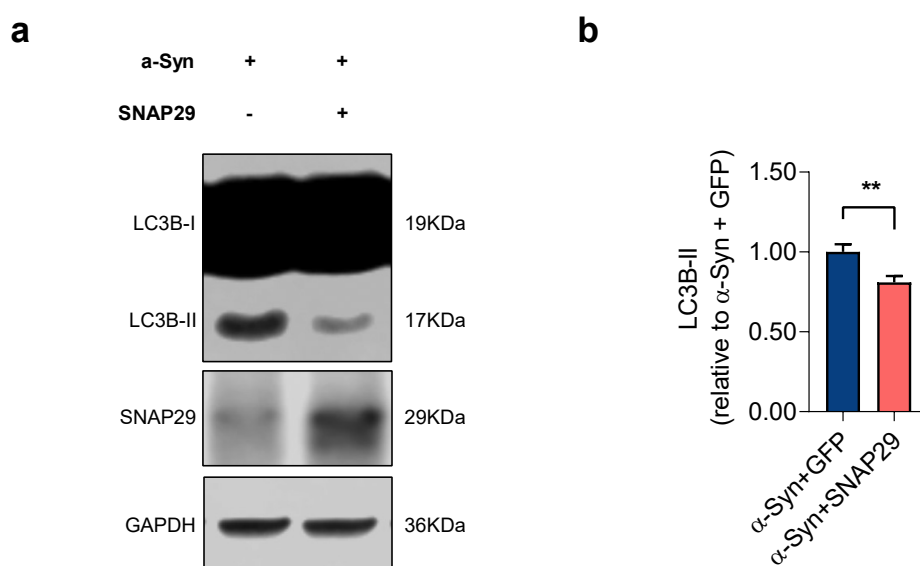


**Figure 17 SNAP29 co-expression rescues the  $\alpha$ -Syn-induced impairment of autophagy turnover.** **a,b** Western blot and bar graphs illustrating a decreased abundance of LC3B-II in  $\alpha$ -Syn overexpressing cells in response to transfection with SNAP29 (n = 9/condition). For comparison of the means, an unpaired t-test was used; \*\*P < 0.01. Data are shown as means  $\pm$  SEM.

### 3.4.2 Co-expressing SNAP29 rescues the defected autophagy turnover in $\alpha$ -Syn transduced LUHMES cells

Likewise, the result of the RFP-GFP-LC3B autophagy reporter assay showed a decreased number of GFP-positive dots in SNAP29 co-expressing  $\alpha$ -Syn transduced neurons, suggesting that SNAP29 co-expression partially attenuated the  $\alpha$ -Syn-mediated increase in autophagosomes and normalized the ratio between autophagosomes and autophagolysosomes (Figure 18).

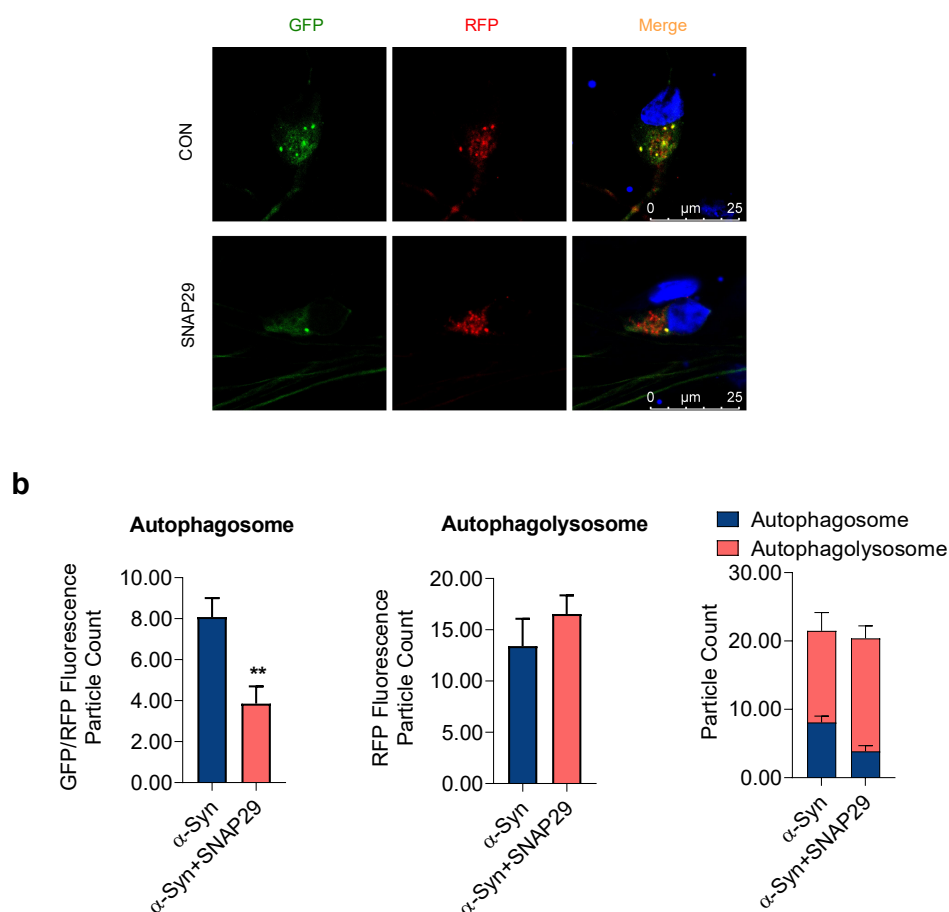


**Figure 18 SNAP29 co-expression rescues the  $\alpha$ -Syn-induced impairment of autophagosome-lysosome fusion. c** Photomicrographs from confocal microscopy of neurons transduced with GFP-RFP-LC3B,  $\alpha$ -Syn and either with SNAP29 or vehicle (VEH). **d** Bar graphs illustrating the count of fluorescence positive particles. SNAP29 co-expression led to a significant decrease in GFP/RFP fluorescence positive particles (left

graph), whereas RFP-fluorescence positive particles remained unchanged (middle graph). The ratio of GFP/RFP double-positive autophagosomes to RFP-positive autophagolysosomes is increased in response to SNAP29 transduction (for  $\alpha$ -Syn  $n = 25$  cells, for  $\alpha$ -Syn+SNAP29  $n = 28$  cells). For comparison of the means, an unpaired t-test was used;  $**P < 0.01$ . Data are shown as means  $\pm$  SEM.

### 3.4.3 Co-expressing SNAP29 attenuates the cytotoxicity of $\alpha$ -Syn overexpression

Consistent with previous result of our lab,  $\alpha$ -Syn-transduced cells release more LDH to the cell culture medium than GFP-transduced cells, indicating  $\alpha$ -Syn overexpression to induce cell death in LUHMES cells. Besides, rapamycin treatment potentiated  $\alpha$ -Syn-induced cell death in LUHMES cells, similar to its effect on autophagosome accumulation and EV release, as demonstrated by an increased LDH release and decreased MTT signal in these neurons (**Figure 19**).

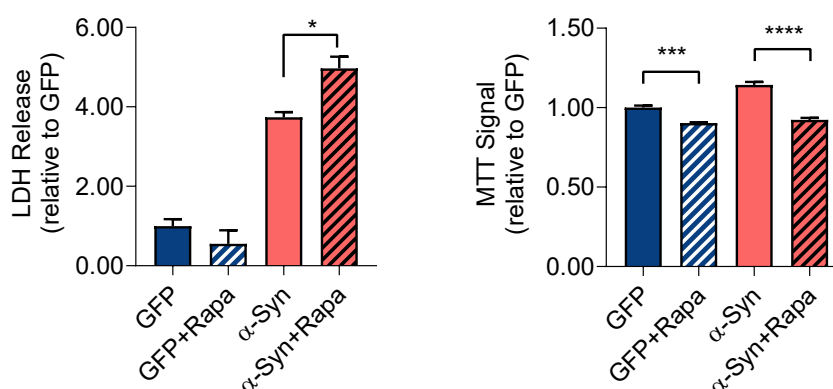


**Figure 19  $\alpha$ -Syn overexpression induces cell death.** Bar graphs illustrating the quantification of LDH in the culture medium (left) and the MTT signal (right) in response to  $\alpha$ -Syn overexpression or to treatment with rapamycin (100 nM; 24 hrs) ( $n = 4$ /condition). For comparison of the means, one-way ANOVA with Tukey's post hoc test was used. \*\*\*\* $P < 0.0001$ , \*\*\* $P < 0.001$ , \* $P < 0.05$ . Data are shown as means  $\pm$  SEM.

Notably, co-expressing SNAP29 in  $\alpha$ -Syn transduced neurons decreased LDH release and enhanced the MTT signal, suggesting that re-introducing SNAP29 attenuates cellular death (**Figure 20**). These results illustrate that the loss of SNAP29 in  $\alpha$ -Syn-transduced neurons contributes to  $\alpha$ -Syn-associated neuronal death.

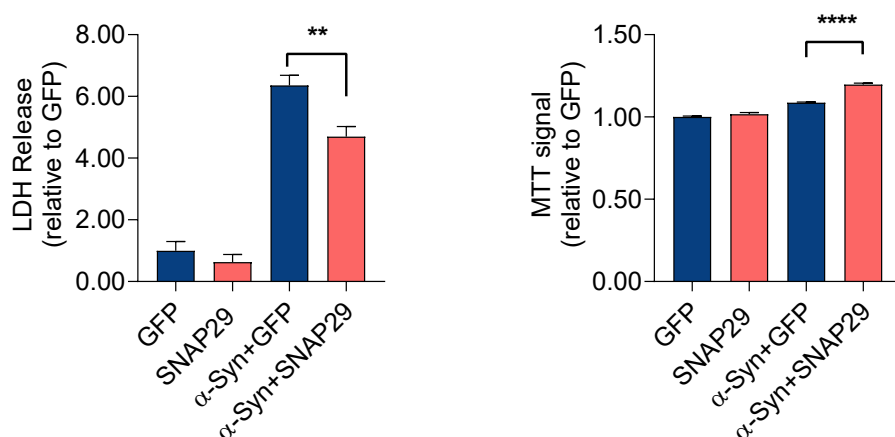


**Figure 20 co-expressing SNAP29 in  $\alpha$ -Syn transduced neurons attenuated cellular death.** Bar graphs illustrating the quantification of LDH in the culture medium (left) and the MTT signal (right) in response to  $\alpha$ -Syn and SNAP29 expression (n = 8/condition). For comparison of the means, one-way ANOVA with Tukey's post hoc test was used. \*\*\*\*P < 0.0001, \*\*P < 0.01. Data are shown as means  $\pm$  SEM.

#### **3.4.4 Co-expressing SNAP29 attenuates the abundance of EVs in $\alpha$ -Syn-transduced LUHMES cell medium**

Western blot results showed co-expressing SNAP29 in  $\alpha$ -Syn-transduced neurons likewise normalized the  $\alpha$ -Syn-mediated increase of EV markers Alix/AIP1, Flotillin-1 and CD81 in EV-enriched medium pellets. And nano-particle tracking analysis showed a decreased particle concentration in SNAP29 co-expressing cell medium (**Figure 21**).

In summary, our results thus suggest that  $\alpha$ -Syn overexpression affected autophagy turnover by impairing SNAP29-mediated autophagolysosome fusion, and that the loss of SNAP29 in  $\alpha$ -Syn-transduced cells led to increased EV release as well as cell death in cultured DAergic neurons.

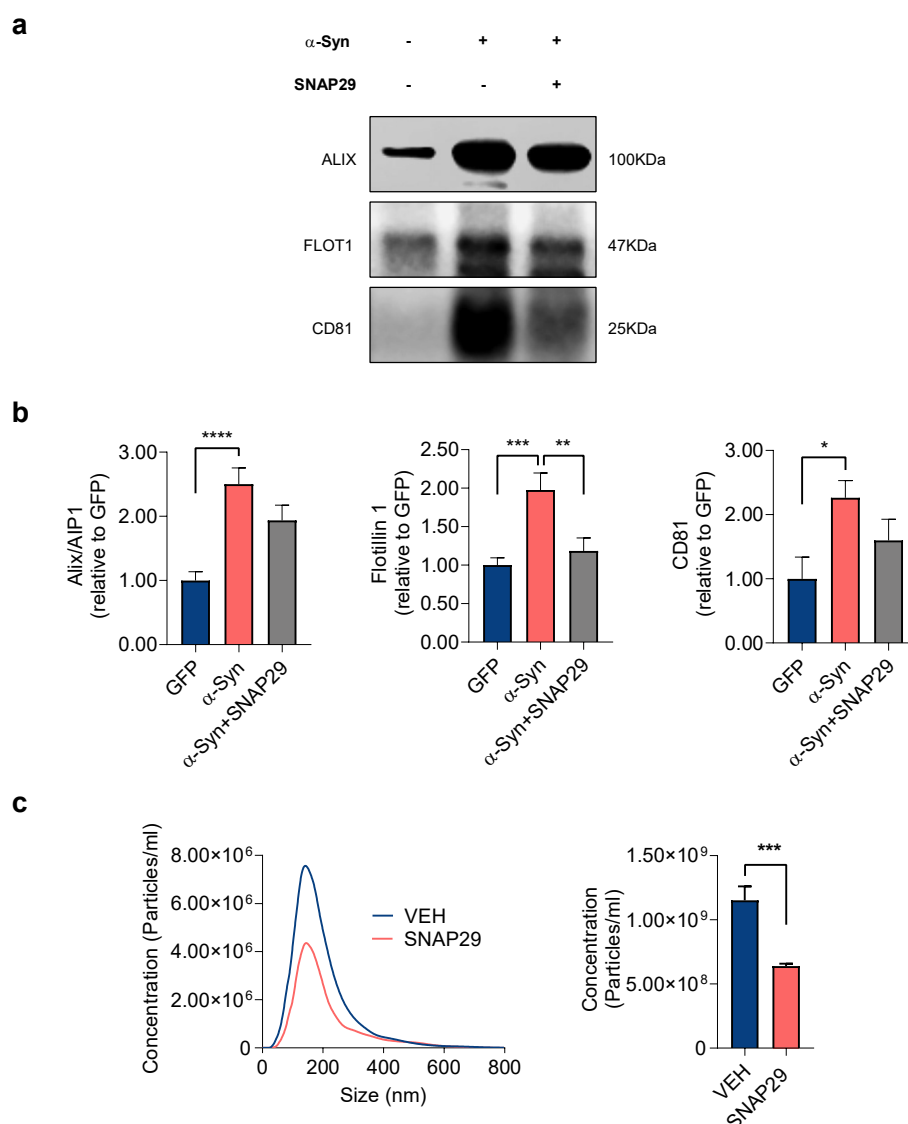


**Figure 21 SNAP29 co-expression attenuated  $\alpha$ -Syn-induced increase on EVs release.** **e,f** Western blot and bar graphs illustrating the decreased abundance of the EV-associated proteins Alix/AIP1, Flotillin-1 and CD81 in EV-enriched medium pellets from cells in response to SNAP29 co-expression (n = 9/condition). **g** Results from NTA illustrating a decreased amount of EVs in response to transducing cells with SNAP29 (n = 9/condition). For comparison of the means, one-way ANOVA with Tukey's post hoc test was used in panel b; a two-tailed unpaired t-test was used in panel c. \*\*\*\*P < 0.0001, \*\*\*P < 0.001, \*\*P < 0.01, \*P < 0.05. Data are shown as means  $\pm$  SEM.

## 3.5 $\alpha$ -Syn directly interacts with SNAP29

### 3.5.1 SNAP29 three-dimensional structure was predicted with good quality

Because our results demonstrated a decrease of SNAP29 in response to  $\alpha$ -Syn overexpression and since  $\alpha$ -Syn has been suggested to directly interact with SNARE complex proteins at presynaptic sites [144], we hypothesized SNAP29 likewise to interact with  $\alpha$ -Syn. In order to examine such a protein-protein interaction and since the complete tertiary structure of SNAP29 has not been established before, we first generated a computationally modelled structure of SNAP29. Using the Rosetta protein structure prediction algorithm, SNAP29 domains were first predicted as independent folding units. Units that had homologous structures were modeled with Rosetta comparative modeling, while Rosetta ab initio modelling was used where no homologous structures were found by sequence homology. Thereafter, the units were assembled into full chain models, and a total of 5 top-scored structure models were returned, which were next optimized by PyRosetta FastRelax. The Rosetta scores and protein structure geometry evaluation scores (see below) of all the five models increased after FastRelax optimization (**Table 2**).



Model #		Rosetta Score	VERIFY*	ERRAT**	PROCHECK***
#1	original	-652.90	70.54	98.34	92.10
	relaxed	-733.38	60.47	97.19	93.40
#2	original	-563.17	79.84	91.32	90.30
	relaxed	-685.85	85.27	92.15	90.30
#3	original	-625.03	77.91	98.00	93.00
	relaxed	-695.10	79.07	99.20	92.50
#4	original	-640.56	79.07	93.95	96.00
	relaxed	-689.68	93.41	95.95	95.20
#5	original	-672.05	79.46	90.36	93.00
	relaxed	-748.22	86.05	91.57	93.40

**Table 2 Rosetta scores and protein structure geometry evaluation scores of the SNAP29 models.** \* percentage of the residues have averaged 3D-1D score  $\geq 0.2$ ; \*\* Overall quality factor; \*\*\* percentage of the residues in most favored regions.

To validate the reliability of the predicted models, protein structure geometry evaluations were performed. Among the five SNAP29 models, model #4 showed a good PROCHECK (Ramachandran plot: 95.2% most favored), Verify 3D (93.41% residues were in allowed regions), ERRAT (95.95), and ProSA analysis result (z-score: -6.49). These results confirmed the quality of our predicted model of SNAP29. Thus, we select model #4 for the subsequent docking analysis (**Figure 22**).

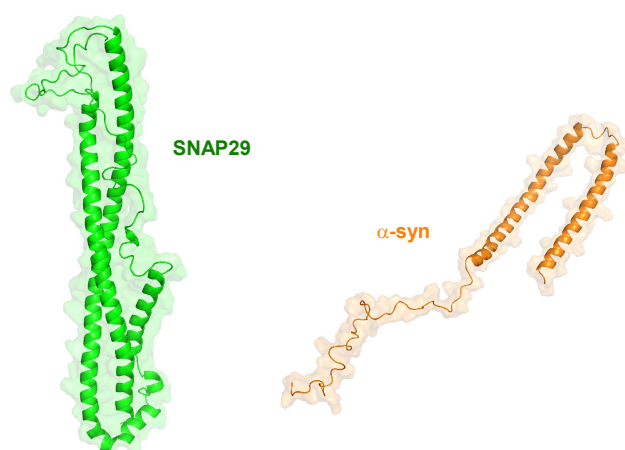


**Figure 22 The computationally modelled tertiary structure of SNAP29 and  $\alpha$ -Syn.**

### **3.5.2 Protein-protein docking simulations indicates sufficiently strong binding between $\alpha$ -Syn and SNAP29**

Given that SNAP29 and  $\alpha$ -Syn may interact with each other, we performed a flexible protein-protein docking analysis using the protein docking prediction server SwarmDock. A total of 492 docking complexes were identified, and representative docking complexes were evaluated using jsPISA. The analysis showed a low binding energy for all six representative possible docking poses (**Figure 23, Table 3**). These bioinformatical results support a sufficiently strong binding between SNAP29 and  $\alpha$ -Syn, and in principle support a potential PPI between the two molecules.

### **3.5.3 Co-IP indicated a direct binding between $\alpha$ -Syn and SNAP29**

In order to further validate our bioinformatic analysis with experimental evidence, we conducted a co-immunoprecipitation with SNAP29 as a bait in neurons that were transduced with  $\alpha$ -Syn or GFP (**Figure 24**). In order to better preserve weak or transient PPIs, the cells were treated with formaldehyde, a mild and reversible crosslinker with a very short spacer length (2.3–2.7 Å) that selectively cross-links closely associated proteins [113]. Western blot confirmed a pulldown of  $\alpha$ -Syn with SNAP29, thus demonstrating a physical binding of  $\alpha$ -Syn and SNAP29 in cultured DAergic neurons. In summary, these results further support a relevant PPI between  $\alpha$ -Syn and SNAP29.

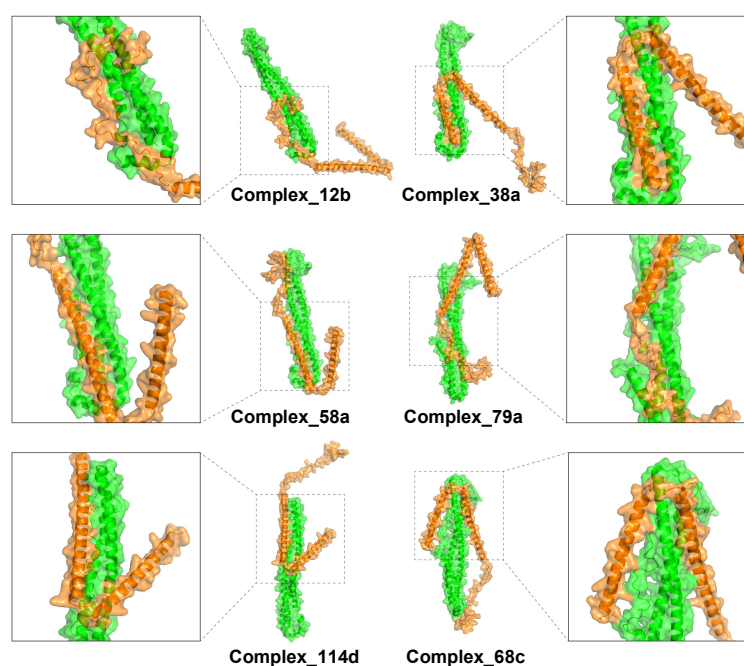


**Figure 23** Potential binding sites and complexes between SNAP29 and  $\alpha$ -Syn.

Complex #	Interface area ( $\text{\AA}^2$ )	Solvation Energy (kcal/mol)	Total Binding Energy (kcal/mol)	Hydrophobic P-value	Hydrogen Bonds	Salt Bridges	Disulphide Bonds
# 12b	986.5	-7633	-12.6	0.6641	7	5	0
# 38a	1389	-15.05	-20.17	0.6599	4	9	0
# 58a	1243	-18.92	-21.88	0.4065	5	2	0
# 79a	1303	-16.09	-22.84	0.472	11	5	0
# 114d	1310	-16.55	-21.88	0.5421	12	0	0
# 68c	1582	-16.94	-23.39	0.6159	12	3	0

**Table 3** The bioenergetic and biophysical characteristics of the indicated complexes between SNAP29 and  $\alpha$ -Syn. All complexes exhibit a low total binding energy, thus demonstrating an energetically favorable binding between SNAP29 and  $\alpha$ -Syn.

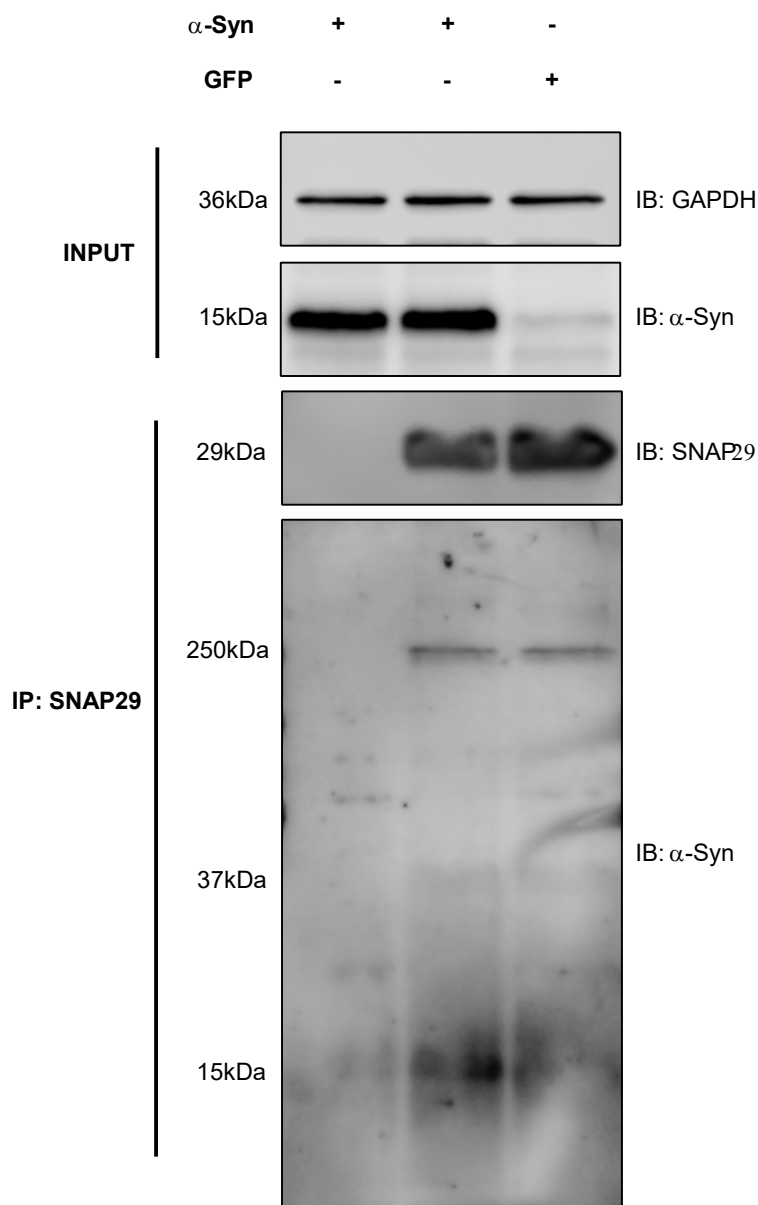


**Figure 24  $\alpha$ -Syn physically interacts with SNAP29 in cultured neurons.** Western blot illustrating the result of a Co-IP with SNAP29 as a bait. Reacting the membrane with an antibody against  $\alpha$ -Syn revealed a clearly visible band in  $\alpha$ -Syn-transduced neurons at around 15 kDa. The left lane represents a negative control (no SNAP29 antibody during IP). Representative result from 3 independent experiments.

### 3.6 SNAP29 is lost from neuromelanin-positive neurons of the human SNc in LBP cases

In addition to experiments in cultured DAergic neurons, we finally investigated the abundance of SNAP29 in SNc DAergic neurons in post-mortem human brain tissue from eleven patients with LBP at different stages and six control cases. Based on the Braak staging and recommendations of Brain Net Europe [93, 145], all cases were checked and staged for LBP by an experienced neuropathologist (**Appendix E**). Next, for SNAP29 quantification, midbrain sections from each case were randomly selected and SNAP29 fluorescent intensity in the cytoplasm of neuromelanin-positive neurons was quantified. For LBP cases, neuromelanin-positive cells in SNc showed a stage-dependent decrease of SNAP29, whereas robust SNAP29 staining was observed in almost all neuromelanin-positive cells in control cases. In addition to the overall reduction, we observed the decreased abundance of SNAP29 to be already present at Braak stage 1, where LBs are per definition restricted to the dorsal motor nucleus of the vagus nerve (DMV). There's no difference in the fixation time of the tissues between the control and LBP group (**Figure 25**). These results imply that the decrease of SNAP29 is an early pathological event during the progression of Lewy pathology in PD that may precede and enhance the appearance of LBs in SNc neurons. Taken together, our results from investigating post-mortem brain tissue demonstrate the validity of our results from cultured cells in patient-derived material.

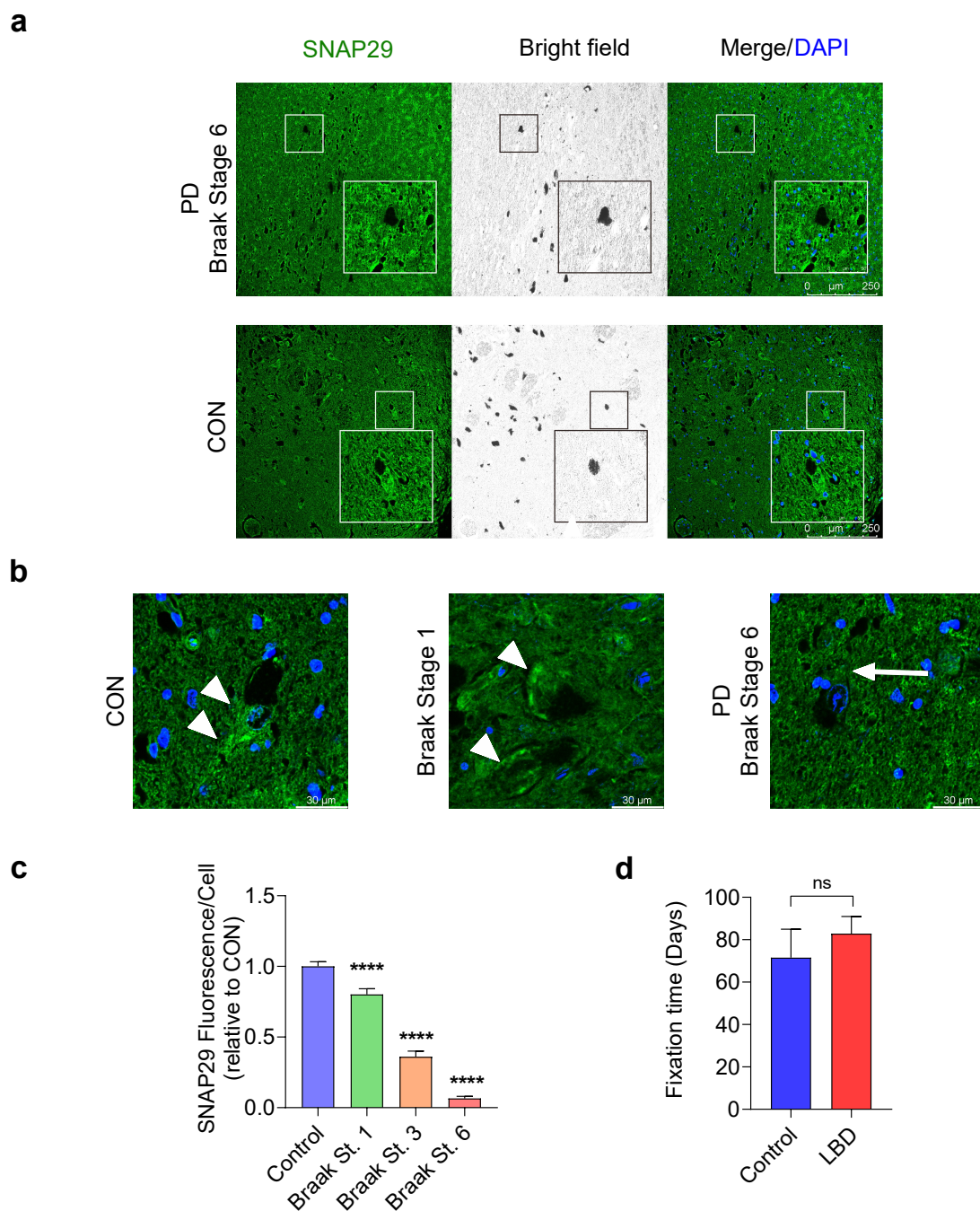


**Figure 25 The abundance of SNAP29 is stage-dependently decreased in neuromelanin-positive neurons from LBP cases.** **a** Representative photomicrograph from immunohistochemical staining of SNc post-mortem brain tissue. Tissue sections were stained with an antibody against SNAP29 (green), revealing a cytoplasmic staining pattern for SNAP29 in neuromelanin-positive neurons. Upper row: Pictures from a PD case

at Braak Stage 6; lower row: pictures from a control case which had no LBP. Insert: 2.5 x magnification. **b** High magnification merged photomicrographs from a control case (left panel), a Braak stage 1 case (middle panel), and a Braak stage 6 PD patient (right panel) and. Note the absence of cytoplasmic SNAP29 fluorescence in PD (arrow), whereas control neurons show a clear cytoplasmic SNAP29 fluorescence signal (arrowhead). The signal of stage 1 case is weaker than that of the control one. **c** Bar graph illustrating a stage-dependent decline of SNAP29 in LBP cases. **d** Bar graph illustrating the fixation time of tissue in control and LBP group. For comparison of the means, a one-way ANOVA with Tukey's post hoc test was used. \*\*\*\* $P < 0.0001$ , ns: no significance; Data are shown as means  $\pm$  SEM.

## 4. Discussion

### 4.1 $\alpha$ -Syn overexpression induces a complex modulation of autophagy

Our results show that  $\alpha$ -Syn overexpression impairs autophagy flux by attenuating autophagolysosome fusion and by inhibiting autophagy initiation. Overexpression of  $\alpha$ -Syn induced a reduced abundance of the v-SNARE protein SNAP29 (**Figure 13**), thus resulting in a SNARE-mediated autophagolysosome fusion defect (**Figure 7, Figure 8**). On the other hand,  $\alpha$ -Syn overexpression activated mTOR complex-associated signaling cascades (**Figure 6**) [12], therefore inhibiting autophagy initiation. In addition, the  $\alpha$ -Syn overexpression related autophagolysosome fusion defect resulted in increased release of EVs. These results suggest a complex modulation of autophagy by  $\alpha$ -Syn overexpression, building on and confirming numerous previous reports, which collectively demonstrate an inhibitory effect of  $\alpha$ -Syn overexpression on autophagy through a number of distinct mechanisms. For example,  $\alpha$ -Syn overexpression damaged autophagy in mammalian cell lines and transgenic mice by inhibiting RAB1A, and resulted in a mislocalization of the early autophagy protein ATG9 and decreased formation of omegasomes, which could be rescued by RAB1A overexpression [146, 147]. A significant increase of autophagic vesicular structures was observed in rat PC12 cell lines expressing the  $\alpha$ -Syn A53T mutant. Besides,  $\alpha$ -Syn aggregates compromised the retrograde transport of autophagosomes [148, 149] and disrupted the activity of the lysosomal aspartyl protease cathepsin D (CTSD) and the autophagic degradation process [64, 150, 151]. A more recent study using PC12 cells demonstrated that overexpressed  $\alpha$ -Syn bound to both cytosolic and nuclear high mobility group box 1 (HMGB1), impaired the cytosolic translocation of HMGB1, blocked HMGB1-Becn1 (BECN1) binding while strengthened BECN1-BCL2 binding.  $\alpha$ -Syn overexpression was reported in a more recent study to



impair the cytosolic translocation of high mobility group box 1 (HMGB1), thereby affects the binding between HMGB1 and Beclin 1 (BECN1) and promotes BECN1-BCL2 binding. Deregulation of these molecular events by  $\alpha$ -Syn overexpression inhibited autophagy, which was restored by BECN1 overexpression and HMGB1 knockdown [70], although this mechanism remains a matter of debate [152, 153].

Moreover, previous research demonstrated an additional role of mTOR not only in autophagy initiation but also for autophagolysosome fusion. UV radiation resistance associated gene (UVRAG) and Rubicon (RUBCN) are two components of the PI3K complex, which acts upstream of mTOR. UVRAG and RUBCN are reported to be involved in autophagolysosome fusion through Rab7 [53, 154, 155], although they appear to have opposite effects: UVRAG promotes autophagolysosome fusion, whereas RUBCN inhibits it [156, 157]. These findings add another layer of complexity to  $\alpha$ -Syn-mediated autophagy manipulation. In summary, the  $\alpha$ -Syn overexpression mediated activation of mTOR-associated pathways would therefore additively contribute to impairing the autophagolysosome fusion but through a mechanism distinct from affecting SNAP29. However, because co-expressing SNAP29 partially rescued the effect of  $\alpha$ -Syn, we favor a mechanism where the impairment of SNARE-dependent autophagolysosome fusion predominates. Future research should address the specific effect of  $\alpha$ -Syn overexpression on the different steps of autophagy flux to dissect the specific consequences.

However, these results should be interpreted with caution, since they are obtained from an artificial cell model. Furthermore, although  $\alpha$ -Syn aggregation is a common feature of both sporadic and familial PD and  $\alpha$ -Syn overexpression leads to aggregation, the  $\alpha$ -Syn overexpression model may not be capable of representing features of sporadic PD. As PD is a complex heterogeneous disease, whether these mechanisms act as a main factor for the initiation or promotion of PD patients remains to be established.

## **4.2 Impaired autophagy and $\alpha$ -Syn accumulation form a bidirectional pathogenic loop in synucleinopathies**

As described above, our results show an impairment of autophagy upon  $\alpha$ -Syn overexpression. A study of aggregated  $\alpha$ -Syn demonstrated a similar result of impaired lysosomal function, and analysis of autophagy-related protein markers suggested a decreased autophagosome clearance [64]. Intriguingly, numerous studies indicated that  $\alpha$ -Syn is degraded by autophagy [158-161] and autophagolysosome inhibition conversely blocked  $\alpha$ -Syn degradation and potentiated its toxicity [62], exacerbated  $\alpha$ -Syn pathology, thus forming a bidirectional pathogenic loop.

For instance, evidence showed the autophagy gene ATG7 deletion in mice midbrain DAergic neurons resulted in p62 and Ub-labeled inclusions and DAergic neuron impairments [72, 75, 162]. In CNS-specific ATG7 knockout mice,  $\alpha$ -Syn was found to accumulate in presynaptic terminals [162]. The conditional knockout of ATG7 in mice DAergic neurons led to locomotor disorders, although the autophagy defect may lead to a compensatory increase in dopamine release [73]. Different from these studies, a recent report by Fussi et al. reported a protective effect of ATG5 knockdown in cultured DAergic neurons [163]. These studies indicate an association between autophagy deficiency or blockade of autophagy flux and  $\alpha$ -Syn pathology, therefore supporting a bidirectional functional interplay between overexpressed  $\alpha$ -Syn and autophagy.

Additional evidence from investigating post-mortem patient-derived tissue likewise support an important role of autophagy for PD, suggesting that the aggregation of  $\alpha$ -Syn may be a consequence of impaired autophagy turnover. In two recent large meta-analyses of genome-wide association studies (GWAS), PD candidate loci were strongly enriched for lysosomal and autophagy functions [164, 165]. In accord, autophagic degeneration was observed in DAergic neurons in the SNc of PD patients [166]. In addition to

$\alpha$ -Syn, lots of autophagy-related proteins were identified in LBs [167, 168], and a recent post-mortem study of PD brains reported organelles and lipid membranes which reminiscent of autophagosomes and lysosomes [169]. Furthermore, in PD the majority of LBs in the SNc were found to be immunoreactive for the autophagy-related protein LC3 [65, 170], and LC3-II levels were also significantly increased in the SNc [166].

In accord with these previous neuropathological results, our own data demonstrate a stage-dependent decline of SNAP29 in post-mortem brain tissue from LBP cases (**Figure 25**). In addition to the overall reduction, we found less SNAP29 at Braak stage 1 as compared to cases that had no LBP. Interestingly, LBs are by definition restricted to neurons of the medulla oblongata such as the dorsal motor nucleus of the vagus nerve at Braak stage 1. Because we found a decline of SNAP29 to be evident at Braak stage 1, these results imply that the decrease of SNAP29 is an early pathological event during the progression of LBP in PD that may precede and enhance the appearance of LBs in SNc neurons. Our results thus add specific insights into the early pathological changes in PD.

According to literature, impairments at various stages of this system result in accumulation and toxicity of  $\alpha$ -Syn. For further studies, it needs more emphasis to find the origin of this vicious cycle, and to address whether cells with  $\alpha$ -Syn accumulation benefit from stimulated autophagy. Our own results from cultured DAergic neurons demonstrated that increasing the generation of LC3B-II-positive autophagosomes, for instance by application of rapamycin, results in incremental cell death in  $\alpha$ -Syn transduced cells (**Figure 19**). Conversely, enhancing autophagy turnover by SNAP29 overexpression decreased  $\alpha$ -Syn overexpression induced cell death (**Figure 20**). Our results thus are consistent with the model where overexpressed  $\alpha$ -Syn augments DAergic neuron cell death by inhibiting autophagosome turnover. These mechanistic insights will support the development of

novel molecular targets to modulate  $\alpha$ -Syn-associated autophagy changes and eventually attenuate cell death in PD.

### **4.3 The potential role of SNAP29 in $\alpha$ -Syn overexpression related autophagy defects**

In the macroautophagy process, autophagosomes ultimately fuse with late endosomes or lysosomes to form amphisomes or autolysosomes, respectively. In accord, experimental research demonstrated that autophagosome-to-lysosomes fusion is vital for neuronal integrity [171]. During the maturation process, autophagosomes will obtain the required molecular machinery to be able to fuse with specific vesicles. In principle, the homotypic fusion is driven by SNARE-complexes. Autophagosome-lysosome fusion is known to be mediated by specific SNARE molecules including STX17, VAMP7/8, SNAP29, STX17, and YKT6 [58, 141, 142]. Notably, previous reports identified two distinct SNARE complexes to mediate autophagosome/lysosome fusion: STX17–SNAP29–VAMP7/8 [58, 171] and YKT6–SNAP29–STX7 [142], thus identifying SNAP29 as a ubiquitous SNARE protein implicated in different pathways of autophagosome/lysosome fusion.

SNAP29 is a member of the Qb/Qc subfamily of SNARE proteins. In vertebrates, this sub-family includes SNAP-23, SNAP-25, SNAP-29, and SNAP-47. Whereas SNAP-23 and SNAP-25 participate in regulated exocytosis, SNAP-29 mediates the autophagosome-lysosome fusion [172]. Our results from investigating the abundance of SNAP23 and SNAP29 demonstrated a reduction for both in  $\alpha$ -Syn-transduced neurons, thus suggesting a family-specific effect of  $\alpha$ -Syn overexpression (**Figure 13**). Future research should address the particular impact of the structural organization of SNAP25 family members for their vulnerability against  $\alpha$ -Syn.

Because qRT-PCR showed gene expression of SNAP29 to be unaffected in  $\alpha$ -Syn-transduced cells (**Figure 13**), our results exclude a transcriptional regulation and instead favor a posttranscriptional effect. Since  $\alpha$ -Syn has been shown to physically interact with synaptic SNARE proteins chaperoning their assembly [144], a possible scenario would be that  $\alpha$ -Syn physically interacts with SNAP29 to facilitate its degradation. Indeed, our protein-protein docking stimulations and Co-IP experiments all suggest  $\alpha$ -Syn to physically interact and bind to SNAP29 in cultured neurons (**Figure 23**, **Figure 24**). However, the specific intermolecular interaction between both molecules and the consequences of such an interaction for the abundance of SNAP29 are yet to be elucidated and warrant further investigation. Future studies should examine if the binding is required for the effect of  $\alpha$ -Syn overexpression on SNAP29 protein abundance and the molecular and structural requirements of such a protein-protein interaction, where the particular molecular domains of SNAP25 family members with dual Qb and Qc SNARE motifs may provide a structural basis for specific binding.

#### **4.4 The “crosstalk” between $\alpha$ -Syn-related autophagy defects and increased release of EVs**

Our results demonstrate an increased release of EVs in  $\alpha$ -Syn-transduced neurons (**Figure 9**). Notably,  $\alpha$ -Syn-mediated EV release was functionally connected to autophagy turnover in cultured neurons, as autophagy induction by rapamycin further increased EV release, mirroring to the effect of blocking autophagy turnover by bafilomycin A1 (**Figure 11**) or SNAP29 knockdown (**Figure 16**). Conversely, enhancing autophagy flux by SNAP29 overexpression led to a reduced abundance of EVs. Taken these results together, they suggest that EV release may compensate for the accumulation of autophag-

gosomes in  $\alpha$ -Syn-transduced cells. In accord,  $\alpha$ -Syn-induced EVs carried increased autophagy-related molecules (**Figure 12**), thus suggesting their generation from amphisomes (MVB/autophagosome hybrid organelles).

Several studies demonstrated a link between the autophagy-lysosome pathway and EV release. For instance, evidence from both mammalian cell and mouse models revealed the conjugation of the ubiquitin-like protein ISG15 to enhance protein degradation, accompanied by reduced MVBs within the cells and exosome release. Conversely, prevention of endosome–lysosome fusion rescued exosome release [173]. Another recent study in the CD63 knockout model showed autophagy to degrade aberrant endocytic vacuoles associated with the loss of CD63, whereas blockage of autophagy degradation partially normalizes CD63 knockout-related exosome biogenesis decrease [174]. Taken together, these and several other reports [175, 176] suggest a model, where autophagosomes fuse with MVBs to produce amphisomes, which can either be degraded by fusing with lysosomes or result in EV release by fusing with the plasma membrane [177].

In addition, the ATPase ion pump ATP13A2 has been shown to maintain the balance between the EVs release of  $\alpha$ -Syn and its autophagic degradation in several neuronal cell lines. On one hand, ATP13A2 loss defects lysosomal function and impairs  $\alpha$ -Syn degradation by downregulation of SYT11, whereas ATP13A2 upregulation reduces  $\alpha$ -Syn overexpression related toxicity [178]. On the other hand, ATP13A2 regulates intraluminal zinc ion levels in MVBs, mediating  $\alpha$ -Syn externalization by EVs release [179].

Evidence showed that EV release may be a compensatory manner for proteotoxic stress alleviation when autophagy or lysosomal function is impaired. For example, studies demonstrated autophagy-dependent  $\alpha$ -Syn release to be enhanced when autophagosome maturation was inhibited by tubulin polymerization-promoting protein (p25 $\alpha$ , or

TPPP) overexpression [180]. Whereas the elevation of  $\alpha$ -Syn secretion through EVs regulated by secretory membrane carrier protein 5 (SCAMP5) overexpression reduced autophagosome–lysosome fusion and lysosomal degradation of  $\alpha$ -Syn [181]. Consistent with our own data (**Figure 11**), evidence showed lysosomal inhibition with bafilomycin A1 to increase EV released  $\alpha$ -Syn in both  $\alpha$ -Syn overexpressing cell and animal model [74, 182]. A more recent study showed an increased number of amphisomes in the cells and increased levels of autophagy-associated proteins in EVs upon lysosomal inhibition [183]. This evidence further supports EV secretion to be utilized as a compensatory manner for cellular waste disposal. Ironically, cellular waste disposed of in such a manner may be taken up by neighbouring neurons, therefore contributing to the propagation of the disease phenotype. Future research should thus specifically address the relevance of the autophagolysosomal SNARE protein SNAP29 for cell-to-cell transmission of  $\alpha$ -Syn aggregates.

In summary, these observations indicate a “crosstalk” between the autophagy-lysosome pathway and EV release. Nevertheless, because of the complexity of the secretion process, additional considerations need to be aware of when applying this model. For instance, when it comes to IL-1 $\beta$  secretion, evidence indicated LC3B-positive IL-1 $\beta$  carrier vesicles may directly fuse with the plasma membrane, since functional MVBs are needed in this process [184], but the autophagosome–lysosome fusion is dispensable [185]. Further in-depth studies are therefore required, in particular in the context of  $\alpha$ -Syn-associated neurodegenerative conditions, where autophagy and EV release appear to be likewise intimately linked.

## 5. Summary

In the present work, we investigated the effect of  $\alpha$ -Syn overexpression on autophagy in cultured human dopaminergic neurons. We found  $\alpha$ -Syn overexpression to impair autophagy turnover by attenuating the fusion of autophagosomes with lysosomes in these cells. Mechanistically,  $\alpha$ -Syn overexpression inhibited autophagolysosome fusion by interacting with and by decreasing the abundance of SNAP29, a key member of the SNARE complex that mediates the fusion of intracellular vesicular compartments. Besides, we found that normalizing SNAP29 attenuates the autophagy defect and rescues cells from  $\alpha$ -Syn toxicity. Furthermore, our results suggest a cross talk between impaired autophagy turnover and increased EVs release, suggesting a possible mode that accumulated  $\alpha$ -Syn promotes the trans-neuronal spreading of its toxic species, which may be involved in the progression of PD.

In addition to investigating cultured cells, we studied SNAP29 protein levels in postmortem brain tissue from cases with different stages of PD. Notably, we found SNAP29 to be likewise lost in neuromelanin-positive SNc neurons of postmortem brain tissue from cases that had LBP, thus demonstrating the validity of our findings in the diseased human CNS. In summary, we therefore believe that our results reveal a novel and previously unknown interaction between  $\alpha$ -Syn and intracellular SNARE proteins and characterize the consequences of such an interaction for autophagy in dopaminergic neurons.



## References

1. Parkinson, J., *An essay on the shaking palsy. 1817.* J Neuropsychiatry Clin Neurosci, 2002. **14**(2): p. 223-36; discussion 222.
2. de Rijk, M.C., et al., *Prevalence of Parkinson's disease in Europe: A collaborative study of population-based cohorts. Neurologic Diseases in the Elderly Research Group.* Neurology, 2000. **54**(11 Suppl 5): p. S21-3.
3. Golbe, L.I., *Young-onset Parkinson's disease: a clinical review.* Neurology, 1991. **41**(2 ( Pt 1)): p. 168-73.
4. Muthane, U.B., et al., *Early onset Parkinson's disease: are juvenile- and young-onset different?* Mov Disord, 1994. **9**(5): p. 539-44.
5. Hely, M.A., et al., *Sydney Multicenter Study of Parkinson's disease: non-L-dopa-responsive problems dominate at 15 years.* Mov Disord, 2005. **20**(2): p. 190-9.
6. Goodarzi, Z., et al., *Detecting depression in Parkinson disease: A systematic review and meta-analysis.* Neurology, 2016. **87**(4): p. 426-37.
7. Parkinson Study, G., *Dopamine transporter brain imaging to assess the effects of pramipexole vs levodopa on Parkinson disease progression.* JAMA, 2002. **287**(13): p. 1653-61.
8. Marshall, V. and D. Grosset, *Role of dopamine transporter imaging in routine clinical practice.* Mov Disord, 2003. **18**(12): p. 1415-23.
9. Whone, A.L., et al., *Slower progression of Parkinson's disease with ropinirole versus levodopa: The REAL-PET study.* Ann Neurol, 2003. **54**(1): p. 93-101.
10. Kitamura, Y., J. Kakimura, and T. Taniguchi, *Antiparkinsonian drugs and their neuroprotective effects.* Biol Pharm Bull, 2002. **25**(3): p. 284-90.
11. Dawson, T.M. and V.L. Dawson, *Neuroprotective and neurorestorative strategies for Parkinson's disease.* Nat Neurosci, 2002. **5 Suppl**: p. 1058-61.
12. Tan, Y., et al., *Loss of fragile X mental retardation protein precedes Lewy pathology in Parkinson's disease.* Acta Neuropathol, 2020. **139**(2): p. 319-345.
13. Del Rey, N.L., et al., *Advances in Parkinson's Disease: 200 Years Later.* Front Neuroanat, 2018. **12**: p. 113.
14. Dauer, W. and S. Przedborski, *Parkinson's disease: mechanisms and models.* Neuron, 2003. **39**(6): p. 889-909.
15. Holdorff, B., *Friedrich Heinrich Lewy (1885-1950) and his work.* J Hist Neurosci, 2002. **11**(1): p. 19-28.
16. Spillantini, M.G., et al., *Alpha-synuclein in Lewy bodies.* Nature, 1997. **388**(6645): p. 839-40.
17. Spillantini, M.G., et al., *alpha-Synuclein in filamentous inclusions of Lewy bodies from Parkinson's disease and dementia with lewy bodies.* Proc Natl Acad Sci U S A, 1998. **95**(11): p. 6469-73.
18. Polymeropoulos, M.H., et al., *Mutation in the alpha-synuclein gene identified in families with Parkinson's disease.* Science, 1997. **276**(5321): p. 2045-7.
19. Clayton, D.F. and J.M. George, *The synucleins: a family of proteins involved in synaptic function, plasticity, neurodegeneration and disease.* Trends Neurosci, 1998. **21**(6): p. 249-54.
20. Ltic, S., et al., *Alpha-synuclein is expressed in different tissues during human fetal development.* J Mol Neurosci, 2004. **22**(3): p. 199-204.

21. Filippini, A., M. Gennarelli, and I. Russo, *alpha-Synuclein and Glia in Parkinson's Disease: A Beneficial or a Detrimental Duet for the Endo-Lysosomal System?* Cell Mol Neurobiol, 2019. **39**(2): p. 161-168.
22. Lykkebo, S. and P.H. Jensen, *Alpha-synuclein and presynaptic function: implications for Parkinson's disease*. Neuromolecular Med, 2002. **2**(2): p. 115-29.
23. Dev, K.K., et al., *Part II: alpha-synuclein and its molecular pathophysiological role in neurodegenerative disease*. Neuropharmacology, 2003. **45**(1): p. 14-44.
24. Giasson, B.I., et al., *A hydrophobic stretch of 12 amino acid residues in the middle of alpha-synuclein is essential for filament assembly*. J Biol Chem, 2001. **276**(4): p. 2380-6.
25. Schmidt, F., et al., *Single-channel electrophysiology reveals a distinct and uniform pore complex formed by alpha-synuclein oligomers in lipid membranes*. PLoS One, 2012. **7**(8): p. e42545.
26. Ganguly, U., et al., *Alpha-synuclein, Proteotoxicity and Parkinson's Disease: Search for Neuroprotective Therapy*. Curr Neuropharmacol, 2018. **16**(7): p. 1086-1097.
27. Conway, K.A., J.D. Harper, and P.T. Lansbury, *Accelerated in vitro fibril formation by a mutant alpha-synuclein linked to early-onset Parkinson disease*. Nat Med, 1998. **4**(11): p. 1318-20.
28. Ghosh, D., et al., *The Parkinson's disease-associated H50Q mutation accelerates alpha-Synuclein aggregation in vitro*. Biochemistry, 2013. **52**(40): p. 6925-7.
29. Greenbaum, E.A., et al., *The E46K mutation in alpha-synuclein increases amyloid fibril formation*. J Biol Chem, 2005. **280**(9): p. 7800-7.
30. Ruf, V.C., et al., *Different Effects of alpha-Synuclein Mutants on Lipid Binding and Aggregation Detected by Single Molecule Fluorescence Spectroscopy and ThT Fluorescence-Based Measurements*. ACS Chem Neurosci, 2019. **10**(3): p. 1649-1659.
31. Kruger, R., et al., *Ala30Pro mutation in the gene encoding alpha-synuclein in Parkinson's disease*. Nat Genet, 1998. **18**(2): p. 106-8.
32. Singleton, A.B., et al., *alpha-Synuclein locus triplication causes Parkinson's disease*. Science, 2003. **302**(5646): p. 841.
33. Zarranz, J.J., et al., *The new mutation, E46K, of alpha-synuclein causes Parkinson and Lewy body dementia*. Ann Neurol, 2004. **55**(2): p. 164-73.
34. Goedert, M., *Familial Parkinson's disease. The awakening of alpha-synuclein*. Nature, 1997. **388**(6639): p. 232-3.
35. Okochi, M., et al., *Constitutive phosphorylation of the Parkinson's disease associated alpha-synuclein*. J Biol Chem, 2000. **275**(1): p. 390-7.
36. Anderson, J.P., et al., *Phosphorylation of Ser-129 is the dominant pathological modification of alpha-synuclein in familial and sporadic Lewy body disease*. J Biol Chem, 2006. **281**(40): p. 29739-52.
37. Visanji, N.P., et al., *alpha-Synuclein-Based Animal Models of Parkinson's Disease: Challenges and Opportunities in a New Era*. Trends Neurosci, 2016. **39**(11): p. 750-762.
38. Baba, M., et al., *Aggregation of alpha-synuclein in Lewy bodies of sporadic Parkinson's disease and dementia with Lewy bodies*. Am J Pathol, 1998. **152**(4): p. 879-84.
39. Braak, H., et al., *Staging of brain pathology related to sporadic Parkinson's disease*. Neurobiol Aging, 2003. **24**(2): p. 197-211.
40. Aarsland, D., et al., *Cognitive decline in Parkinson disease*. Nat Rev Neurol, 2017. **13**(4): p. 217-231.
41. Doty, R.L., *Olfactory dysfunction in Parkinson disease*. Nat Rev Neurol, 2012. **8**(6): p. 329-39.
42. Kordower, J.H., et al., *Lewy body-like pathology in long-term embryonic nigral transplants in Parkinson's disease*. Nat Med, 2008. **14**(5): p. 504-6.

43. Kordower, J.H., et al., *Transplanted dopaminergic neurons develop PD pathologic changes: a second case report*. *Mov Disord*, 2008. **23**(16): p. 2303-6.
44. Li, J.Y., et al., *Lewy bodies in grafted neurons in subjects with Parkinson's disease suggest host-to-graft disease propagation*. *Nat Med*, 2008. **14**(5): p. 501-3.
45. Wakabayashi, K., et al., *Parkinson's disease: an immunohistochemical study of Lewy body-containing neurons in the enteric nervous system*. *Acta Neuropathol*, 1990. **79**(6): p. 581-3.
46. Pan-Montojo, F., et al., *Progression of Parkinson's disease pathology is reproduced by intragastric administration of rotenone in mice*. *PLoS One*, 2010. **5**(1): p. e8762.
47. Holmqvist, S., et al., *Direct evidence of Parkinson pathology spread from the gastrointestinal tract to the brain in rats*. *Acta Neuropathol*, 2014. **128**(6): p. 805-20.
48. Svensson, E., et al., *Vagotomy and subsequent risk of Parkinson's disease*. *Ann Neurol*, 2015. **78**(4): p. 522-9.
49. Klionsky, D.J., *Autophagy revisited: a conversation with Christian de Duve*. *Autophagy*, 2008. **4**(6): p. 740-3.
50. Mizushima, N., et al., *Autophagy fights disease through cellular self-digestion*. *Nature*, 2008. **451**(7182): p. 1069-75.
51. Mizushima, N. and M. Komatsu, *Autophagy: renovation of cells and tissues*. *Cell*, 2011. **147**(4): p. 728-41.
52. Hosokawa, N., et al., *Nutrient-dependent mTORC1 association with the ULK1-Atg13-FIP200 complex required for autophagy*. *Mol Biol Cell*, 2009. **20**(7): p. 1981-91.
53. Tabata, K., et al., *Rubicon and PLEKHM1 negatively regulate the endocytic/autophagic pathway via a novel Rab7-binding domain*. *Mol Biol Cell*, 2010. **21**(23): p. 4162-72.
54. McEwan, D.G., et al., *PLEKHM1 regulates autophagosome-lysosome fusion through HOPS complex and LC3/GABARAP proteins*. *Mol Cell*, 2015. **57**(1): p. 39-54.
55. Tian, X., J. Teng, and J. Chen, *New insights regarding SNARE proteins in autophagosome-lysosome fusion*. *Autophagy*, 2020: p. 1-9.
56. Itoh, T., et al., *OATL1, a novel autophagosome-resident Rab33B-GAP, regulates autophagosomal maturation*. *J Cell Biol*, 2011. **192**(5): p. 839-53.
57. Diao, J., et al., *ATG14 promotes membrane tethering and fusion of autophagosomes to endolysosomes*. *Nature*, 2015. **520**(7548): p. 563-6.
58. Itakura, E., C. Kishi-Itakura, and N. Mizushima, *The hairpin-type tail-anchored SNARE syntaxin 17 targets to autophagosomes for fusion with endosomes/lysosomes*. *Cell*, 2012. **151**(6): p. 1256-69.
59. Davis, S., J. Wang, and S. Ferro-Novick, *Crosstalk between the Secretory and Autophagy Pathways Regulates Autophagosome Formation*. *Dev Cell*, 2017. **41**(1): p. 23-32.
60. Ponpuak, M., et al., *Secretory autophagy*. *Curr Opin Cell Biol*, 2015. **35**: p. 106-16.
61. Martinez-Vicente, M. and A.M. Cuervo, *Autophagy and neurodegeneration: when the cleaning crew goes on strike*. *Lancet Neurol*, 2007. **6**(4): p. 352-61.
62. Klucken, J., et al., *Alpha-synuclein aggregation involves a bafilomycin A 1-sensitive autophagy pathway*. *Autophagy*, 2012. **8**(5): p. 754-66.
63. Ebrahimi-Fakhari, D., et al., *Distinct roles in vivo for the ubiquitin-proteasome system and the autophagy-lysosomal pathway in the degradation of alpha-synuclein*. *J Neurosci*, 2011. **31**(41): p. 14508-20.
64. Hoffmann, A.C., et al., *Extracellular aggregated alpha synuclein primarily triggers lysosomal dysfunction in neural cells prevented by trehalose*. *Sci Rep*, 2019. **9**(1): p. 544.
65. Tanji, K., et al., *Alteration of autophagosomal proteins (LC3, GABARAP and GATE-16) in Lewy body disease*. *Neurobiol Dis*, 2011. **43**(3): p. 690-7.

66. Alvarez-Erviti, L., et al., *Chaperone-mediated autophagy markers in Parkinson disease brains*. Arch Neurol, 2010. **67**(12): p. 1464-72.
67. Arotcarena, M.L., et al., *Transcription factor EB overexpression prevents neurodegeneration in experimental synucleinopathies*. JCI Insight, 2019. **4**(16).
68. Decressac, M., et al., *TFEB-mediated autophagy rescues midbrain dopamine neurons from alpha-synuclein toxicity*. Proc Natl Acad Sci U S A, 2013. **110**(19): p. E1817-26.
69. Lei, Z., G. Cao, and G. Wei, *A30P mutant alpha-synuclein impairs autophagic flux by inactivating JNK signaling to enhance ZKSCAN3 activity in midbrain dopaminergic neurons*. Cell Death Dis, 2019. **10**(2): p. 133.
70. Song, J.X., et al., *HMGB1 is involved in autophagy inhibition caused by SNCA/alpha-synuclein overexpression: a process modulated by the natural autophagy inducer corynoxine B*. Autophagy, 2014. **10**(1): p. 144-54.
71. Torra, A., et al., *Overexpression of TFEB Drives a Pleiotropic Neurotrophic Effect and Prevents Parkinson's Disease-Related Neurodegeneration*. Mol Ther, 2018. **26**(6): p. 1552-1567.
72. Ahmed, I., et al., *Development and characterization of a new Parkinson's disease model resulting from impaired autophagy*. J Neurosci, 2012. **32**(46): p. 16503-9.
73. Hunn, B.H.M., et al., *Impairment of Macroautophagy in Dopamine Neurons Has Opposing Effects on Parkinsonian Pathology and Behavior*. Cell Rep, 2019. **29**(4): p. 920-931 e7.
74. Poehler, A.M., et al., *Autophagy modulates SNCA/alpha-synuclein release, thereby generating a hostile microenvironment*. Autophagy, 2014. **10**(12): p. 2171-92.
75. Sato, S., et al., *Loss of autophagy in dopaminergic neurons causes Lewy pathology and motor dysfunction in aged mice*. Sci Rep, 2018. **8**(1): p. 2813.
76. Zaborowski, M.P., et al., *Extracellular Vesicles: Composition, Biological Relevance, and Methods of Study*. Bioscience, 2015. **65**(8): p. 783-797.
77. Thery, C., L. Zitvogel, and S. Amigorena, *Exosomes: composition, biogenesis and function*. Nat Rev Immunol, 2002. **2**(8): p. 569-79.
78. Vlassov, A.V., et al., *Exosomes: current knowledge of their composition, biological functions, and diagnostic and therapeutic potentials*. Biochim Biophys Acta, 2012. **1820**(7): p. 940-8.
79. Eirin, A., et al., *MicroRNA and mRNA cargo of extracellular vesicles from porcine adipose tissue-derived mesenchymal stem cells*. Gene, 2014. **551**(1): p. 55-64.
80. Huang, X., et al., *Characterization of human plasma-derived exosomal RNAs by deep sequencing*. BMC Genomics, 2013. **14**: p. 319.
81. Mittelbrunn, M., et al., *Unidirectional transfer of microRNA-loaded exosomes from T cells to antigen-presenting cells*. Nat Commun, 2011. **2**: p. 282.
82. Ridder, K., et al., *Extracellular vesicle-mediated transfer of genetic information between the hematopoietic system and the brain in response to inflammation*. PLoS Biol, 2014. **12**(6): p. e1001874.
83. Raposo, G., et al., *Accumulation of major histocompatibility complex class II molecules in mast cell secretory granules and their release upon degranulation*. Mol Biol Cell, 1997. **8**(12): p. 2631-45.
84. Zitvogel, L., et al., *Eradication of established murine tumors using a novel cell-free vaccine: dendritic cell-derived exosomes*. Nat Med, 1998. **4**(5): p. 594-600.
85. Chiasserini, D., et al., *Proteomic analysis of cerebrospinal fluid extracellular vesicles: a comprehensive dataset*. J Proteomics, 2014. **106**: p. 191-204.
86. Fruhbeis, C., et al., *Neurotransmitter-triggered transfer of exosomes mediates oligodendrocyte-neuron communication*. PLoS Biol, 2013. **11**(7): p. e1001604.

87. Frohlich, D., et al., *Multifaceted effects of oligodendroglial exosomes on neurons: impact on neuronal firing rate, signal transduction and gene regulation*. Philos Trans R Soc Lond B Biol Sci, 2014. **369**(1652).
88. Guitart, K., et al., *Improvement of neuronal cell survival by astrocyte-derived exosomes under hypoxic and ischemic conditions depends on prion protein*. Glia, 2016. **64**(6): p. 896-910.
89. Dickens, A.M., et al., *Astrocyte-shed extracellular vesicles regulate the peripheral leukocyte response to inflammatory brain lesions*. Sci Signal, 2017. **10**(473).
90. Kumar, A., et al., *Microglial-derived microparticles mediate neuroinflammation after traumatic brain injury*. J Neuroinflammation, 2017. **14**(1): p. 47.
91. Chartier-Harlin, M.C., et al., *Alpha-synuclein locus duplication as a cause of familial Parkinson's disease*. Lancet, 2004. **364**(9440): p. 1167-9.
92. Nalls, M.A., et al., *Large-scale meta-analysis of genome-wide association data identifies six new risk loci for Parkinson's disease*. Nat Genet, 2014. **46**(9): p. 989-93.
93. Braak, H. and K. Del Tredici, *Neuropathological Staging of Brain Pathology in Sporadic Parkinson's disease: Separating the Wheat from the Chaff*. J Parkinsons Dis, 2017. **7**(s1): p. S71-S85.
94. Goedert, M., et al., *100 years of Lewy pathology*. Nat Rev Neurol, 2013. **9**(1): p. 13-24.
95. Jellinger, K.A., *A critical evaluation of current staging of alpha-synuclein pathology in Lewy body disorders*. Biochim Biophys Acta, 2009. **1792**(7): p. 730-40.
96. Jellinger, K.A., *Neuropathology and pathogenesis of extrapyramidal movement disorders: a critical update-I. Hypokinetic-rigid movement disorders*. J Neural Transm (Vienna), 2019. **126**(8): p. 933-995.
97. Bieri, G., A.D. Gitler, and M. Brahic, *Internalization, axonal transport and release of fibrillar forms of alpha-synuclein*. Neurobiol Dis, 2018. **109**(Pt B): p. 219-225.
98. Lopes da Fonseca, T., A. Villar-Pique, and T.F. Outeiro, *The Interplay between Alpha-Synuclein Clearance and Spreading*. Biomolecules, 2015. **5**(2): p. 435-71.
99. Prusiner, S.B., *Novel proteinaceous infectious particles cause scrapie*. Science, 1982. **216**(4542): p. 136-44.
100. Polanco, J.C., et al., *Exosomes taken up by neurons hijack the endosomal pathway to spread to interconnected neurons*. Acta Neuropathol Commun, 2018. **6**(1): p. 10.
101. Saman, S., et al., *Exosome-associated tau is secreted in tauopathy models and is selectively phosphorylated in cerebrospinal fluid in early Alzheimer disease*. J Biol Chem, 2012. **287**(6): p. 3842-9.
102. Sardar Sinha, M., et al., *Alzheimer's disease pathology propagation by exosomes containing toxic amyloid-beta oligomers*. Acta Neuropathol, 2018. **136**(1): p. 41-56.
103. Shi, M., et al., *Plasma exosomal alpha-synuclein is likely CNS-derived and increased in Parkinson's disease*. Acta Neuropathol, 2014. **128**(5): p. 639-650.
104. Thompson, A.G., et al., *Extracellular vesicles in neurodegenerative disease - pathogenesis to biomarkers*. Nat Rev Neurol, 2016. **12**(6): p. 346-57.
105. Spencer, B., et al., *alpha-Synuclein interferes with the ESCRT-III complex contributing to the pathogenesis of Lewy body disease*. Hum Mol Genet, 2016. **25**(6): p. 1100-15.
106. Tsunemi, T., K. Hamada, and D. Krainc, *ATP13A2/PARK9 regulates secretion of exosomes and alpha-synuclein*. J Neurosci, 2014. **34**(46): p. 15281-7.
107. Kunadt, M., et al., *Extracellular vesicle sorting of alpha-Synuclein is regulated by sumoylation*. Acta Neuropathol, 2015. **129**(5): p. 695-713.
108. Emmanouilidou, E., et al., *Cell-produced alpha-synuclein is secreted in a calcium-dependent manner by exosomes and impacts neuronal survival*. J Neurosci, 2010. **30**(20): p. 6838-51.

109. Danzer, K.M., et al., *Exosomal cell-to-cell transmission of alpha synuclein oligomers*. Mol Neurodegener, 2012. **7**: p. 42.
110. Stuenkel, A., et al., *Induction of alpha-synuclein aggregate formation by CSF exosomes from patients with Parkinson's disease and dementia with Lewy bodies*. Brain, 2016. **139**(Pt 2): p. 481-94.
111. Bruch, J., et al., *PERK activation mitigates tau pathology in vitro and in vivo*. EMBO Mol Med, 2017. **9**(3): p. 371-384.
112. Scholz, D., et al., *Rapid, complete and large-scale generation of post-mitotic neurons from the human LUHMES cell line*. J Neurochem, 2011. **119**(5): p. 957-71.
113. Klockenbusch, C. and J. Kast, *Optimization of formaldehyde cross-linking for protein interaction analysis of non-tagged integrin beta1*. J Biomed Biotechnol, 2010. **2010**: p. 927585.
114. Wang, G., et al., *Tyramide signal amplification method in multiple-label immunofluorescence confocal microscopy*. Methods, 1999. **18**(4): p. 459-64.
115. Ulmer, T.S., et al., *Structure and dynamics of micelle-bound human alpha-synuclein*. J Biol Chem, 2005. **280**(10): p. 9595-603.
116. Kim, D.E., D. Chivian, and D. Baker, *Protein structure prediction and analysis using the Robetta server*. Nucleic Acids Res, 2004. **32**(Web Server issue): p. W526-31.
117. Raman, S., et al., *Structure prediction for CASP8 with all-atom refinement using Rosetta*. Proteins, 2009. **77 Suppl 9**: p. 89-99.
118. Song, Y., et al., *High-resolution comparative modeling with RosettaCM*. Structure, 2013. **21**(10): p. 1735-42.
119. Chaudhury, S., S. Lyskov, and J.J. Gray, *PyRosetta: a script-based interface for implementing molecular modeling algorithms using Rosetta*. Bioinformatics, 2010. **26**(5): p. 689-91.
120. Conway, P., et al., *Relaxation of backbone bond geometry improves protein energy landscape modeling*. Protein Sci, 2014. **23**(1): p. 47-55.
121. Khatib, F., et al., *Algorithm discovery by protein folding game players*. Proc Natl Acad Sci U S A, 2011. **108**(47): p. 18949-53.
122. Nivon, L.G., R. Moretti, and D. Baker, *A Pareto-optimal refinement method for protein design scaffolds*. PLoS One, 2013. **8**(4): p. e59004.
123. Tyka, M.D., et al., *Alternate states of proteins revealed by detailed energy landscape mapping*. J Mol Biol, 2011. **405**(2): p. 607-18.
124. Laskowski, R.A., et al., *AQUA and PROCHECK-NMR: programs for checking the quality of protein structures solved by NMR*. J Biomol NMR, 1996. **8**(4): p. 477-86.
125. Eisenberg, D., R. Luthy, and J.U. Bowie, *VERIFY3D: assessment of protein models with three-dimensional profiles*. Methods Enzymol, 1997. **277**: p. 396-404.
126. Colovos, C. and T.O. Yeates, *Verification of protein structures: patterns of nonbonded atomic interactions*. Protein Sci, 1993. **2**(9): p. 1511-9.
127. Sippl, M.J., *Recognition of errors in three-dimensional structures of proteins*. Proteins, 1993. **17**(4): p. 355-62.
128. Wiederstein, M. and M.J. Sippl, *ProSA-web: interactive web service for the recognition of errors in three-dimensional structures of proteins*. Nucleic Acids Res, 2007. **35**(Web Server issue): p. W407-10.
129. Torchala, M. and P.A. Bates, *Predicting the structure of protein-protein complexes using the SwarmDock Web Server*. Methods Mol Biol, 2014. **1137**: p. 181-97.
130. Torchala, M., et al., *A Markov-chain model description of binding funnels to enhance the ranking of docked solutions*. Proteins, 2013. **81**(12): p. 2143-9.

131. Torchala, M., et al., *SwarmDock: a server for flexible protein-protein docking*. Bioinformatics, 2013. **29**(6): p. 807-9.
132. Krissinel, E., *Crystal contacts as nature's docking solutions*. J Comput Chem, 2010. **31**(1): p. 133-43.
133. Krissinel, E., *Stock-based detection of protein oligomeric states in jsPISA*. Nucleic Acids Res, 2015. **43**(W1): p. W314-9.
134. Di Nardo, A., et al., *Neuronal Tsc1/2 complex controls autophagy through AMPK-dependent regulation of ULK1*. Hum Mol Genet, 2014. **23**(14): p. 3865-74.
135. Jang, M., et al., *AMPK contributes to autophagosome maturation and lysosomal fusion*. Sci Rep, 2018. **8**(1): p. 12637.
136. Kim, J., et al., *AMPK and mTOR regulate autophagy through direct phosphorylation of Ulk1*. Nat Cell Biol, 2011. **13**(2): p. 132-41.
137. Bjorkoy, G., et al., *p62/SQSTM1 forms protein aggregates degraded by autophagy and has a protective effect on huntingtin-induced cell death*. J Cell Biol, 2005. **171**(4): p. 603-14.
138. Klionsky, D.J., et al., *Guidelines for the use and interpretation of assays for monitoring autophagy (3rd edition)*. Autophagy, 2016. **12**(1): p. 1-222.
139. Guo, B., et al., *O-GlcNAc-modification of SNAP-29 regulates autophagosome maturation*. Nat Cell Biol, 2014. **16**(12): p. 1215-26.
140. Hamasaki, M., et al., *Autophagosomes form at ER-mitochondria contact sites*. Nature, 2013. **495**(7441): p. 389-93.
141. Jiang, P., et al., *The HOPS complex mediates autophagosome-lysosome fusion through interaction with syntaxin 17*. Mol Biol Cell, 2014. **25**(8): p. 1327-37.
142. Matsui, T., et al., *Autophagosomal YKT6 is required for fusion with lysosomes independently of syntaxin 17*. J Cell Biol, 2018. **217**(8): p. 2633-2645.
143. Burre, J., M. Sharma, and T.C. Sudhof, *Cell Biology and Pathophysiology of alpha-Synuclein*. Cold Spring Harb Perspect Med, 2018. **8**(3).
144. Burre, J., et al., *Alpha-synuclein promotes SNARE-complex assembly in vivo and in vitro*. Science, 2010. **329**(5999): p. 1663-7.
145. Braak, H. and K. Del Tredici, *Neuroanatomy and pathology of sporadic Parkinson's disease*. Adv Anat Embryol Cell Biol, 2009. **201**: p. 1-119.
146. Stefanis, L., et al., *Expression of A53T mutant but not wild-type alpha-synuclein in PC12 cells induces alterations of the ubiquitin-dependent degradation system, loss of dopamine release, and autophagic cell death*. J Neurosci, 2001. **21**(24): p. 9549-60.
147. Winslow, A.R., et al., *alpha-Synuclein impairs macroautophagy: implications for Parkinson's disease*. J Cell Biol, 2010. **190**(6): p. 1023-37.
148. Volpicelli-Daley, L.A., et al., *Formation of alpha-synuclein Lewy neurite-like aggregates in axons impedes the transport of distinct endosomes*. Mol Biol Cell, 2014. **25**(25): p. 4010-23.
149. Tanik, S.A., et al., *Lewy body-like alpha-synuclein aggregates resist degradation and impair macroautophagy*. J Biol Chem, 2013. **288**(21): p. 15194-210.
150. Dinter, E., et al., *Rab7 induces clearance of alpha-synuclein aggregates*. J Neurochem, 2016. **138**(5): p. 758-74.
151. Moors, T.E., et al., *Subcellular orchestration of alpha-synuclein variants in Parkinson's disease brains revealed by 3D multicolor STED microscopy*. bioRxiv, 2019.
152. Koch, J.C., et al., *Alpha-Synuclein affects neurite morphology, autophagy, vesicle transport and axonal degeneration in CNS neurons*. Cell Death Dis, 2015. **6**: p. e1811.

153. Oliveira, L.M., et al., *Elevated alpha-synuclein caused by SNCA gene triplication impairs neuronal differentiation and maturation in Parkinson's patient-derived induced pluripotent stem cells*. Cell Death Dis, 2015. **6**: p. e1994.
154. Liang, C., et al., *Beclin1-binding UVRAG targets the class C Vps complex to coordinate autophagosome maturation and endocytic trafficking*. Nat Cell Biol, 2008. **10**(7): p. 776-87.
155. Matsunaga, K., et al., *Two Beclin 1-binding proteins, Atg14L and Rubicon, reciprocally regulate autophagy at different stages*. Nat Cell Biol, 2009. **11**(4): p. 385-96.
156. Sun, Q., et al., *The RUN domain of rubicon is important for hVps34 binding, lipid kinase inhibition, and autophagy suppression*. J Biol Chem, 2011. **286**(1): p. 185-91.
157. Kim, Y.M., et al., *mTORC1 phosphorylates UVRAG to negatively regulate autophagosome and endosome maturation*. Mol Cell, 2015. **57**(2): p. 207-18.
158. Yan, J.Q., et al., *E46K Mutant alpha-Synuclein Is Degraded by Both Proteasome and Macroautophagy Pathway*. Molecules, 2018. **23**(11).
159. Webb, J.L., et al., *Alpha-Synuclein is degraded by both autophagy and the proteasome*. J Biol Chem, 2003. **278**(27): p. 25009-13.
160. Vogiatzi, T., et al., *Wild type alpha-synuclein is degraded by chaperone-mediated autophagy and macroautophagy in neuronal cells*. J Biol Chem, 2008. **283**(35): p. 23542-56.
161. Sarkar, S., et al., *Trehalose, a novel mTOR-independent autophagy enhancer, accelerates the clearance of mutant huntingtin and alpha-synuclein*. J Biol Chem, 2007. **282**(8): p. 5641-52.
162. Friedman, L.G., et al., *Disrupted autophagy leads to dopaminergic axon and dendrite degeneration and promotes presynaptic accumulation of alpha-synuclein and LRRK2 in the brain*. J Neurosci, 2012. **32**(22): p. 7585-93.
163. Fussi, N., et al., *Exosomal secretion of alpha-synuclein as protective mechanism after upstream blockage of macroautophagy*. Cell Death Dis, 2018. **9**(7): p. 757.
164. Nalls, M.A., et al., *Identification of novel risk loci, causal insights, and heritable risk for Parkinson's disease: a meta-analysis of genome-wide association studies*. Lancet Neurol, 2019. **18**(12): p. 1091-1102.
165. Chang, D., et al., *A meta-analysis of genome-wide association studies identifies 17 new Parkinson's disease risk loci*. Nat Genet, 2017. **49**(10): p. 1511-1516.
166. Anglade, P., et al., *Apoptosis and autophagy in nigral neurons of patients with Parkinson's disease*. Histochem J, 1997. **29**(1): p. 25-31.
167. Xia, Q., et al., *Proteomic identification of novel proteins associated with Lewy bodies*. Front Biosci, 2008. **13**: p. 3850-6.
168. Wakabayashi, K., et al., *The Lewy body in Parkinson's disease and related neurodegenerative disorders*. Mol Neurobiol, 2013. **47**(2): p. 495-508.
169. Shahmoradian, S.H., et al., *Lewy pathology in Parkinson's disease consists of crowded organelles and lipid membranes*. Nat Neurosci, 2019. **22**(7): p. 1099-1109.
170. Dehay, B., et al., *Pathogenic lysosomal depletion in Parkinson's disease*. J Neurosci, 2010. **30**(37): p. 12535-44.
171. Takats, S., et al., *Autophagosomal Syntaxin17-dependent lysosomal degradation maintains neuronal function in Drosophila*. J Cell Biol, 2013. **201**(4): p. 531-9.
172. Kadkova, A., J. Radecke, and J.B. Sorensen, *The SNAP-25 Protein Family*. Neuroscience, 2019. **420**: p. 50-71.
173. Villarroja-Beltri, C., et al., *ISGylation controls exosome secretion by promoting lysosomal degradation of MVB proteins*. Nat Commun, 2016. **7**: p. 13588.



174. Hurwitz, S.N., et al., *Tetraspanin CD63 Bridges Autophagic and Endosomal Processes To Regulate Exosomal Secretion and Intracellular Signaling of Epstein-Barr Virus LMP1*. J Virol, 2018. **92**(5).
175. Patel, K.K., et al., *Autophagy proteins control goblet cell function by potentiating reactive oxygen species production*. EMBO J, 2013. **32**(24): p. 3130-44.
176. Chen, Y.D., et al., *Exophagy of annexin A2 via RAB11, RAB8A and RAB27A in IFN-gamma-stimulated lung epithelial cells*. Sci Rep, 2017. **7**(1): p. 5676.
177. Xu, J., R. Camfield, and S.M. Gorski, *The interplay between exosomes and autophagy - partners in crime*. J Cell Sci, 2018. **131**(15).
178. Bento, C.F., et al., *The Parkinson's disease-associated genes ATP13A2 and SYT11 regulate autophagy via a common pathway*. Nat Commun, 2016. **7**: p. 11803.
179. Kong, S.M., et al., *Parkinson's disease-linked human PARK9/ATP13A2 maintains zinc homeostasis and promotes alpha-Synuclein externalization via exosomes*. Hum Mol Genet, 2014. **23**(11): p. 2816-33.
180. Ejlerskov, P., et al., *Tubulin polymerization-promoting protein (TPPP/p25alpha) promotes unconventional secretion of alpha-synuclein through exophagy by impairing autophagosome-lysosome fusion*. J Biol Chem, 2013. **288**(24): p. 17313-35.
181. Yang, Y., et al., *Secretory carrier membrane protein 5 is an autophagy inhibitor that promotes the secretion of alpha-synuclein via exosome*. PLoS One, 2017. **12**(7): p. e0180892.
182. Alvarez-Erviti, L., et al., *Lysosomal dysfunction increases exosome-mediated alpha-synuclein release and transmission*. Neurobiol Dis, 2011. **42**(3): p. 360-7.
183. Minakaki, G., et al., *Autophagy inhibition promotes SNCA/alpha-synuclein release and transfer via extracellular vesicles with a hybrid autophagosome-exosome-like phenotype*. Autophagy, 2018. **14**(1): p. 98-119.
184. Zhang, M., et al., *Translocation of interleukin-1beta into a vesicle intermediate in autophagy-mediated secretion*. Elife, 2015. **4**.
185. Kimura, T., et al., *Dedicated SNAREs and specialized TRIM cargo receptors mediate secretory autophagy*. EMBO J, 2017. **36**(1): p. 42-60.

## Appendix A: Cell Culture Materials and Regents

Material	Cat. Num.	Supplier
Thermo Scientific™ Nunc™ EasYFlask™ Cell Culture Flasks		
Nunc EasYFlask 75cm <sup>2</sup>	10364131	Thermo Fisher Scientific
Nunc EasYFlask 25cm <sup>2</sup>	12034917	
Thermo Scientific™ Nunc™ Cell-Culture Treated Multidishes		
6-Well Cell Culture Dish	10119831	Thermo Fisher Scientific
12-Well Cell Culture Dish	10098870	
24-Well Cell Culture Dish	10604903	
48-Well Cell Culture Dish	10644901	
100mm Cell Culture Dish	10508921	
Stericup Quick Release-GP Sterile Vacuum Filtration System		
Stericup-GP 250mL	S2GPU02RE	Millipore
Stericup-GP 500mL	S2GPU05RE	
Poly-L-ornithine solution	P4957	Sigma-Aldrich
Bovine fibronectin	1030-FN	Bio-Techne
Dulbecco's Modified Eagle's Medium/Nutrient Mixture F-12 Ham (DMEM/F-12)	D8062	Sigma-Aldrich
N-2 Supplement (100X)	17502048	Thermo Fisher Scientific
Recombinant Human FGF-basic (154 a.a.)	100-18B	PeproTech
Tetracycline hydrochloride	T7660	Sigma-Aldrich
N6,2'-O-Dibutyryl adenosine 3',5'-cyclic monophosphate sodium salt (Dibutyryl cyclic-AMP)	D0627	Sigma-Aldrich
Recombinant Human GDNF Protein	212-GD	Bio-Techne
Dulbecco's phosphate-buffered saline (DPBS), no calcium, no magnesium	14190169	Thermo Fisher Scientific
Fetal Bovine Serum (FBS/FCS)	F9665	Sigma-Aldrich
Trypsin-EDTA solution	T3924	Sigma-Aldrich
Trypan Blue solution	T8154	Sigma-Aldrich
Bafilomycin A1	B1793	Sigma-Aldrich
Rapamycin	R0395	Sigma-Aldrich
Premo™ Autophagy Tandem Sensor RFP-GFP-LC3B Kit	P36239	Thermo Fisher Scientific

## Appendix B: Buffers and Solutions

Buffer	Components	Supplier (Cat. Num)
RIPA Buffer	25 mM Tris	Roth (4855.2)
	150 mM NaCl	Sigma (S9888)
	0.1% (w/v) SDS	Roth (2326.2)
	0.5% (w/v) sodium deoxycholate	Sigma (D6750)
	1% (v/v) Triton X-100	Sigma (93443)
	pH 7.4	
Tris-Glycine Running Buffer	25 mM Tris	Roth (4855.2)
	192 mM Glycine	Roth (3908.3)
	0.1% (w/v) SDS	Roth (2326.2)
	pH 8.3	
Transfer Buffer	25 mM Tris	Roth (4855.2)
	192 mM Glycine	Roth (3908.3)
	pH 8.3	
Tris-buffered saline with Tween 20 (TBS-T)	10 mM Tris	Roth (4855.2)
	137 mM NaCl	Sigma (S9888)
	0.05% (v/v) Tween-20	Sigma (P1379)
	pH 7.3	
Stripping Buffer	62.5 mM Tris-HCL	Sigma (T3253)
	2% (w/v) SDS	Roth (2326.2)
	pH 6.8	
	Add 0.8% (v/v) $\beta$ -mercaptoethanol before use	Sigma (M6250)
Phosphate buffered saline (PBS)	8mM Na <sub>2</sub> HPO <sub>4</sub>	Roth (P030.2)
	1.5mM KH <sub>2</sub> PO <sub>4</sub>	Roth (3904.1)
	137mM NaCl	Sigma (S9888)
	2.7mM KCl	Roth (6781.1)
	pH 7.4	
TE Buffer	50 mM Tris	Roth (4855.2)
	1 mM EDTA	Roth (8040.1)
	0.5% (v/v) Triton X-100	Sigma (93443)
	pH 8.0	
Formaldehyde solution	4% (w/v) Paraformaldehyde (For autophagy reporter assay)	Roth (0335.4)
	1% (w/v) Paraformaldehyde (For co-IP assay)	Roth (0335.4)
	Dissolve in DPBS	Thermo Fisher (14190169)
	pH 6.9	
Glycine solution	1.25M Glycine	Roth (3908.3)
	Filter sterilize (0.22 $\mu$ m)	

## Appendix C: Antibodies

Antibody	Cat. No.	Application	Dilution	Supplier
AKT	9272S	WB	1:1000	Cell Signaling Technology
Alix (E6P9B)	92880S	WB	1:500	Cell Signaling Technology
Alpha-synuclein (14H2L1)	701085	WB for co-IP	1:500	Thermo Fisher Scientific
Alpha-synuclein (C-20)	sc-7011-R	WB	1:1000	Santa Cruz
CD81 (B-11)	sc-166029	WB	1:500	Santa Cruz
Flotillin-1 (D2V7J)	18634S	WB	1:500	Cell Signaling Technology
GAPDH (6C5)	sc-32233	WB	1:1000	Santa Cruz
LC3B (D11)	3868S	WB	1:1000	Cell Signaling Technology
Phospho-Akt (Ser473)	9271S	WB	1:1000	Cell Signaling Technology
Phospho-S6 Ribosomal Protein Ser240/244	2215S	WB	1:1000	Cell Signaling Technology
S6 Ribosomal Protein (5G10)	2217S	WB	1:1000	Cell Signaling Technology
SNAP29	MAB7869	WB	1:250	R&D Systems
SNAP29	MAB7869	IHC	1:50	R&D Systems
SNAP29 [EPR9198(2)]	ab181151	co-IP	1:50	Abcam
SQSTM1/p62 (D5L7G)	88588S	WB	1:500	Cell Signaling Technology
Syntaxin 17 (D3D7H)	31261S	WB	1:1000	Cell Signaling Technology
VAMP8	13060S	WB	1:1000	Cell Signaling Technology
YKT6	PA5-56565	WB	1:1000	Thermo Fisher Scientific
Horse Anti-Mouse IgG Antibody (H+L), Biotinylated	Provided in PK-4002	IHC	1:200	Vector
Peroxidase Labeled Goat anti-Mouse IgG H+L	PI-2000	WB	1:5000	Vector
Peroxidase Labeled Goat anti-Rabbit IgG H&L	PI-1000	WB	1:5000	Vector

## Appendix D: PCR Primers

Gene		Primer	Sequence 5' to 3'
SNAP29	Synaptosomal-associated protein, 29kDa	Forward Primer	TCATGTACGAGTCCGAGAAGG
		Reverse Primer	CCCAAACACGCTCTTAATGCTAT
RPL22	Ribosomal protein L22	Forward Primer	CACGAAGGAGGAGTGACTGG
		Reverse Primer	TGTGGCACACCACTGACATT
GPBP1	GC-rich promotor binding protein 1	Forward Primer	ATCATTCGGTCTTCAACCTTCC
		Reverse Primer	ATCCTCAGTTAAGGGAGCACA
GAPDH	Glyceraldehyde-3-phosphate dehydrogenase	Forward Primer	TCGGAGTCAACGGATTTGGT
		Reverse Primer	CCTGGAAGATGGTGATGGGA
ACTB	Actin beta	Forward Primer	TCACCAACTGGGACGACATG
		Reverse Primer	GAGGCGTACAGGGATAGCAC

## Appendix E: Information of Human Brain Samples

	Case #	Braak Stage	Age at Disease Onset (yrs.)	Clinical Symptoms	Age at Death (yrs.)	Sex	Tissue Fixation Time (days)
<b>LBD</b>	1	5	unknown	PD, D, Dep	82	f	83
	3	6	unknown	PD	86	f	71
	4	3	n.a.	-	54	m	83
	5	3	unknown	PD	58	m	103
	7	6	65	PD	82	m	42
	8	6	49	PD, D	69	m	68
	10	6	54 (PD), 69 (D)	PD, D	74	m	100
	11	6	73	PD	82	f	113
	32	1	n.a.	RLS	90	f	377
	33	1	n.a.	RLS	95	f	352
<b>Control</b>	34	1	n.a.	-	65	f	14
	14	0	n.a.	-	70	m	68
	15	0	n.a.	-	60	f	47
	16	0	n.a.	-	59	f	110
	18	0	n.a.	-	60	m	30
	19	0	n.a.	-	82	m	63
	20	0	n.a.	-	73	f	111

PD: Parkinson's disease; D: Dementia; Dep: Depression; RLS: Restless Legs Syndrome, -: no neurological or psychiatric symptoms; n.a. = not applicable.

## Acknowledgements

First, I would like to thank Dr. med. Thomas Köglsperger and Prof. Dr. Kai Bötzel for giving me the opportunity to perform my doctoral thesis in a wonderful group and for providing an atmosphere and environment that is thoroughly enjoyable to work in. Especially, I would like to express my greatest appreciation to my awesome supervisor Dr. med. Thomas Köglsperger for his continuous support, both in life and research. To me, he is not only a supervisor for my doctoral study and research, but also a perfect mentor in my career development and life plan. He encouraged me to think independently, and always supported my ideas and concepts and gave me the freedom to execute them in my way. Without his close supervision and constant encouragement, this work would never have been possible.

I would like to thank Prof. Dr. Günter U. Höglinger for his generous support and for the good working environment I had during the time when our group was at his Department of Translational Neurodegeneration at the DZNE. Thanks to Prof. Dr. Jochen Herms for welcoming me in his lab and providing research resources.

Special thanks to my colleague Dr. Yi Tan for advice and helpful discussions as well as for sharing his large technical experience and scientific knowledge. Thanks to Felix Machleid for introducing me to the lab and sharing his protocols which accompanied me throughout my thesis. Thanks to Diana Mahlstedt, Rohit Kumar, Pan Gao, Márcia Costa, Valentin Evsyukov, Niko-Petteri Nykänen, Chencheng Pan, Shan Zhao and Jiayu Cao for technical introduction and occasional but invaluable help.

I would like to thank Dr. Sigrid Schwarz for introducing me to qRT-PCR and providing the housekeeping genes primers. Thank Dr. Thomas Arzberger for the help in the post-mortem brain slices study. My thanks also go to all the past and present lab members




who supported me in various respects of science and created a scientifically stimulating working environment.

Additionally, I would like to thank the China Scholarship Council (CSC) for funding me during the first three years of my doctoral study, and Dr. Thomas Köglspurger for an additional 12 months of financial support. Thanks to the International Office of LMU, especially Dr. Dongmei Zhang, for the help and guidance in LMU-CSC program application, as well as providing a well-organized orientation course and living assistance.

At last, I would thank my family, for their endless love, inspiration and unconditional support. And special gratitude to my wife Mengmeng Song for always being there, with faith and love. Thank you for your patience and immense support when I kept you waiting long for dinner again and again, and spent one weekend after another in the lab.



## Affidavit

	LUDWIG- MAXIMILIANS- UNIVERSITÄT MÜNCHEN	Promotionsbüro Medizinische Fakultät		
<b>Affidavit</b>				

Tang, Qilin

\_\_\_\_\_  
Surname, first name

\_\_\_\_\_  
Street

\_\_\_\_\_  
Zip code, town, country

I hereby declare, that the submitted thesis entitled:

**Alpha-Synuclein defects autophagy flux by impairing SNAP29-mediated autophagosome-lysosome fusion**

is my own work. I have only used the sources indicated and have not made unauthorized use of services of a third party. Where the work of others has been quoted or reproduced, the source is always given.

I further declare that the submitted thesis or parts thereof have not been presented as part of an examination degree to any other university.

Munich, 08.12.2020

\_\_\_\_\_  
place, date

Qilin Tang

\_\_\_\_\_  
Signature doctoral candidate